Project No. R924080

Synthesis of Feasibility Analysis of Ultra-High Performance Concrete for Prestressed Concrete Bridge Application – Phases I to V

Final Report
April 2025

Prepared by:

Zhe Wan, Assistant Professor
Craig M. Newtson, Professor
Jesus Duran Varela, Graduate Research Assistant
&
Jannatul Ferdous, Graduate Research Assistant

Department of Civil Engineering
New Mexico State University
PO Box 30001, MSC 3CE
Las Cruces, NM 88003

NM STATE

TECHNICAL PAGE

1. Report No. R924080	2. Recipient's Catalog No.	
3. Title and Subtitle Synthesis of Feasibility Analysis of Ultra-High Performance Concrete for Prestressed Concrete Bridge Application – Phases I to V	**4. Report Date** April 2025	
5. Author(s): Zhe Wan, Craig M. Newtson, Jesus Duran Varela and Jannatul Ferdous	**6. Performing Organization Report No.**	
7. Performing Organization Name and Address New Mexico State University Civil Engineering Department 3035 S Espina St. Las Cruces, NM 88003-8001	**8. Performing Organization Code**	
	9. Contract/Grant No.	
10. Sponsoring Agency Name and Address Research Bureau, NMDOT 7500B Pan American Freeway Albuquerque, NM 87199	**11. Type of Report and Period Covered** Final Report December 12, 2023 – April 12, 2025	
	12. Sponsoring Agency Code NMDOT	
13. Supplementary Notes None		

14. Abstract

UHPC is an advanced construction material characterized by exceptional compressive strength, enhanced tensile properties, and superior durability. Where prestressed concrete girders are used in New Mexico's bridge infrastructure, integrating UHPC offers a cost-effective and sustainable solution to enhance structural strength, longevity, and resilience. This report synthesizes a comprehensive feasibility analysis of UHPC for prestressed concrete bridge applications in New Mexico, spanning fifteen years of research from 2009 to 2024. The study began with an extensive literature review to understand UHPC's material properties and concluded with the application of UHPC as an overlay material for an existing concrete bridge. The report examines both the feasibility and limitations of UHPC use within the state, analyzing findings from all five phases of research.

A parametric study was conducted to evaluate the impact of constant and variable parameters on the flexural and shear performance of prestressed concrete bridges, including three-span configurations from the I-25/Doña Ana Interchange and the Sunland Park River Crossing. An economic analysis assessed the feasibility of producing locally optimized UHPC mixtures, aiming to reduce costs while enhancing material performance. Various mixture proportions were tested by adjusting supplementary cementitious materials (silica fume and fly ash), sand content and size, water-to-cement ratio, steel fiber type and content, admixture type, and curing conditions. The optimized UHPC mixture was identified based on workability, compressive strength, and flexural strength. The final mixture was further evaluated for unit weight, modulus of elasticity, modulus of rupture, durability, creep, and shrinkage to ensure its suitability for structural applications.

To validate the structural performance of UHPC, a comparative study was conducted on Bridge 5296, a structurally deficient bridge in need of repair. Longitudinal and transverse flexural tests were performed on bridge girders, alongside compressive strength tests on girders and cube samples of the same UHPC mixture. Additional UHPC applications, including joint connections, shear keys in concrete bridges, and composite beams, were explored. The efficacy of UHPC as an overlay material was further evaluated through direct tension pullout tests on the bridge deck of Bridge 7032 in Socorro, NM, assessing the bond strength between the UHPC overlay and the existing concrete surface. Recommendations were developed for material selection, substrate surface preparation, placement techniques, material handling, and UHPC mixing to facilitate practical implementation.

Beyond the feasibility analysis, this report presents a roadmap of UHPC research and applications, encompassing material optimization, mechanical property improvements, and real-world infrastructure deployment. The roadmap synthesizes significant global research, highlights current applications, and identifies challenges in UHPC implementation, such as workability retention, standardized design guidelines, reinforcement detailing, and sustainability concerns. By addressing these challenges, this report provides insights into future research directions essential for the broader adoption of UHPC in transportation infrastructures.

15. Key Words		16. Distribution Statement	
UHPC; mixture proportions; material properties; optimization; application; overlay; rehabilitation		Available from NMDOT Research Bureau	
17. Security Classification of this Report	18. Security Classification of this page	19. Number of Pages	20. Price
None	None	169	N/A

PREFACE

Since 2009, a collaborative research initiative funded by the New Mexico Department of Transportation (NMDOT) has been dedicated to evaluating the feasibility of Ultra-High Performance Concrete (UHPC) for bridge design and rehabilitation across the state. This long-term study has encompassed a wide range of research activities, including literature review, mixture development, parametric studies on bridge design, mechanical property evaluation, durability testing, structural design, the construction and monitoring of a UHPC-girder bridge completed in 2017, and the assessment of UHPC as an overlay material for the rehabilitation of existing concrete bridge decks. As a result, the project has progressed through five distinct phases, each addressing critical aspects of UHPC's application in bridge infrastructure.

Given the extensive research conducted over the past fifteen years, the NMDOT has recognized the need for a comprehensive synthesis that consolidates the findings from all five research phases into a single, cohesive document. This report serves as a centralized resource, integrating key insights, methodologies, and results to provide a clear and accessible overview of UHPC research and its implications for bridge infrastructure.

Beyond summarizing the findings from all five phases, this synthesis situates UHPC advancements within the broader landscape of global research and real-world applications. The roadmap presented in this report offers a comprehensive analysis of significant UHPC studies worldwide, highlighting current implementations by researchers, identifying persistent challenges in mixtures development and structural integration, and outlining future directions for UHPC expansion. By examining these critical aspects, this report not only consolidates past research but also provides a strategic framework for advancing UHPC implementation in transportation infrastructure.

NOTICE

DISCLAIMER

ABSTRACT

UHPC is an advanced construction material characterized by exceptional compressive strength, enhanced tensile properties, and superior durability. Where prestressed concrete girders are used in New Mexico's bridge infrastructure, integrating UHPC offers a cost-effective and sustainable solution to enhance structural strength, longevity, and resilience. This report synthesizes a comprehensive feasibility analysis of UHPC for prestressed concrete bridge applications in New Mexico, spanning fifteen years of research from 2009 to 2024. The study began with an extensive literature review to understand UHPC's material properties and concluded with the application of UHPC as an overlay material for an existing concrete bridge. The report examines both the feasibility and limitations of UHPC use within the state, analyzing findings from all five phases of research.

A parametric study was conducted to evaluate the impact of constant and variable parameters on the flexural and shear performance of prestressed concrete bridges, including three-span configurations from the I-25/Doña Ana Interchange and the Sunland Park River Crossing. An economic analysis assessed the feasibility of producing locally optimized UHPC mixtures, aiming to reduce costs while enhancing material performance. Various mixture proportions were tested by adjusting supplementary cementitious materials (silica fume and fly ash), sand content and size, water-to-cement ratio, steel fiber type and content, admixture type, and curing conditions. The optimized UHPC mixture was identified based on workability, compressive strength, and flexural strength. The final mixture was further evaluated for unit weight, modulus of elasticity, modulus of rupture, durability, creep, and shrinkage to ensure its suitability for structural applications.

To validate the structural performance of UHPC, a comparative study was conducted on Bridge 5296, a structurally deficient bridge in need of repair. Longitudinal and transverse flexural tests were performed on bridge girders, alongside compressive strength tests on girders and cube samples of the same UHPC mixture. Additional UHPC applications, including joint connections, shear keys in concrete bridges, and composite beams, were explored. The efficacy of UHPC as an overlay material was further evaluated through direct tension pullout tests on the bridge deck of Bridge 7032 in Socorro, NM, assessing the bond strength between the UHPC overlay and the existing concrete surface. Recommendations were developed for material selection, substrate surface preparation, placement techniques, material handling, and UHPC mixing to facilitate practical implementation.

Beyond the feasibility analysis, this report presents a roadmap of UHPC research and applications, encompassing material optimization, mechanical property improvements, and real-world infrastructure deployment. The roadmap synthesizes significant global research, highlights current applications, and identifies challenges in UHPC implementation, such as workability retention, standardized design guidelines, reinforcement detailing, and sustainability concerns. By addressing these challenges, this report provides insights into future research directions essential for the broader adoption of UHPC in transportation infrastructures.

TABLE OF CONTENTS

LIST OF FIGURES

LIST OF TABLES

LAYOUT OF REPORT

In this report, Section 1 provides an Introduction, outlining the objectives and scope of the study. Section 2 examines the Feasibility and Limitations of UHPC, addressing its potential advantages and constraints in bridge applications. Section 3 focuses on UHPC Mixture Development, detailing the process of optimizing mixture proportions using locally available materials. Section 4 presents the Material Properties of the Optimized UHPC, evaluating key characteristics such as strength, durability, and workability. Section 5 compares UHPC and HPC through Laboratory and Field Analyses, assessing their structural performance under various conditions. Section 6 explores the Application of UHPC in New Mexico, documenting real-world implementations and case studies. Section 7 presents a Roadmap for UHPC Exploration, synthesizing research advancements, global applications, and strategic directions for future implementation. Section 8 discusses Current Challenges and Future Work, identifying barriers to widespread adoption and areas for further research. Finally, Section 9 provides a Summary, encapsulating key findings and conclusions from the study.

1. INTRODUCTION

Ultra-high performance concrete (UHPC) is an advanced material technology which combines enhanced fibrous and cementitious materials to achieve high compressive strength (>21.7 ksi), ductility and exceptional durability (B. A. Graybeal, 2006). UHPC tends to have a low water to binder ratio and can achieve adequate rheological properties by combining optimized granular packing with high range water reducing admixtures (Du et al., 2021; Ullah et al., 2022). Moreover, the appropriate addition of fibers to UHPC continues to improve its tensile cracking resistance, post-cracking strength, ductility, and energy absorption capacity (Wille et al., 2011). Given its low water-to-binder ratio (w/b, 0.15–0.25), high particle packing density (0.825–0.855), high-volume of steel fibers (≥2%, by volume), and proper addition of chemical admixtures, UHPC exhibits good flowability and exceptional mechanical properties (Du et al., 2021). Despite improved strength and mechanical properties, UHPC is limited by its extensive material cost (Azmee & Shafiq, 2018). However, by lowering the cross-sections of structural elements and integrating cost effective materials, UHPC can result in sustainable construction, saving materials and labor costs (Abbas et al., 2016).

For the past two decades, UHPC has been gaining increased interest in many countries including Australia, Austria, Canada, China, the Czech Republic, France, Germany, Italy, Japan, Malaysia, the Netherlands, New Zealand, Slovenia, South Korea, Switzerland, and the United States (Azmee & Shafiq, 2018) with its usage ranging from building components, bridges, architectural features, repair and rehabilitation, vertical components such as windmills towers and utilities towers to oil and gas industry applications, off-shore structures, hydraulic structures and overlay materials. To date, in the United States, more than 200 bridges in 27 states and the District of Columbia have been constructed using UHPC materials (Haber & Graybeal, 2019). One emerging application for UHPC in the U.S. highway bridge sector is for bridge repair, retrofit, and rehabilitation. Since 2016, at least 10 U.S. bridges have been repaired or rehabilitated using UHPC-class materials and exhibited unique aspects in their repair approaches, such as the use of UHPC for joint closures, deck overlays, or localized structural strengthening. Each of these projects used relatively small volumes of UHPC material and were viewed as relatively low risk by the bridge owners (Haber & Graybeal, 2019).

Various states such as Iowa, New York, and Florida are actively exploring and adopting UHPC for their infrastructure projects. The first UHPC bridge in the United States was built in Wapello County, Iowa, Mars Hill Bridge. The 109.91 ft. long bridge was constructed using UHPC, which helped reduce the number of prestressing tendons and the girder depth in the bridge (Bierwagen & Abu-Hawash, 2016). In 2011, the first precast UHPC waffle bridge deck panels were installed in the Little Cedar Creek Bridge in Wapello County, Iowa (Wipf et al., 2011). Referring to the rehabilitation of deteriorated bridge decks and columns, Buchanan County, Iowa implemented in 2017 the first bridge deck overlay on Mud Creek Bridge, showing satisfactory bonding and crack resistance properties (Wibowo & Sritharan, 2018). On the field test, it was found that, when UHPC is used as an overlay, to avoid the use of framework and limit the material cost, it should be designed for a thixotropic behavior (Du et al., 2021).

The Florida Department of Transportation implemented UHPC in the repair of an existing bridge connection (constructed in 1978) with precast, prestressed concrete voided-slab beams. After years of service, as reflective cracking became apparent in the bridge's asphalt overlay, instead of

replacing the superstructure, FDOT decided to remove the existing connection regions using hydrodemolition, installing additional reinforcement, and replacing the removed concrete with UHPC. Laboratory testing of similar connections using UHPC between adjacent box beams has demonstrated that UHPC can create full composite action and robust performance (Haber & Graybeal, 2019).

NYSDOT (New York State Department of Transportation) has successfully utilized the beneficial properties of UHPC in a large number of accelerated bridge construction projects (Fuda J. M., 2019). In 2009 two projects were successfully implemented in New York, Route 31 Bridge in Lyons and Route 23 Bridge in Oneonta (Du et al., 2021). Additionally, New Jersey has implemented the use of UHPC in concrete decks, joint repairs, as well as overlay tests on at least 8 bridge decks (Murphy et al., 2019). Several more UHPC projects within New York State are under construction, in design, or in the planning phases. As shown in Figure 1.1, New York has been near the forefront in integrating UHPC in their repairs.
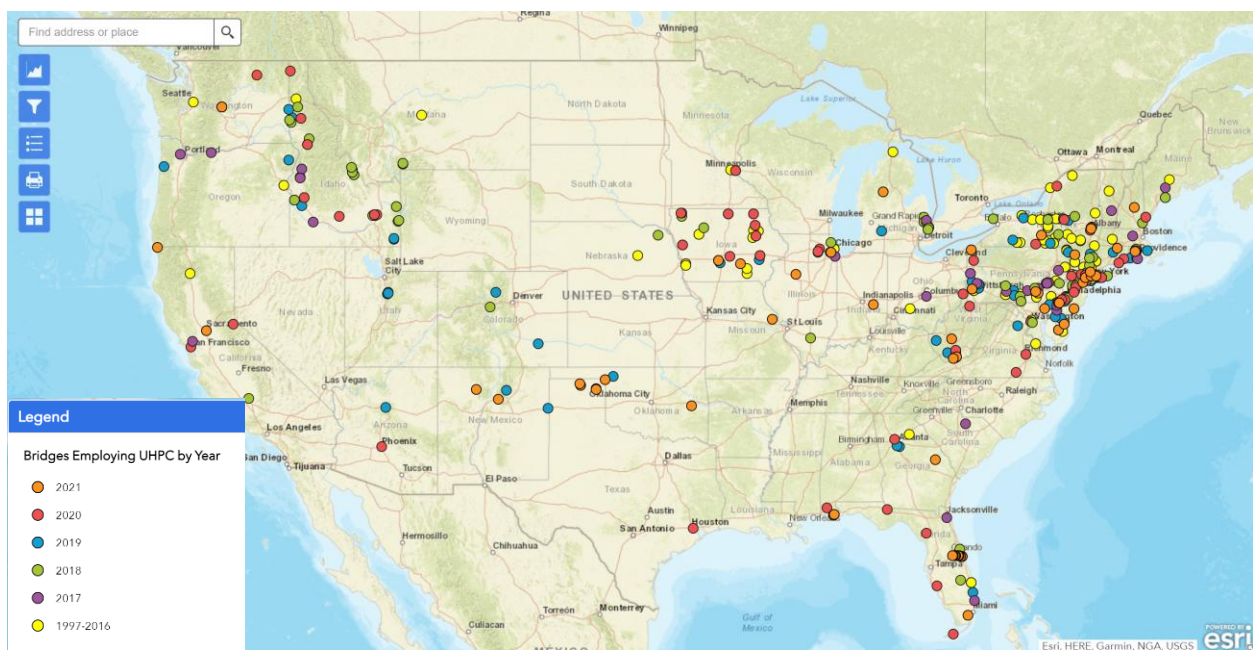
Figure 1.1. Interactive map of bridges employing UHPC in the United States (FHWA and Turner-Fairbank Highway Research Center in McLean, VA, USA)

1.1 UHPC Applicated to New Mexico

In New Mexico, research into UHPC has been ongoing since 2009 (Weldon et al., 2009), encompassing a broad spectrum of activities including feasibility studies, mixture development, parametric analyses of bridge designs, and monitoring of a UHPC-girder bridge. Given that approximately 50% of the state's bridges are built with prestressed concrete, integrating UHPC into construction and repair activities could significantly enhance both the cost-efficiency and performance of these structures, potentially extending their service life by up to twice as long (Weldon et al., 2009). The state's extreme temperatures and intense sun exposure can create thermal moments that can rapidly degrade traditional concrete, but UHPC's superior toughness helps maintain structural integrity under such conditions. Additionally, its durability against freeze-thaw cycles (Akeed et al., 2022) reduces maintenance needs. This extended service life is

16

particularly valuable in New Mexico's remote areas, where frequent repairs and upgrades for aging infrastructure, such as bridges, incur additional costs for travel and labor.

One significant drawback of UHPC is its higher initial cost compared to traditional concrete. To address this issue, in 2007, a research team at NMSU began investigating the development of UHPC using local New Mexico materials (Isabel A. Rodriguez, 2012). This research included conducting mechanical analyses, such as compressive and flexural tests, and the results revealed the potential for incorporating UHPC into bridge design in New Mexico. Subsequently, additional investigations related to UHPC application were initiated at NMSU with financial support from NMDOT. The research spanned 15 years and was divided into five phases, with each phase targeting a specific aspect of UHPC application.

The first phase of this research went from April 7, 2009 to July 31, 2010 (Weldon et al., 2009), where a literature review was conducted to understand the characteristics and properties of UHPC. On completion of the review, trial designs as well as cost analyses were performed on typical prestressed concrete bridges to investigate the merits and feasibility of UHPC in New Mexico. Working with the cost constraints and characteristics of UHPC identified in Phase I, Phase II was initiated. In this phase, mixture proportions were prepared using local New Mexico materials. This Phase was completed by June 30, 2012 (Weldon et al., 2012). Then, Phase III began, which continued from December 6, 2012, to December 6, 2016 (Weldon et al., 2016). In this phase, full scale laboratory mechanical tests were performed on UHPC bridge girders, which provided enough information on strength and durability of UHPC for NMDOT to specify the material for the replacement of a small bridge near Las Cruces. Bridge 9706 was designed with one span of UHPC prestressed girders and one with HPC girders, instrumented with vibrating wire strain gauges and fiber optic sensors for long term monitoring of the bridge. In Phase IV, Bridge 9706 was subjected to load testing, which was completed by May 2022 (Weldon et al., 2022). From the results obtained from the laboratory and field testing, an analytical model was developed that was used further to investigate the bridge behavior. Additionally, the application of UHPC on some additional case studies (joint application, shear keys) were also investigated. Finally, in Phase V of this project, a non-proprietary UHPC overlay was placed on Bridge No. 7032, with strain gauges and thermocouples installed for long-term monitoring (Alvarez et al., 2024). Lastly, some necessary suggestions were presented for contracts related to UHPC overlay projects.

Given the extensive and detailed nature of the reports associated with each phase of the research, the NMDOT recognizes the need for a more streamlined approach. To facilitate a more efficient understanding and utilization of the research findings, the NMDOT aims to consolidate these individual reports into a single comprehensive synthesis. This synthesis will serve as a condensed yet comprehensive document, encompassing the entirety of the research initiatives, high-level findings, and the roadmap that describes the course of action for all five UHPC research phases.

Objectives

There were three specific objectives of this research:

- Compile the individual reports (Phases I, II, III, IV, V) into a single synthesis, providing a concise overview of research initiatives and high-level findings.
- Develop a roadmap to incorporate UHPC into bridge design in New Mexico, based on the research findings.

- Ensure that the compiled synthesis is practical and accessible for NMDOT personnel, enabling them to implement the research findings effectively.

1.2 Organization of the Synthesis

The organization of this report (Figure 1.2) begins with an assessment of the feasibility and limitations of using UHPC in New Mexico, followed by the development of optimized mixtures and evaluation of their properties. A comparative analysis of UHPC and HPC is conducted under similar conditions to evaluate their performance. Additionally, the potential applications of UHPC are explored. A roadmap is provided to review existing applications and guide future implementation. Finally, the summary section offers a comprehensive overview of the findings.
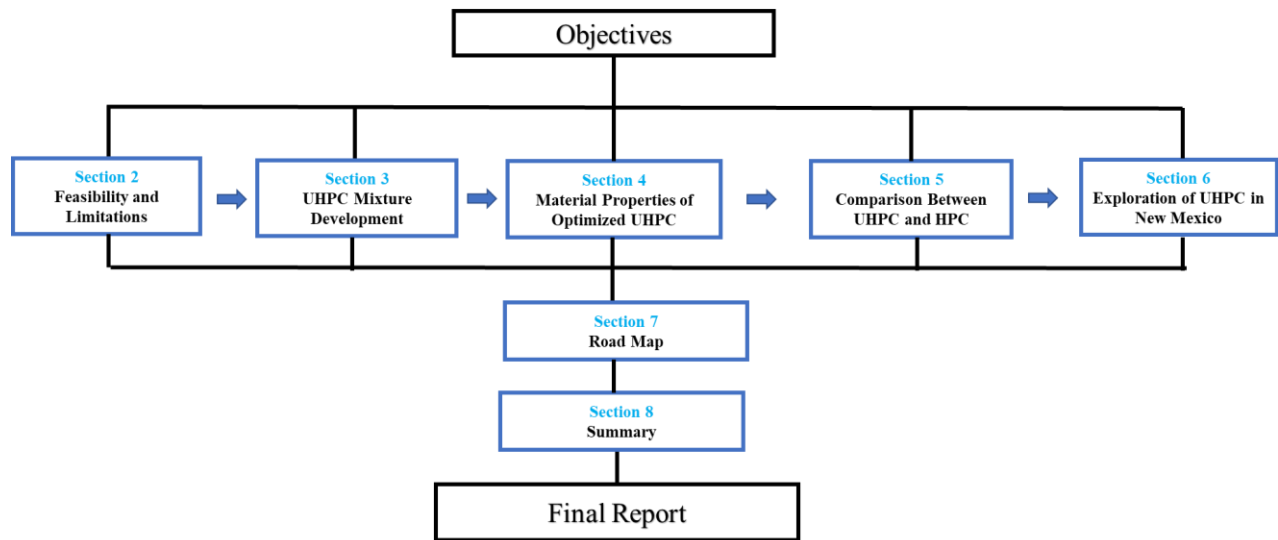
Figure 1.2. Organization of the synthesis

2. FEASIBILITY AND LIMITATIONS

The successful implementation of UHPC in the state of New Mexico requires a comprehensive analysis to evaluate the feasibility and limitations of its application. This analysis examines factors affecting UHPC's performance, cost-effectiveness, and practicality under the state's specific conditions.

2.1 Feasibility

The feasibility of using UHPC in prestressed bridges was analyzed through a parametric study on representative bridges in New Mexico. Specifically, CONSPAN®, a numerical software for designing and analyzing precast and prestressed beams, was utilized. The matrix analysis in the software was designed to compare the flexural and shear performance of UHPC and HPC for various types of girder cross sections commonly used in New Mexico's prestressed concrete bridges. Additionally, the study examined the impact of negative moment reinforcement in two- and three-span bridges.

Three types of bridges commonly used in New Mexico were identified for analysis: single simple span, two-span continuous, and three-span continuous bridges. Specifically, the I-25/Doña Ana Interchange, consisting of six AASHTO BT-63 girders spaced at 7.25 ft, was selected to represent the single-span bridge (Figure 2.1). The Sunland Park River Crossing Bridge, designed with ten modified BT-54 prestressed concrete girders spaced at 6.8 ft and comprising seven spans (two-span continuous, three-span continuous and two-span continuous), was selected to represent both two- and three-span continuous bridges (Figures 2.2 and 2.3).

The goal was to explore the potential for material savings by using UHPC. Due to its high strength, UHPC was expected to reduce the number and/or size of the girders when compared to HPC, potentially lowering overall concrete volume and leading to material savings.

Figure 2.1. North Bound Structure of I-25 Doña Ana Interchange (UHPC Phase I, Figure 4.1)

Figure 2.2. Two span unit of Sunland Park River Crossing (UHPC Phase I, Figure 4.5)

Figure 2.3. Three span unit of Sunland Park River Crossing (UHPC Phase I, Figure 4.6)

2.1.1 Parametric Study

A parametric study was conducted to assess the impact of varying parameters on bridge performance. This study compared the performance of the as-designed bridges made with HPC to that of an equivalent bridge utilizing UHPC. The design matrix used in the software incorporated both constant and variable parameters to evaluate the performance and cost-effectiveness of UHPC under different configurations.

Constant Parameters

Constant parameters included deck width, deck compressive strength, strand pattern, and girder length. Specifically, the deck overhang was set at 3.38 ft for the I-25/Doña Ana Interchange and 4.25 ft for the Sunland Park Bridge. The compressive strength of deck was considered to be 4,000 psi, a typical value for conventional concrete. The span length was 112.5 ft for the I-25/Doña Ana Interchange and 121.92 ft for the Sunland Park River Crossing Bridge. Both straight and harped strand patterns were used consistent comparisons.

Variable Parameters

The variable parameters included the number of girder lines, deck thickness, release and final compressive strengths, modulus of elasticity, modulus of rupture, and the diameter of prestressing strands.

- Number of girder lines:

  I-25/Doña Ana Interchange: 4 to 6 girders

  Sunland Park Bridge: 6 to 10 girders

- Deck thickness:

  I-25/Doña Ana Interchange: 7.5 to 9.5 in.

20

Sunland Park Bridge: 8 to 10.5 in.

- Girder compressive strength:

    Both bridges: 9.5, 15, 17.5, 20, and 22.5 ksi.

For each compressive strength level, the required number of 0.6 in. and 0.7 in. prestressing strands was determined. The modulus of elasticity values were calculated using the AASHTO code (AASHTO, 2017), the AFGC/SETRA equation (AFGC-SETRA, 2002), and the Graybeal equation (B. A. Graybeal, 2006). Additionally, the modulus of rupture was analyzed under two conditions:

- Limited per AASHTO provisions
- Limited to 1.16 ksi, as per Gowripalan and Gilbert (2000)

These variables were chosen for their potential influence on bridge performance, cost, and material usage. The study aimed to explore how UHPC's unique properties can be optimized to enhance structural efficiency.

Flexure analysis

A flexure analysis is essential to ensure that the bridge can support the anticipated vehicle loads without excessive bending or deformation. This analysis aimed to optimize the number and size of girders in various bridge designs while preserving sufficient load-bearing capacity. By preventing excessive or repeated bending, the bridge is protected from material fatigue, cracking, and potential long-term damage.

CONSPAN offers options for simulating girder types currently utilized by the NMDOT, including AASHTO BT-63, BT-54, Type III, Type II and Type I. The software was used to adjust the variable parameters and analyze bridge designs with different girder number and type. This methodology was applied to the three selected bridge types.

Two prestressing strand sizes were used, 0.6 in. and 0.7 in. in diameter. The primary difference between them was their cross-sectional area - the 0.7 in. strands provide 35% more cross-sectional area than the 0.6 in. strands, despite only a 17% increase in diameter. The larger strands offer advantages, such as labor savings and increased prestressing force, which were achieved with fewer strands. The objective was to achieve the great amount of savings in UHPC volume, while using the fewest strands.

The results indicate that the enhanced compressive and tensile strength of UHPC can lead to significant concrete savings compared to HPC. Live load deflections were evaluated for all designs, with an allowable deflection limit of L/800 or 1.7 in. All deflections satisfied the serviceability requirements.

The following sections present the specific simulations conducted along with their corresponding results.

I-25/Doña Ana Interchange

The I-25/Doña Ana Interchange bridge incorporated 36 prestressing strands of 0.6 in. diameter, distributed as follows: 24 straight strands, 6 harped strands, and 6 debonded partial-length strands in the top flange. These strands were strategically placed to control stresses and achieve the required flexural moment capacity.

Based on the strand configuration used in the I-25/Doña Ana Interchange bridge, two base configurations using different diameters of prestressing strands were developed for analysis. These configurations, shown below, featured harped and straight strand patterns, excluding the debonded partial-length strands in the top flange (UHPC Phase I, Section 4.1.5).

Methodology

Two configurations were set up for the analysis, varying in prestressing strands diameter.
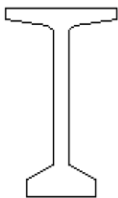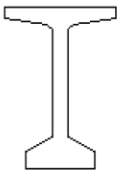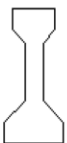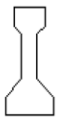
- Base Configuration 1: Used 0.6 in. diameter strands, incorporating 28 strands (26 straight and 2 harped).
- Base Configuration 2: Used 0.7 in. diameter strands, incorporating 22 strands (20 straight and 2 harped).

The design matrix considered the number of girders (six, five, and four), the types of girders (BT-63, BT-54, Type III, Type II, and Type I) (Table 2.1), five compressive strengths (9.5, 15, 17.5, 20 and 22.5 ksi), as well as three values of deck thickness (7.5, 8.5 and 9.5 in.) (Table 2.2), based on configurations 1 and 2. The matrix was tested beginning with BT-63 and progress sequentially to type I, stopping if a configuration failed to meet the viability requirements of the LFD specifications.

Furthermore, the modulus of rupture was analyzed under two conditions:

- Limited per AASHTO provisions
- Limited to 1.16 ksi

Table 2.1. Design Matrix for I-25/Doña Ana Interchange (UHPC Phase I, Table 4.1)

Number of Girders	Types of Girders				
	BT - 63	BT - 54	Type III	Type II	Type I
6	I	II	III	IV	V
5	VI	VII	VII	IX	X
4	XI	XII	XIII	XIV	XV

22

Results

By increasing the diameter of the strands (from configuration 1 to configuration 2) and the compressive strength, additional UHPC volume savings (Table 2.2) as well as savings in the number of strands were achieved. Furthermore, when limiting the MOR value to 1.16 ksi instead of the LFD limit, further savings could be achieved (UHPC concrete volume and number strands) using both sizes of strands. Additionally, with the increase in volume of normal-strength concrete (deck thickness increased from 7.5 to 9.5 in), the UHPC volume decreased, which can reduce both material and labor costs. Testing results are presented below.

Using 0.6 in diameter strands:

- MOR calculated with LFD Code:

Four configurations (I, II, VI and VII) met the requirements (Table 2.2). A 23% reduction in UHPC volume for the girders was achieved by utilizing 46 strands of 0.6 in diameter and increasing the deck thickness (made of normal-strength concrete) from 7.5 to 8.5 in., with a configuration of five girder lines of Type BT-54.

Additionally, live load deflections ranged from 1.104 in. at a compressive strength of 15 ksi to 0.977 in. at 22.5 ksi. For comparison, the baseline configuration, which used six girder lines of Type BT-63 with a compressive strength of 9.5 ksi and 28 strands, resulted in a live load deflection of 0.771 in.

- MOR limited to 1.16 ksi.:

Five configurations (I, II, VI, VII and XI) met the requirements (Table 2.2). A 33% savings in UHPC volume was achieved by utilizing 42 strands of 0.6-in. diameter and increasing the deck thickness (made of normal-strength concrete) from 7.5 to 9.5 in., with a configuration of four girder lines of Type BT-63.

Additionally, live load deflections ranged from 0.897 in. at a compressive strength of 15 ksi to 0.785 in. at 22.5 ksi. For comparison, the baseline configuration, which used six girder lines of Type BT-63 with a compressive strength of 9.5 ksi and 28 strands, resulted in a live load deflection of 0.771 in.

Using 0.7 in. diameter strands:

- MOR calculated with LFD Code:

Five configurations (I, II, VI, VII and XI) met the requirements (Table 2.2). A 33% reduction in UHPC volume was achieved by utilizing 34 strands of 0.7-in. diameter and increasing the deck thickness (made of normal-strength concrete) from 7.5 to 9.5 in., with a configuration of four girder lines of Type BT-63.

Additionally, live load deflections ranged from 0.874 in. at a compressive strength of 15 ksi to 0.772 in. at 22.5 ksi. For comparison, the baseline configuration, which consisted of six girder lines of Type BT-63 with a compressive strength of 9.5 ksi and 22 strands, resulted in a live load deflection of 0.767 in.

- MOR limited to 1.16 ksi:

Six configurations (I, II, VI, VII, XI and XII) met the requirements (Table 2.2). A 38% reduction in UHPC volume was achieved by utilizing 46 strands of 0.7-in. diameter and increasing the deck thickness (made of normal-strength concrete) from 7.5 to 9.5 in., with a configuration of four girder lines of Type BT-54.

Additionally, live load deflections ranged from 1.057 in. at a compressive strength of 20 ksi and 36 strands to 1.104 in. at 22.5 ksi. For comparison, the baseline configuration, which used six girder lines of Type BT-63 with a compressive strength of 9.5 ksi and 22 strands, resulted in a live load deflection of 0.767 in.

The configurations that yielded the greatest concrete savings for I-25/Doña Ana Interchange consisted of two optimized designs (Table 2.2).

- Configuration XI: utilized 42 strands of 0.6 in. diameter and increased the deck thickness (made of normal-strength concrete) from 7.5 to 9.5 in., with a configuration of four girder lines of Type BT-63, resulting in 33% savings in girder volume by incorporating UHPC.

- Configuration XII: utilized 46 strands of 0.7 in. diameter and increased the deck thickness (made of normal-strength concrete) from 7.5 to 9.5 in., with a configuration of four girder lines of Type BT-54, resulting in 38% reduction in girder volume by incorporating UHPC.

Table 2.2. Flexure analysis results for I-25/Doña Ana Interchange

Viable Cross-Section Configurations	Compressive Strength of UHPC, ksi	Deck Thickness, in.	Tensile Stress Limit according to LFD						Tensile Stress Limit of 1.16 ksi					
			Live Load Deflections with Strands, in.		Savings in Concrete Volume in Girders, %		Number of Strands		Live Load Deflections with Strands, in.		Savings in Concrete Volume in Girders, %		Number of Strands	
			0.6 in. strands	0.7 in. strands	0.6 in. strands	0.7 in. strands	0.6 in. strands	0.7 in. strands	0.6 in. strands	0.7 in. strands	0.6 in. strands	0.7 in. strands	0.6 in. strands	0.7 in. strands
I (6 BT-63 Girder Lines)	9.5	7.5	0.0304	0.0302	0%	0%	28	22	0.0304	0.0302	0%	0%	28	22
	15		0.0295	0.02933			26	20	0.0298	0.0298			22	16
	17.5		0.0281	0.02795			26	20	0.0283	0.0283			22	16
	20		0.0269	0.02677			26	20	0.0271	0.0271			22	16
	22.5		0.0259	0.02579			26	20	0.0261	0.0261			22	16
II (6 BT-54 Girder Lines)	9.5	7.5	0.0423	0.04217	8%	8%	36	26	0.0423	0.0422	8%	8%	36	26
	15		0.0408	0.04051			34	26	0.0412	0.0411			30	22
	17.5		0.0389	0.0389			34	24	0.0393	0.0391			30	22
	20		0.0374	0.03732			34	24	0.0376	0.0376			30	22
	22.5		0.036	0.03598			34	24	0.0363	0.0362			30	22
VI (5 BT-63 Girder Lines)	9.5	8.5	0.0325	0.03244	17%	17%	36	26	0.0325	0.0324	17%	17%	36	26
	15		0.0315	0.03146			34	24	0.0319	0.0317			28	22
	17.5		0.03	0.02996			34	24	0.0302	0.0302			30	22
	20		0.0287	0.02874			34	24	0.029	0.0289			30	22
	22.5		0.0278	0.02768			32	24	0.0279	0.0278			30	22
VII (5 BT-54 Girder Lines)	9.5	8.5	-	-	23%	23%	-	-	-	-	23%	23%	-	-
	15		0.0435	0.04307			48	32	0.044	0.0436			42	28
	17.5		0.0415	0.0411			48	32	0.042	0.0416			40	28
	20		0.0434	0.03949			46	32	0.0402	0.0399			40	28
	22.5		0.0385	0.03811			46	32	0.0388	0.0385			40	28
XI (4 BT-63 Girder Lines)	9.5	9.5	-	0.03441	-	33%	-	-	-	-	33%	33%	-	-
	15		-	0.03441			-	34	0.0353	0.0349			42	30
	17.5		-	0.03283			-	34	0.0335	0.0332			42	30
	20		-	0.0315			-	34	0.0321	0.0319			42	30
	22.5		-	0.03039			-	34	0.0309	0.0307			42	30
XII (4 BT-54 Girder Lines)	9.5	9.5	-	-	-	-	-	-	-	-		38%	-	-
	15		-	-			-	-	-	-			-	-
	17.5		-	-			-	-	-	-			-	-
	20		-	-			-	-	-	0.0416			-	46
	22.5		-	-			-	-	-	0.0435			-	46
- non viable design														

Sunland Park Bridge – Two Span Continuous Unit

The Sunland Park Bridge incorporated 40 prestressing strands of 0.6 in. diameter, distributed as follows: 32 straight strands and 8 harped strands. These strands were strategically placed to control stresses and achieve the required flexural moment capacity.

Based on the strand configuration used in the Sunland Park Bridge, two base configurations using different diameters of prestressing strands were developed for analysis.

Methodology

Two configurations were set up for the analysis, differing in the diameter of the prestressing strands:

- Base Configuration 1: used 0.6-in. diameter strands, incorporating 40 strands (32 straight strands and 8 harped strands).
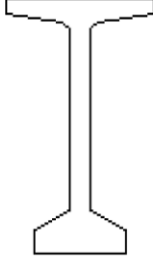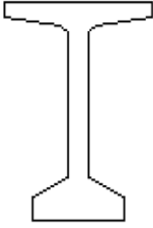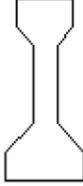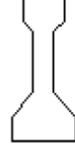
- Base Configuration 2: used 0.7-in. diameter strands, incorporating 26 strands (20 straight strands and 6 harped strands).

The design matrix considered the number of girders (ten, nine, eight, seven and six), types of girders (BT-63 and BT-54) (Table 2.3), five compressive strengths (9.5, 15, 17.5, 20, to 22.5 ksi) as well as four values of deck thickness (8, 8.5, 9 and 10.5 in.) (Table 2.4) based on configurations 1 and 2. The matrix was evaluated beginning with 10 BT-54 and progressing sequentially to 6 BT-63, stopping if a configuration failed to meet the viability requirements of the LFD specifications.

The modulus of rupture was analyzed under two conditions:

- Limited per AASHTO provisions
- Limited to 1.16 ksi

Table 2.3. Design matrix for Sunland Park Bridge (UHPC Phase I, Table 4.9)

Number of Girders	Type of Girders				
	BT-63	BT-54	Type III	Type II	Type I
10	N/A	I	-	-	-
9	N/A	V	-	-	-
8	N/A	IX	-	-	-
7	N/A	XIII	-	-	-
6	XVII-b	XVII-a	-	-	-

Note: the AASHTO Type I, II and III were found to be unsatisfactory girder types for this structure.

Results

By increasing the diameter of the strands (from configuration 1 to configuration 2) and the compressive strength, additional UHPC volume savings (Table 2.4) as well as savings in the number of strands were achieved. Furthermore, when limiting the MOR value to 1.16 ksi instead of the LFD limit, further savings can be achieved (UHPC concrete volume and number strands) using both sizes of strands. Additionally, with the increase in volume of normal-strength concrete (deck thickness increased from 8 to 10.5 in.), the UHPC volume decreased which can reduce both the material and labor cost. Testing results are shown below.

Using 0.6 in. diameter strands:

- MOR calculated with LFD Code:

Three configurations (I, V and IX) met the requirements (Table 2.4). A 20% reduction in UHPC volume for the girders was achieved by utilizing 48 strands of 0.6 in. diameter and increasing the deck thickness (made of normal-strength concrete) from 8 to 8.5 in., with a configuration of eight girder lines of Type BT-54.

Additionally, live load deflections ranged from 0.999 in. at a compressive strength of 15 ksi and 52 strands to 0.884 in. at 22.5 ksi. For comparison, the baseline configuration, which used ten girder lines of Type BT-54 with a compressive strength of 9.5 ksi and 40 strands, resulted in a live load deflection of 0.877 in.

- MOR limited to 1.16 ksi:

Three configurations (I, V and IX) met the requirements (Table 2.4). A 20% savings in UHPC volume was achieved by utilizing 42 strands of 0.6-in. diameter and increasing the deck thickness (made of normal-strength concrete) from 8 to 8.5 in., with a configuration of eight girder lines of Type BT-54.

Additionally, live load deflections ranged from 0.864 in. at a compressive strength of 15 ksi with 40 strands to 0.886 in. at 22.5 ksi. For comparison, the baseline configuration, which used 10 girder lines of Type BT-54 with a compressive strength of 9.5 ksi and 40 strands, resulted in a live load deflection of 0.877 in.

Using 0.7 in diameter strands:

- MOR calculated with LFD Code:

Five configurations (I, V, IX, XIII and XVII-b) met the requirements (Table 2.4). A 30% reduction in UHPC volume was achieved by utilizing 36 strands of 0.7 in. diameter and increasing the deck thickness (made of normal-strength concrete) from 8 to 9 in., with a configuration of seven girder lines of Type BT-54.

Additionally, live load deflections ranged from 1.067 in. at a compressive strength of 15 ksi to 0.946 in. at 22.5 ksi. For comparison, the baseline configuration, which consisted of 10 girder lines of Type BT-54 with a compressive strength of 9.5 ksi and 26 strands, resulted in a live load deflection of 0.878 in.

- MOR limited to 1.16 ksi:

Five configurations (I, V, IX, XIII and XVII-b) met the requirements (Table 2.4). A 43% reduction in UHPC volume was achieved by utilizing 38 strands of 0.7-in. diameter and increasing the deck thickness (made of normal-strength concrete) from 8 to 10.5 in., with a configuration of 6 girder lines of Type BT-63.

Additionally, live load deflections ranged from 0.869 in. at a compressive strength of 15 ksi and 36 strands to 0.748 in. at 22.5 ksi. For comparison, the baseline configuration, which used 10 girder

lines of Type BT-54 with a compressive strength of 9.5 ksi and 26 strands, resulted in a live load deflection of 0.878 in.

The configurations that yielded the greatest concrete savings for the Sunland Park Bridge two-span continuous unit consisted of two optimized designs (Table 2.4).

- Configuration IX: utilized 42 strands of 0.6-in. diameter and increased the deck thickness (made of normal-strength concrete) from 8 to 8.5 in., with a configuration of eight girder lines of Type BT-54, resulting in 20% savings in UHPC volume.

- Configuration XVII-b: utilized 38 strands of 0.7 in. diameter and increased the deck thickness (made of normal-strength concrete) from 8 to 10.5 in., with a configuration of 6 girder lines of Type BT-63, resulting in 43% reduction in UHPC volume.

Table 2.4. Flexure analysis results for Sunland Park Bridge – Two span unit

Viable Cross-Section Configurations	Compressive Strength of UHPC, ksi	Deck Thickness, in.	Tensile Stress Limit according to LFD						Tensile Stress Limit of 1.16 ksi					
			Live Load Deflections with Strands, in.		Savings in Concrete Volume in Girders, %		Number of Strands		Live Load Deflections with Strands, in.		Savings in Concrete Volume in Girders, %		Number of Strands	
			0.6 in. strands	0.7 in. strands	0.6 in. strands	0.7 in. strands	0.6 in. strands	0.7 in. strands	0.6 in. strands	0.7 in. strands	0.6 in. strands	0.7 in. strands	0.6 in. strands	0.7 in. strands
I (10 BT-54 Girder Lines)	9.5	8	0.0345	0.0346	0%	0%	40	26	0.0345	0.0346	0%	0%	40	26
	15		0.0342	0.0345			36	22	0.0344	0.0345			32	22
	17.5		0.0326	0.0329			36	22	0.0329	0.0329			32	22
	20		0.0313	0.0315			36	22	0.0315	0.0315			32	22
	22.5		0.0302	0.0304			36	22	0.0305	0.0304			30	22
V (9 BT-54 Girder Lines)	9.5	8	0.0305	0.038	10%	10%	46	32	0.0305	0.038	10%	10%	46	32
	15		0.0369	0.0371			42	26	0.0371	0.0371			36	26
	17.5		0.0352	0.0354			42	26	0.0354	0.0354			36	26
	20		0.0339	0.0339			40	26	0.034	0.0339			36	26
	22.5		0.0327	0.0328			40	26	0.0328	0.0328			36	26
IX (8 BT-54 Girder Lines)	9.5	8.5	-	-	20%	20%	-	-	-	-	20%	20%	-	-
	15		0.0393	0.0394			52	28	0.034	0.0394			40	28
	17.5		0.0376	0.0376			50	28	0.0328	0.0376			42	28
	20		0.0361	0.0359			50	30	0.0362	0.0359			42	30
	22.5		0.0348	0.0347			48	30	0.0349	0.0347			42	30
XIII (7 BT-54 Girder Lines)	9.5	9	-	-	-	30%	-	-	-	-	-	30%	-	-
	15		-	0.042			-	36	-	0.042			-	36
	17.5		-	0.0364			-	36	-	0.0364			-	36
	20		-	0.0386			-	36	-	0.0386			-	36
	22.5		-	0.0372			-	36	-	0.0372			-	36
XVII-b (6 BT-63 Girder Lines)	9.5	10.5	-	-	-	43%	-	-	-	-	-	43%	-	-
	15		-	0.0342			-	36	-	0.0342			-	36
	17.5		-	0.0318			-	38	-	0.0318			-	38
	20		-	0.0305			-	38	-	0.0305			-	38
	22.5		-	0.0294			-	38	-	0.0294			-	38

- non viable design

<u>Sunland Park Bridge - Three Span Continuous Unit</u>

The three-span continuous unit of the Sunland Park Bridge had two distinct girder cross sections. Spans 3 and 5 shared an identical strand layout, while span 4 had a separate strand layout.

<u>*Sunland Park Bridge – Three Span Unit – Spans 3 & 5*</u>

Spans 3 and 5 incorporated 40 prestressing strands of 0.6 in. diameter, distributed as follows: 30 straight strands and 10 harped strands. These strands were strategically placed to control stresses and achieve the required flexural moment capacity. Based on the strand configuration, two base configurations were developed for analysis.

Methodology

Two configurations were set up for the analysis, differing in prestressing strand diameter.

- Base configuration 1: used 0.6-in. diameter strands, incorporating 40 strands (30 straight strands and 10 harped strands).
- Base configuration 2: used 0.7-in. diameter strands, incorporating 26 strands (20 straight strands and 6 harped strands).

The design matrix considers the number of girders (ten, nine, eight, seven and six), types of girders (BT-63 and BT-54) (Table 2.3), five compressive strengths (9.5, 15, 17.5, 20, to 22.5 ksi) as well as four values of deck thickness (8, 8.5, 9 and 10.5 in.) (Table 2.5) based on configurations 1 and 2. The matrix was evaluated beginning with 10 BT-54 and progressing sequentially to 6 BT-63, stopping if a configuration failed to meet the viability requirements of the LFD specifications.

Furthermore, the modulus of rupture was analyzed under two conditions:

- Limited per AASHTO provisions
- Limited to 1.16 ksi

Results

By increasing the diameter of the strands (from configuration 1 to configuration 2) and the compressive strength, additional UHPC volume savings (Table 2.5) as well as savings in the number of strands were achieved. Furthermore, when limiting the MOR value to 1.16 ksi instead of the LFD limit, further savings can be achieved (UHPC concrete volume and number strands) using both sizes of strands. Additionally, with the increase in volume of normal-strength concrete (deck thickness increased from 8 to 10.5 in.), the UHPC volume decreased which can reduce both the material and labor cost. Analysis results are shown below.

<u>*Using 0.6 in. diameter strands:*</u>

- MOR calculated with LFD Code:

Three configurations (I, V and IX) met the requirements (Table 2.5). A 20% reduction in UHPC volume for the girders was achieved by utilizing 46 strands of 0.6 in. diameter and increasing the

deck thickness (made of normal-strength concrete) from 8 to 8.5 in., with a configuration of eight girder lines of Type BT-54.

Additionally, live load deflections ranged from 0.993 in. at a compressive strength of 15 ksi with 48 strands to 0.879 in. at 22.5 ksi. For comparison, the baseline configuration, which used ten girder lines of Type BT-54 with a compressive strength of 9.5 ksi and 36 strands, resulted in a live load deflection of 0.875 in.

- MOR limited to 1.16 ksi:

Three configurations (I, V and IX) met the requirements (Table 2.5). A 20% savings in UHPC volume was achieved by utilizing 40 strands of 0.6 in. diameter and increasing the deck thickness (made of normal-strength concrete) from 8 to 8.5 in. with a configuration of eight girder lines of Type BT-54.

Additionally, live load deflections ranged from 0.998 in. at a compressive strength of 15 ksi with 40 strands to 0.882 in. at 22.5 ksi. For comparison, the baseline configuration, which used 10 girder lines of Type BT-54 with a compressive strength of 9.5 ksi and 36 strands, resulted in a live load deflection of 0.875 in.

Using 0.7 in. diameter strands:

- MOR calculated with LFD Code:

Five principal configurations (I, V, IX, XIII and XVII-b) met the requirements (Table 2.5). A 30% savings in UHPC volume was achieved by utilizing 36 strands of 0.7 in. diameter and increasing the deck thickness (made of normal-strength concrete) from 8 to 9 in. with a configuration of seven girder lines of Type BT-54.

Additionally, live load deflections ranged from 1.100 in. at a compressive strength of 15 ksi with 34 strands to 0.940 in. at 22.5 ksi. For comparison, the baseline configuration, which used 10 girder lines of Type BT-54 with a compressive strength of 9.5 ksi and 26 strands, resulted in a live load deflection of 0.873 in.

- MOR limited to 1.16 ksi:

Five principal configurations (I, V, IX, XIII and XVII-b) met the requirements (Table 2.5). A 43% savings in UHPC volume was achieved by utilizing 32 strands of 0.7 in. diameter and increasing the deck thickness (made of normal-strength concrete) from 8 to 10.5 in. with a configuration of six girder lines of Type BT-63.

Additionally, live load deflections ranged from 0.637 in. at a compressive strength of 17.5 ksi with 30 strands to 0.584 in. at 22.5 ksi. For comparison, the baseline configuration-which used 10 girder lines of Type BT-54 with a compressive strength of 9.5 ksi and 26 strands-resulted in a live load deflection of 0.680 in.

The results indicate that the improved compressive and tensile strength of UHPC can lead to significant concrete savings compared to HPC. Live load deflections were evaluated for all

designs, with an allowable deflection limit of L/800 or 1.8 in. All deflections satisfied the serviceability requirements.

Table 2.5 Flexure analysis results for Sunland Park Bridge - Three span unit - Span 3 and 5

Viable Cross-Section Configurations	Compressive Strength of UHPC, ksi	Deck Thickness, in.	Tensile Stress Limit according to LFD						Tensile Stress Limit of 1.16 ksi					
			Live Load Deflections with Strands, in.		Savings in Concrete Volume in Girders, %		Number of Strands		Live Load Deflections with Strands, in.		Savings in Concrete Volume in Girders, %		Number of Strands	
			0.6 in. strands	0.7 in. strands	0.6 in. strands	0.7 in. strands	0.6 in. strands	0.7 in. strands	0.6 in. strands	0.7 in. strands	0.6 in. strands	0.7 in. strands	0.6 in. strands	0.7 in. strands
I (10 BT-54 Girder Lines)	9.5	8	0.0344	0.0344	0%	0%	36	26	0.0344	0.0268	0%	0%	36	26
	15		0.0341	0.0343			34	22	0.0344	0.0267			30	20
	17.5		0.0325	0.0327			34	22	0.0328	0.0255			30	20
	20		0.0312	0.0313			34	22	0.0314	0.0244			30	20
	22.5		0.0302	0.0302			32	22	0.0303	0.0235			30	20
V (9 BT-54 Girder Lines)	9.5	8	0.0372	-	10%	10%	42	-	-	-	10%	10%	42	-
	15		0.0311	0.0313			40	24	0.0313	0.0244			34	22
	17.5		0.0351	0.0353			38	24	0.0353	0.0277			34	20
	20		0.0337	0.0339			38	24	0.0339	0.0266			34	20
	22.5		0.0326	0.0327			36	24	0.0327	0.0256			34	20
IX (8 BT-54 Girder Lines)	9.5	8.5	-	-	20%	20%	-	-	-	-	20%	20%	-	-
	15		0.0391	0.0392			48	28	0.0393	0.0307			40	24
	17.5		0.0373	0.0374			48	28	0.0375	0.0293			40	24
	20		0.0359	0.0359			46	28	0.036	0.0281			40	24
	22.5		0.0346	0.0346			46	28	0.0347	0.0271			40	24
XIII (7 BT-54 Girder Lines)	9.5	9	-	-	-	20%	-	-	-	-	-	30%	-	-
	15		-	0.0433			-	34	-	0.0339			-	30
	17.5		-	0.0401			-	34	-	0.0314			-	30
	20		-	0.0383			-	36	-	0.0302			-	30
	22.5		-	0.037			-	36	-	0.0291			-	30
XVII-b (6 BT-63 Girder Lines)	9.5	10.5	-	-	-	43%	-	-	-	-	-	43%	-	-
	15		-	-			-	-	-	-			-	-
	17.5		-	0.0318			-	36	-	0.0251			-	30
	20		-	0.0305			-	36	-	0.0239			-	32
	22.5		-	0.0294			-	36	-	0.023			-	32

- non viable design

Sunland Park Bridge – Three span unit – Span 4

Span 4 incorporated 34 prestressing strands of 0.6 in. diameter, distributed as follows: 28 straight strands and 6 harped strands. These strands were strategically placed to control stresses and achieve the required flexural moment capacity. Based on the strand configuration, two base configurations were developed for analysis.

Methodology

Two configurations were set up for the analysis, differing in prestressing strand diameter:

- Base Configuration 1: used 0.6-in. diameter strands, incorporating 34 strands (28 straight strands and 6 harped strands)
- Base Configuration 2: used 0.7-in. diameter strands, incorporating 24 strands (18 straight strands and 6 harped strands)

The design matrix considered the number of girders (ten, nine, eight, seven and six), types of girders (BT-63 and BT-54) (Table 2.3), five compressive strengths (9.5, 15, 17.5, 20, to 22.5 ksi)

as well as four values of deck thickness (8, 8.5, 9 and 10.5 in.)(Table 2.6) based on configurations 1 and 2. The matrix was evaluated beginning with 10 BT-54 and progressing sequentially to 6 BT-63, stopping if a configuration failed to meet the viability requirements of the LFD specifications.

Furthermore, the modulus of rupture was analyzed under two conditions:

- Limited per AASHTO provisions
- Limited to 1.16 ksi

Results

By increasing the diameter of the strands (from configuration 1 to configuration 2) and the compressive strength, additional UHPC volume savings (Table 2.6) as well as savings in the number of strands were achieved. Furthermore, when limiting the MOR value to 1.16 ksi instead of the LFD limit, further savings can be achieved (UHPC concrete volume and number strands) using both sizes of strands. Additionally, with the increase in volume of normal-strength concrete (deck thickness increases from 8 to 10.5 in.), the UHPC volume decreased which can reduce both the material and labor cost. Analysis results are shown below.

Using 0.6 in. diameter strands:

- MOR calculated with LFD Code:

Three configurations (I, V and IX) meet the requirements (Table 2.6). A 20% reduction in UHPC volume for the girders was achieved by utilizing 38 strands of 0.6 in. diameter and increasing the deck thickness (made of normal-strength concrete) from 8 to 8.5 in., with a configuration of eight girder lines of Type BT-54.

Additionally, live load deflections range from 0.774 in. at a compressive strength of 15 ksi with 40 strands to 0.685 in. at 22.5 ksi. For comparison, the baseline configuration, which uses ten girder lines of Type BT-54 with a compressive strength of 9.5 ksi and 32 strands, results in a live load deflection of 0.683 in.

- MOR limited to 1.16 ksi:

Five configurations (I, V and IX) met the requirements (Table 2.6). A 20% savings in UHPC volume was achieved by utilizing 34 strands of 0.6 in. diameter and increasing the deck thickness (made of normal-strength concrete) from 8 to 8.5 in. with a configuration of eight girder lines of Type BT-54.

Additionally, live load deflections ranged from 0.781 in. at a compressive strength of 15 ksi and 34 strands to 0.688 in. at 22.5 ksi. For comparison, the baseline configuration, which used 10 girder lines of Type BT-54 with a compressive strength of 9.5 ksi and 32 strands, resulted in a live load deflection of 0.683 in.

Using 0.7 in. diameter strands:

- MOR calculated with LFD Code:

Five configurations (I, V, IX, XIII and XVII-b) met the requirements (Table 2.6). A 30% savings in UHPC volume was achieved by utilizing 34 strands of 0.7 in. diameter and increasing the deck thickness (made of normal-strength concrete) from 8 to 9 in. with a configuration of seven girder lines of Type BT-54.

Additionally, live load deflections ranged from 0.852 in. at a compressive strength of 15 ksi to 0.731 in. at 22.5 ksi. For comparison, the baseline configuration, which used 10 girder lines of Type BT-54 with a compressive strength of 9.5 ksi and 24 strands, resulted in a live load deflection of 0.680 in.

- MOR limited to 1.16 ksi:

Five configurations (I, V, IX, XIII and XVII-b) met the requirements (Table 2.6). A 43% savings in UHPC volume was achieved by utilizing 32 strands of 0.7 in. diameter and increasing the deck thickness (made of normal-strength concrete) from 8 to 10.5 in. with a configuration of six girder lines of Type BT-63.

Additionally, live load deflections ranged from 0.637 in. at a compressive strength of 17.5 ksi with 30 strands to 0.584 in. at 22.5 ksi. For comparison, the baseline configuration, which used 10 girder lines of Type BT-54 with a compressive strength of 9.5 ksi and 24 strands, resulted in a live load deflection of 0.680 in.

The configurations that yielded the greatest concrete savings for Sunland Park Bridge three span continuous unit consisted of two optimized designs (Table 2.6).

- Configuration IX: utilized 40 strands of 0.6 in. diameter and increased the deck thickness (made of normal-strength concrete) from 8 to 8.5 in. with a configuration of eight girder lines of Type BT-54, resulting in 20% savings in UHPC volume.
- Configuration XVII-b: utilized 32 strands of 0.7 in. diameter and increased the deck thickness (made of normal-strength concrete) from 8 to 10.5 in. with a configuration of six girder lines of Type BT-63, resulting in 43% savings in UHPC volume.

Concrete volume savings can be achieved by replacing HPC with UHPC. Typically, increasing the deck thickness (made from normal-strength concrete) and adjusting the number of strands is necessary to achieve these savings. The reduction in girder size and quantity demonstrates the advantages of UHPC's enhanced properties.

Table 2.6 Flexure analysis results for Sunland Park Bridge - Three span unit - Span 4

Viable Cross-Section Configurations	Compressive Strength of UHPC, ksi	Deck Thickness, in.	Tensile Stress Limit according to LFD						Tensile Stress Limit of 1.16 ksi					
			Live Load Deflections with Strands, in.		Savings in Concrete Volume in Girders, %		Number of Strands		Live Load Deflections with Strands, in.		Savings in Concrete Volume in Girders, %		Number of Strands	
			0.6 in. strands	0.7 in. strands	0.6 in. strands	0.7 in. strands	0.6 in. strands	0.7 in. strands	0.6 in. strands	0.7 in. strands	0.6 in. strands	0.7 in. strands	0.6 in. strands	0.7 in. strands
I (10 BT-54 Girder Lines)	9.5	8	0.0269	0.0268	0%	0%	32	24	0.0269	0.0268	0%	0%	32	24
	15		0.0266	0.0266			30	22	0.0269	0.0267			26	20
	17.5		0.0254	0.0253			30	22	0.0256	0.0255			26	20
	20		0.0244	0.0233			30	20	0.0246	0.0244			26	20
	22.5		0.0236	0.0235			28	20	0.0237	0.0235			26	20
V (9 BT-54 Girder Lines)	9.5	8	0.029	-	10%	10%	36	-	0.029	-	10%	10%	36	-
	15		0.0243	0.0243			34	24	0.0245	0.0244			28	22
	17.5		0.0275	0.0274			32	24	0.0277	0.0277			28	20
	20		0.0264	0.0263			32	24	0.0266	0.0266			28	20
	22.5		0.0254	0.0334			32	24	0.0256	0.0256			28	20
IX (8 BT-54 Girder Lines)	9.5	8.5	-	-	20%	20%	-	-	-	-	20%	20%	-	-
	15		0.0305	0.0304			40	28	0.0307	0.0307			34	24
	17.5		0.0291	0.029			40	28	0.0293	0.0293			34	24
	20		0.028	0.0278			38	28	0.0281	0.0281			34	24
	22.5		0.027	0.0269			38	28	0.0271	0.0271			34	24
XIII (7 BT-54 Girder Lines)	9.5	9	-	-	-	30%	-	-	-	-	-	30%	-	-
	15		-	0.0335			-	34	-	0.0339			-	30
	17.5		-	0.0311			-	34	-	0.0314			-	30
	20		-	0.0298			-	34	-	0.0302			-	30
	22.5		-	0.0288			-	34	-	0.0291			-	30
XVII-b (6 BT-63 Girder Lines)	9.5	10.5	-	-	-	43%	-	-	-	-	-	43%	-	-
	15		-	-			-	-	-	-			-	-
	17.5		-	0.0246			-	36	-	0.0251			-	30
	20		-	0.0237			-	34	-	0.0239			-	32
	22.5		-	0.0229			-	34	-	0.023			-	32

\- non viable design

Shear analysis

In contrast to flexure analysis, where the greatest stress occurs at the center of the span, the maximum shear force is concentrated near the supports. To reinforce a beam against shear loads, stirrups are typically used. Unlike flexural failure, which involves noticeable displacement, shear failure occurs suddenly and without significant warning, making shear analysis essential for ensuring structural safety.

The methodology used for the analysis was based on the French AFGC/SETRA recommendations and the MIT research on Ductal. Loads and forces were calculated using the AASHTO LRDF specifications. The ultimate limit state is based on the premise that crack-bridging steel fibers can carry a portion of the shear load.

The shear analysis was conducted using the optimum results from the flexure analysis, considering the number and type of girders for the respective bridges:

I-25/Doña Ana Interchange:

- Four girder lines of Type BT-63 girders using 0.6-in. diameter strands (Table 2.2: Configuration XI).
- Four girder lines of Type BT-54 girders using 0.7-in. diameter strands (Table 2.2: Configuration XII).

Sunland Park Bridge Two span continuous unit:

- Eight girder lines of modified Type BT-54 girders using 0.6 in diameter strands (Table 2.4: Configuration IX).
- Six girder lines of Type BT-63 girders using 0.7 in. diameter strands (Table 2.4: Configuration XVII-b).

Sunland Park Bridge Three span continuous unit:

- Eight girder lines of modified Type BT-54 girders using 0.6 in diameter strands (Table 2.5 and 2.6: Configuration IX).
- Six girder lines of Type BT-63 girders using 0.7 in diameter strands (Table 2.5 and 2.6: Configuration XVII-b).

The CONSPAN® software was used to calculate the ultimate shear forces for these bridge configurations in accordance with AASHTO LRFD specifications.

The objective of the parametric study was to minimize UHPC volume in girders while ensuring structural integrity. Two approaches were evaluated to achieve the required shear capacity: increasing girder size or incorporating shear stirrups for reinforcement. To effectively reduce UHPC volume while meeting shear capacity requirements, the latter approach was identified as the better solution.

I-25/Doña Ana Interchange

Using 4 girder lines of Type BT-63 girders with 0.6 in. diameter strands, sufficient shear resistance was achieved without shear stirrups. Considering a factored shear load of 392.5 kips, the design shear strength was 415.9, 430, 435.7 and 440.9 kips for compressive strengths of 15, 17.5, 20 and 22.5 ksi, respectively. Results show that the shear capacity exceeds the factored shear load by 5.7%, 8.7%, 9.9% and 11%, respectively.

Conversely, using 4 girder lines of Type BT-54 girders and 0.7 in. diameter strands, the shear capacity requirements were not met. Two solutions were proposed:

Increasing web width

The web width was increased from 6 to 7 in. Considering a factored shear load of 394 kips, the design shear strength was 439.1 and 443.9 kips for compressive strengths of 20 and 22.5 ksi respectively. Results show that the shear capacity exceeds the factored shear load by 10.3% and 11.2%, respectively.

Adding shear stirrups

No. 5 (M16) shear stirrups at 24.0 in. on-center were placed at a distance of 1/10th of the span (12.29 ft) from the supports. Considering a factored shear load of 394 kips, the design shear strength was 481.4 and 486.5 kips for compressive strengths of 20 and 22.5 ksi, respectively. Results show that the shear capacity exceeded the factored shear load by 18.5% and 19%, respectively. Additionally, adding shear stirrups aligned with the goal of minimizing concrete volume while meeting shear capacity requirements. Therefore, it was observed that as compressive strength increased, the shear capacity also increased.

Sunland Park Bridge two span continuous unit

Increasing web width

The web width was increased from 7 to 8 in. Considering a factored shear load of 382.6 kips, the design shear strength was 411, 417.9, 423.9 and 430.8 kips for compressive strengths of 15, 17.5, 20 and 22.5 ksi, respectively. Results show that the shear capacity exceeded the factored shear load by 6.9%, 8.4%, 9.7% and 11.2%, respectively.

Adding shear stirrups

No. 5 (M16) shear stirrups at 24.0 in. on-center were placed at a distance of 1/10th of the span (12.29 ft) from the supports. Considering a factored shear load of 382.6 kips, the design shear strength was 392.8, 398.9, 404.1 and 409.1 kips for compressive strengths of 15, 17.5, 20 and 22.5 ksi, respectively. Results show that the shear capacity exceeded the factored shear load by 2.6%, 4.1%, 5.3% and 6.5%, respectively.

Conversely, using 6 girder lines of Type BT-63 girders and 0.7 in. diameter strands, the shear capacity requirements were also not met. The only way to achieve adequate design shear strength was by using No. 5 (M16) mild steel stirrups, placed at 24 in. up to the first 1/10th point from the face of the support. Considering a factored shear load of 499 kips, the design shear strength was 511.2 kips for a compressive strength of 22.5 ksi. Results show that the shear capacity exceeded the factored shear load by 2.4%.

Sunland Park Bridge Three span continuous unit

Using 8 BT-54 girders and 0.6 in. diameter strands, the shear capacity requirements were not met. Two solutions were proposed:

Increasing the web width (exterior spans)

The web width was increased from 7 to 8 in. Considering a factored shear load of 379.7 kips, the design shear strength was 397.7, 403.4, 410.1 and 414.1 kips for compressive strengths of 15, 17.5, 20 and 22.5 ksi, respectively. Results show that the shear capacity exceeded the factored shear load. Specifically, for compressive strengths of 15, 17.5, 20, and 22.5 ksi, the increases were 4.9%, 6.3%, 7.8%, and 8.3%, respectively.

Increasing web width (interior span)

The web width was increased from 7 to 8 in. Considering a factored shear load of 366.2 kips, the design shear strength was 405.8, 411.9, 417.5, and 422.8 kips for compressive strengths of 15, 17.5, 20, and 22.5 ksi, respectively. Results show that the shear capacity exceeded the factored shear load. Specifically, for compressive strengths of 15 ksi, 17.5 ksi, 20 ksi, and 22.5 ksi, the increases were 10.2%, 11.5%, 12.4%, and 13.4%, respectively.

Adding shear stirrups (exterior spans)

No. 3 (M8) shear stirrups at 24.0 in. on-center were placed at a distance of 1/10th of the span (12.29 ft) from the supports. Considering a factored shear load of 378 kips, the design shear strength was 389.5, 395.5, 402.1 and 407.3 kips for compressive strength of 15, 17.5, 20 and 22.5 ksi, respectively. Results show that the shear capacity exceeded the factored shear load. Specifically, for compressive strengths of 15 ksi, 17.5 ksi, 20 ksi, and 22.5 ksi, the increases were 3%, 4.4%, 6%, and 6.9%, respectively.

Adding shear stirrups (interior spans)

No. 3 (M8) shear stirrups at 24.0 in. on-center were placed at a distance of 1/10th of the span (12.29 ft) from the supports. Considering a factored shear load of 364.5 kips, the design shear strength was 396.7, 403.3, 409.2 and 414.8 kips for compressive strength of 15, 17.5, 20 and 22.5 ksi, respectively. Results show that the shear capacity exceeded the factored shear load. Specifically, for compressive strengths of 15 ksi, 17.5 ksi, 20 ksi, and 22.5 ksi, the increases were 8.1%, 9.6%, 10.9%, and 12.1%, respectively.

Conversely, using 6 BT-63 girders and 0.7 in. diameter strands, the shear capacity requirements were not met. The only way to achieve adequate design shear strength was to use No. 5 (M16) mild steel stirrups, placed at 18 in. Considering a factored shear load of 497.5 kips, the design shear strength was 502.1, 507.5 and 512.4 kips for compressive strengths of 17.5, 20 and 22.5 ksi, respectively. Results show that the shear capacity exceeded the factored shear load by 0.9%, 2.0% and 2.9%, respectively. Additionally, for the interior span, considering a factored shear load of 479.5 kips, the design shear strength was 503.4, 509.1 and 513.8 kips for compressive strength of 17.5, 20 and 22.5 ksi, respectively. Results show that the shear capacity exceeded the factored shear load. Specifically, for compressive strengths of 17.5 ksi, 20 ksi, and 22.5 ksi, the increases were 4.7%, 5.8%, and 6.7%, respectively.

Results indicate that UHPC outperforms HPC in resisting shear forces. The steel fibers in UHPC significantly enhance shear capacity, particularly at the ultimate limit state, which occurs after the girder section has cracked. In some cases, adequate shear capacity can be achieved without the need for stirrups. When shear capacity is insufficient, two solutions are available:

- Slightly increasing the girder size to provide the necessary capacity.
- Adding stirrups to reinforce the girders.

Negative Moment Reinforcement Analysis

As the number of required girders decreased, negative moment reinforcement in the Sunland Park Bridge became a concern due to the increased moments at the pier with fewer girder lines. Consequently, additional mild steel reinforcement may be needed in the deck to effectively resist these moments.

Methodology

The analysis considered two scenarios.

- Limited diaphragm strength: the diaphragm strength was limited to 15 ksi for each girder compressive strength, as the LFD Article 9.7.2.3.2 states that calculations are valid for concrete with compressive strengths up to 15 ksi.
- Matching diaphragm and girder strength: the diaphragm strength was assumed to be equal to the compressive strength of the girder concrete.

A 15% increase in concrete strength, from 15.0 ksi to 22.5 ksi, resulted in only a 1% reduction in the required amount of steel reinforcement. This finding suggests that the LFD specification remains valid for compressive strengths up to 22.5 ksi.

When using six BT-63 girders with 0.7 in. strands, the maximum increase in steel reinforcement was 33% for the two-span continuous unit and 36% for the three span continuous unit. However, this increase was offset by significant concrete savings, since the as-designed bridge used 10 BT-54 girders.

2.1.2 Economic Analysis

To support the adoption of UHPC in the state, an economic analysis was performed. Given the need to allocate state resources efficiently and the higher initial cost of UHPC, its lifespan becomes a critical factor in determining its feasibility for bridge construction.

For the economic analysis, the as-designed (HPC) bridges were compared to the UHPC girders with a design compressive strength of 22.5 ksi. The results indicate that material savings can be achieved when using UHPC.

The total present costs were calculated including the cost of:

- Girder concrete
- Prestressing strands
- Mild steel reinforcement
- Labor
- Normal-strength concrete deck.

The typical life span of bridge girders in New Mexico was assumed to be 75 years. For future cost calculations, it was assumed that UHPC girders will last twice as long as HPC girders. The inflation rate used in the study was based on 2009 data.

The analysis found life-cycle cost benefits from implementing UHPC in both bridge designs (I-25/Doña Ana Interchange and Sunland Park Bridge). It was demonstrated that UHPC can reduce concrete volume, leading to cost savings and shorter construction time. Additional savings may be achieved if the steel fiber content in UHPC is reduced to 1%.

2.2 Limitations and Possible Solutions

The primary limitation to implementing UHPC in New Mexico is its high initial cost. Using commercially available materials, such as patented UHPC from Ductal®, can be up to 10 times more expensive than HPC.

To overcome this cost barrier, developing a non-proprietary UHPC mixture optimized for New Mexico locally available materials is essential. Specifically, utilizing regionally sourced sand, and cementitious components can significantly reduce costs while maintaining performance.

This approach not only supports the state's financial priorities but also reduces material consumption, thereby promoting sustainability in bridge construction.

3. UHPC MIXTURE DEVELOPMENT

UHPC consists of cement, fine sand, quartz powder, micro silica, steel fibers, and high-range water reducing admixture (HRWRA). Several studies have been conducted on these materials, including those by Richard and Cheyrezy (1995), Shaheen and Shrive (2006) and Matte and Moranville (1999).

The baseline mixture for optimization was based on the formulation developed by Allena and Newtson (2010) (UHPC Phase II, page 183, Table 12.3). This mixture includes cement, silica fume, fine sand, steel fibers, water and HRWRA, achieving a 28-day compressive strength of 24,010 psi. These results demonstrate excellent performance and reinforce the feasibility of implementing UHPC in New Mexico. To reduce costs, locally available materials were used, including Type I/II portland cement, silica fume and fine local sand.

To further decrease costs and enhance material properties, the use of supplementary cementitious materials, SCMs, sand size, and sand content was investigated. Specifically, fly ash was being explored as a partial replacement for silica fume, which can improve durability by mitigating alkali-silica reaction (ASR). Additionally, the aggregate top size investigated was sieve No. 4 (0.187 in), which can help reduce labor cost and material waste by minimizing the need for sieving.

The study also detailed the mixing process and curing regimens used. Primarily, compressive strength tests were conducted to evaluate the mixtures using 2 in. and 4 in. cube specimens, along with workability assessments.

The test specimens were cured using curing option 1, with further details provided in Chapter 3.8. After curing, the specimens were tested for seven-day compressive strength following the guidelines of British Standard BS 1881 Part 116 (UHPC Phase II, page 187). The mixture proportions (UHPC Phase II, Tabe 43) and curing regimen remained consistent across all tests, except for specific parameter variations described in each section. Additionally, Glenium 3030 NS from BASF Chemicals was used as the HRWRA (UHPC Phase II, page 182).

3.1 Water to Cementitious Ratio

Methodology

To reduce the required curing temperature and increase the aggregate top size, the water-to-cementitious materials (w/cm) ratio was gradually decreased. The batches used w/cm ratios of 0.20, 0.18, 0.15, and 0.14. Additionally, a w/cm ratio of 0.13 was also tested, but due to poor workability, it was not considered for further investigation.

Findings

As shown in Table 3.1, decreases in w/cm ratio resulted in increased compressive strength. Specifically,

- At a w/cm ratio of 0.20, the compressive strength was 19,120 psi when testing was performed on 2 in. cubes.

- At the lowest w/cm ratio (0.14), the compressive strength reached its greatest value of 25,080 psi when using 2 in. cube specimen.

Based on the results, a w/cm ratio of 0.14 was selected for further investigation.

Table 3.1. Compressive strength varying w/cm ratio (UHPC Phase II, Table 13.1)

w/cm ratio	Average compressive strength, psi (MPa)	
	2 in. (50 mm) cubes	4 in. (100 mm) cubes
0.20	19,120 (131.8)	17,820 (122.9)
0.18	23,020 (158.7)	18,410 (126.9)
0.15	22,430 (154.7)	19,640 (135.4)
0.14	25,080 (172.9)	20,470 (141.1)

3.2 Varying Fly Ash Content

Silica fume has the smallest particles in the UHPC mixture, with an average diameter of approximately 3.9×10^{-6} in., making it small enough to fill voids within the mixture. It enhances strength and durability by creating a denser, more impermeable matrix, which resists chloride diffusion. However, silica fume significantly increases the cost of UHPC due to its high price.

To address this, fly ash was introduced as a cost-effective alternative that can partially replace silica fume in the mixture. Fly ash improves durability by mitigating ASR through alkali control and contributes to long-term strength gains (UHPC Phase V, page 9 and 10).

When portland cement was replaced with fly ash and other pozzolanic materials, drying creep and basic creep were reduced compared to concrete made solely with cement, provided they were loaded to similar fractions of strength (UHPC Phase III, page 49).

Class F fly ash reduces the water demand of the mixture, enhancing workability. This is achieved by broadening the size range in the powder phase (cement and pozzolan), allowing better particle packing between cement and fine fly ash particles (Bagheri et al., 2013). This improved packing reduces porosity, minimizes the amount of water required to fill voids, and ultimately lowers the mixture's permeability.

Methodology

To minimize the use of silica fume and therefore reduce the cost of the mixtures, silica fume was partially replaced by Class F Fly ash, ranging from 12.5% to 100%. The mixture proportions were then tested for average 7-day compressive strengths.

Several batches were produced with fly ash contents ranging from 12.5% to 100% of the SCM content. From each batch, three test specimens of two sizes (2 in. and 4 in. cubes) were used for the compressive strength tests (UHPC Phase II, page 188).

Findings

Compressive strength values greater than 23,600 psi were obtained from the 7-day compressive strength tests on 2 in. cubes with the following replacement percentages (UHPC Phase II, page 189):

- 25%: 24,560 psi
- 37.5%: 24,200 psi
- 55%: 23,970 psi
- 60%: 24,590 psi
- 75%: 23,600 psi

The maximum compressive strength for the 2 in. cubes was 24,590 psi for 60% replacement by fly ash (Table 3.2).

Compressive strength values greater than 21,190 psi from the 7-day compressive strength tests on 4 in. cubes were obtained with the following replacement percentages (UHPC Phase II, page 189):

- 12.5%: 22,120 psi
- 25%: 21,530 psi
- 37.5%: 21,190 psi
- 45%: 21,220 psi
- 75%: 21,450 psi

The maximum compressive strength for the 4 in. cubes was 22,120 psi when 12.5% fly ash was used (Table 3.2).

Table 3.2. Compressive strength with fly ash replacement (w/cm ratio = 0.14) (UHPC Phase II, Table 13.2)

Percentage (%) of silica fume replaced by fly ash	Average compressive strength, psi (MPa)	
	2 in. (50 mm) cubes	4 in. (100 mm) cubes
12.5	23,690 (163.3)	22,120 (152.5)
25	24,560 (169.3)	21,530 (148.4)
37.5	24,200 (170.0)	21,190 (146.1)
40	23,640 (166.9)	20,140 (138.8)
45	20,360 (140.4)	21,220 (146.3)
50	20,110 (138.7)	20,850 (144.0)
55	23,970 (165.2)	20,590 (142.0)
60	24,590 (169.5)	20,770 (143.2)
75	23,600 (162.7)	21,450 (147.9)
100	14,840 (102.3)	15,030 (103.6)

A similar test was conducted by Villanueva in 2015 with the findings on the behavior of compressive strength similar to results provided on Table 3.2. The results are listed below.

Compressive strengths range from:

- 18,830 psi to 20,290 psi for 2 in. cubes
- 19,970 psi to 20,020 psi for 4 in. cubes

Compressive strength values greater than 20,110 psi from the 7-day compressive tests on 2-in. cubes were obtained with the following replacement percentages (UHPC Phase II, page 189):

- 12.5%: 21,180 psi
- 37.5%: 20,290 psi
- 62.5%: 20,110 psi
- 75%: 20,790 psi
- 87.5%: 21,770 psi

The maximum compressive strength for the 2 in. cubes was 21,770 psi when 87.5% fly ash was used.

Compressive strength values greater than 20,940 psi from the 7-day compressive strength tests on 4 in. cubes were obtained with the following replacement percentages (UHPC Phase II, page 189):

- 0%: 20,940 psi
- 12.5%: 20,270 psi
- 37.5%: 21,020 psi

The maximum compressive strength for the 4 in. cubes was 20,270 psi (Table 3.3) when 12.5% fly ash was used. (UHPC Phase V, page 22).

Table 3.3. Compressive strength with varying fly ash (Villanueva 2015)

Fly Ash Content (%)	Avg. 7-Day Compressive Strength, psi [MPa]	
	2 in. (51 mm)	4 in. (102 mm)
0	20,010 [137.9]	20,940 [144.4]
12.5	21,180 [146.0]	20,270 [139.7]
25	19,130 [131.9]	19,860 [136.9]
37.5	20,290 [139.9]	20,020 [138.0]
50	18,830 [129.8]	19,970 [137.7]
62.5	20,110 [138.7]	19,140 [132.0]
75	20,790 [143.4]	18,270 [125.9]
87.5	21,770 [150.1]	18,880 [130.1]

Similar trends between the two tests can be observed:

Results from 2 in. cubes

- When the replacement level was near 50% the compressive strength decreased to very low values.
- The greatest results from both Tables 3.2 and 3.3 were achieved by replacing 60% and 87.5% of the silica fume with fly ash.

Results from 4 in. cubes

- Average compressive strength for 4 in. cubes was generally less than for the 2 in. cubes.
- A more consistent result in compressive strength was seen since variation for 4 in. cubes generally less than for 2 in. cubes across the different replacement levels.

3.3 Fine Aggregate Size and Proportion

Research has shown that using very fine sand, specifically sand passing through a No. 30 sieve, can achieve high compressive strength (Allena and Newtson, 2010). However, this approach results in longer production time and greater labor costs. To mitigate these challenges, the aggregate top size and sand proportions were investigated. Specifically, sand passing through a No. 4 sieve was examined with sand amount tested up to 2100 lb/yd^3.

Typically, the top aggregate size used in UHPC was No. 30. The small maximum aggregate size often increases labor and can lead to material waste. Therefore, a larger aggregate top size was explored to reduce costs while assessing its impact on UHPC compressive strength.

The objective was to increase the sand content in the mixture, thereby reducing cementitious material usage while maintaining sufficient strength. This approach aimed to lower costs and minimize environmental impact. The sand content was investigated with the goal of ensuring no significant reduction in workability or compressive strength of UHPC.

3.3.1 Aggregate Top Size

Methodology

The maximum aggregate size was gradually increased and tested using sieve No. 30, No, 16, No. 8 and No. 4. Compressive strength tests were conducted on 2-in. and 4-in. cubes.

Findings

- When using sand passing through a No. 30 sieve, the average compressive strengths measured on 2 in. and 4 in. cubes were 24,200 psi and 21,190 psi, respectively.
- When sand size was increased to a No. 4 sieve, the compressive strength decreased slightly to 23,870 psi and 21,790 psi for 2 in. and 4 in., respectively.

Although increasing the sand size to a No. 4 sieve results in a minor reduction in compressive strength (Table 3.4), the potential loss of strength was considered acceptable. This adjustment enables the utilization of a broader range of material from different sieve sizes. More importantly, the compressive strength goals, set to exceed 20,000 psi, were still achieved.

Table 3.4. Effect of maximum size of aggregate on compressive strength (UHPC Phase II, Table 13.3)

Sieve No.	Sieve Size, in. (mm)	Compressive Strength, psi (MPa)	
		2 in. (50 mm) cubes	4 in. (100 mm) cubes
30	0.0234 (0.595)	24,200 (170.0)	21,190 (146.1)
16	0.0469 (1.19)	24,640 (169.9)	24,030 (165.7)
8	0.0937 (2.38)	24,430 (168.4)	22,410 (154.4)
4	0.187 (4.76)	23,870 (165.2)	21,790 (150.3)

Final recommendations were to use a No. 4 sieve as the maximum aggregate size. Prior to incorporating fine aggregates into the mixture, they should be passed through a No. 4 sieve, washed over a No. 200 sieve to eliminate dust fines, and then should be oven-dried to eliminate any residual moisture. (UHPC Phase II, page 183).

3.3.2 Sand Proportion

Methodology

Sand proportions were tested to determine the feasibility of increasing sand content in the mixture. Increasing sand content reduces the amount of cementitious materials, thereby lowering cost.

Seven-day compressive strength tests were performed on 2 in. and 4 in. cubes, with sand content ranging from 1,500 lb/yd^3 to 2,100 lb/yd^3 (Table 3.5).

Findings

- The maximum compressive strength for 2 in. cubes was achieved at 1,900 lb/yd³.
- The maximum compressive strength for 4 in. cubes was obtained at 1,500 lb/yd³.
- Sand contents above 2,100 lb/yd³ exhibited poor workability.

Sand contents of 1900 lb/yd^3 provided the greatest compressive strength from 2 in. cube tests, and 2100 lb/yd^3 provided acceptable compressive strength from both 2 in. and 4 in. cube tests. Therefore, these two sand contents were selected for future works to minimize the use of cementitious material in UHPC.

Table 3.5. Effect of amount of sand on compressive strength (UHPC Phase II, Table 13.4)

Sand, lb/yd^3 (kg/m^3)	Compressive Strength, psi (MPa)	
	2 in. (50 mm) Cubes	4 in. (100 mm) Cubes
1,500 (890)	24,110 (166.2)	22,310 (153.8)
1,700 (1009)	23,990 (165.4)	21,940 (151.3)
1,900 (1127)	24,340 (167.8)	21,010 (144.9)
2,100 (1246)	22,940 (158.2)	21,590 (148.9)

3.4 Optimized Mixtures

Mixture proportions were tested during UHPC Phase IV to adjust various parameters:

- Silica fume (SF)/fly ash (FA) content: Varied between 37.5% SF / 62.5% FA and 50% SF / 50% FA.
- Sand content: Varied between 1,900 lb, 1,700 lb, and 1,500 lb.
- Water-to-cementitious material (w/cm) ratio: Varied between 0.14, 0.15, and 0.16.

Methodology

To analyze workability, tests were conducted by measuring slump and spread on each batch, following ASTM C143 and ASTM C1611. Additionally, compressive strength was measured at 7 and 28 days on 2-in. and 4-in. cube specimens. (UHPC Phase IV, page 331).

Results

- All mixtures exceeded the minimum requirement of 17,000 psi on the 28th day when tested with 4 in. cubes (Table 3.7).
- The greatest compressive strength recorded was 20,260 psi, achieved with a 0.16 w/cm ratio, 50FA/50SF content and 1,700 lb of sand, tested on the 28th day in a 2 in. cube.
- Spread measurements ranged from 8.00 to 9.75 in., depending on the fly ash-to-silica fume (FA/SF) ratio and the w/cm ratio (Table 3.6).
- Slump values ranged from 2 in. to 6.5 in., with lower FA/SF content and higher w/cm ratios resulting in higher slump values.
- Mixing time per batch varied between 16 and 32 minutes.

Table 3.6. Slump and spread results (workability) (UHPC Phase IV, Table 4.1)

Mixture		Spread (in.)	Slump (in.)	Avg. Spread (in.)	Mix Time (min)
0.14 w/cm[1] ratio	FA37.5 SF62.5 1900	8.25 8.0 8.25	N/A	8.17	20
0.14 w/cm ratio	FA50 SF50 1900	9.5 9.75 10.0	N/A	9.75	18
0.14 w/cm ratio	FA50 SF50 1700	8.0 8.0 8.0	N/A	8.00	32
0.14 w/cm ratio	FA50 SF50 1500	8.0 8.0 8.0	N/A	8.00	30
0.15 w/cm ratio	FA50 SF50 1900	8.0 8.0 8.25	3.5	8.08	20
0.15 w/cm ratio	FA50 SF50 1700	9.75 9.75 10.0	N/A	9.83	16
0.15 w/cm ratio	FA50 SF50 1500	8.25 8.25 8.0	2	8.17	20
0.16 w/cm ratio	FA50 SF50 1900	8.5 8.5 8.75	2.25	8.58	21.5
0.16 w/cm ratio	FA50 SF50 1700	9.0 9.5 10.0	5.5	9.50	18
0.16 w/cm ratio	FA50 SF50 1500	9.5 9.5 10.0	6.5	9.67	16

[1] w/cm ratio, percent fly ash to silica fume (supplemental cementitious materials)

Table 3.7. Compressive strength results (UHPC Phase IV, Table 4.2)

Mixture		$f_{c,7\text{-}day}$[2] (psi)		$f_{c,28\text{-}day}$[3] (psi)	
		2 in. Cubes	4 in. Cubes	2 in. Cubes	4 in. Cubes
0.14 w/cm[1] ratio	37.5 FA - 62.5 SF 1900 lb sand	-	-	15913.75	17413.33
	50 FA - 50 SF 1900 lb sand	-	-	17077.5	17076.27
	50 FA - 50 SF 1700 lb sand	-	-	16759.58	17396.7
	50 FA - 50 SF 1500 lb sand	16270	15157.2	18647.5	17650.65
0.15 w/cm ratio	50 FA - 50 SF 1900 lb sand	16146.67	15043.45	19320	18275.95
	50 FA - 50 SF 1700 lb sand	15777.5	14875.65	18876.67	17592.2
	50 FA - 50 SF 1500 lb sand	17598.13	15334.7	20095.5	17693.45
0.16 w/cm ratio	50 FA - 50 SF 1900 lb sand	16013.13	14546.9	18210	18562.5
	50 FA - 50 SF 1700 lb sand	17166.25	14055.35	20260.5	17271.9
	50 FA - 50 SF 1500 lb sand	16200	13613.1	19666.5	16889.05

[1] w/cm ratio, percent fly ash to silica fume (supplemental cementitious materials)
[2] 7 - day compressive strength
[3] 28 - day compressive strength

Based on workability and strength, the mixture selected for further optimization was 0.15 w/cm – 50FA/50SF – 1700 lb sand. This means that a 0.15 w/cm ratio was used with a 50% Fly ash and 50% Silica fume blend and 1700 lb of sand. (UHPC Phase IV, page 335).

3.5 Fiber Reinforcement

Incorporating steel fibers enhances both the tensile and compressive properties of the concrete. Additionally, brittle behavior is mitigated, resulting in a more ductile response (UHPC Phase V, page 11). However, determining the optimal fiber content is crucial, since greater fiber content reduces flowability. Studies have indicated that the optimal fiber content ranges between 1 and 3% (Wu et al., 2016).

In UHPC Phase II, which focused on mixture optimization, Nycon-SF Type I fibers were used. In UHPC Phase IV, polyethylene fibers were investigated as a partial replacement for steel fibers.

During UHPC Phase V, when optimizing the mixture for use in overlays, the NMDOT imposed the "Buy America" requirement. As a result, Steel Fibers – U were intended to be used. However, these fibers failed to meet the minimum compressive strength requirements. Consequently, during the mock-up overlay slab tests, modified Steel Fibers – U were introduced to achieve the target compressive strength of 17,000 psi.

3.5.1 Steel Fibers

Nycon-SF Type I is a steel fiber that meets the requirements of ASTM A820. The fibers have a diameter of 0.0008 in. and a length of 0.5 in. Their tensile strength is 285 ksi, while flexural strength is 29,000 ksi. These steel fibers offer high resistance to corrosion and alkalis, along with enhanced material properties.

Replacing traditional steel fibers with Nycon-SF Type I can provide several benefits, including improved material properties, enhanced bond performance, and reduced cost.

Methodology

UHPC Phase III:

Preliminary studies were conducted to verify that Nycon steel fibers provide at least the equivalent strength and durability compared to the fibers being replaced. Specifically, eight 2-in. and eight 4-in. cube specimens were tested.

UHPC Phase IV:

- The evaluation included workability, compressive strength, and flexural strength tests:
- Slump and spread tests were conducted to assess workability.
- Compressive tests were performed on 2 in. and 4 in. cube specimens after 7 days.
- The steel fiber content varied at 0%, 1%, 1.5%, 2%, and 3%.
- Constant parameters included a mixture with 0.14 w/cm ratio, 50FA/50SF, and 1,900 lb of aggregate.
- Subsequently, adjustments were made to improve workability, increasing the w/cm ratio to 0.145 and reducing the sand content to 1,500 lb.

Results

Preliminary Compressive Strength Tests

2 in. cube specimens:

- Lowest compressive strength: 17,950 psi
- Highest compressive strength: 27,955 psi
- Average compressive strength: 23,860 psi

4 in. cube specimens:

- Lowest compressive strength: 21,220 psi
- Highest compressive strength: 23,470 psi

- Average compressive strength: 22,150 psi

These results were positive, as all compressive strengths exceeded the 20,000 psi requirement set by NMDOT (UHPC Phase III, page 28). It should be noted that, by Phase IV, the new compressive strength requirement was 17,000 psi.

The following results are from Phase IV, where steel fiber percent variations were analyzed in terms of workability, compressive and flexural strengths. Percentages started with 0% fibers, then increased to 1%, 1.5%, 2%, and 3% by volume.

Workability Tests (Slump and Spread Measures)

- 1% steel fibers: Slump: 9.5 in. | Spread: 16.3 in.
- 1.5% steel fibers: Slump: 8 in. | Spread: 11.9 in.
- 2% steel fibers: Slump: 8.75 in. | Spread: 12.8 in.
- 3% steel fibers: Slump: 6.5 in. | Spread: 10.5 in.

The results indicate that increasing steel fiber content reduced workability, with a notable decrease at 3% fiber content by volume (UHPC Phase IV, page 337).

Seven-Day Compressive Strength Tests (Table 3.8):

2 in. cubes:

- 3% steel fibers: 25,830 psi (highest value)
- 2% steel fibers: 24,700 psi

4 in. cubes:

- 3% steel fibers: 21,300 psi (highest value)
- 2% steel fibers: 20,330 psi

Flexural Strength (Modulus of Rupture) (Table 3.9)

- Strength increased with steel fiber content up to 2%.
- At fiber content greater than 2%, flexural strength decreased.

Greatest flexural strength recorded: 1,850 psi at 2% steel fiber content.

Table 3.8. Results for varying steel fiber contents (UHPC Phase IV, Table 4.5)

Fiber Percent (%)	Slump, in. [mm]	Avg. Spread, in. [mm]	Curing Regimen	Avg. 7-Day Compressive Strength, psi [MPa]	
				2-in. (51-mm) Cubes	3.94-in.(100-mm) Cubes
Mixture 0.14 w/cm – 50FA/50SF – 1900 lb sand					
0	3.00 [76.2]	9.08 [231]	Ambient	12,410 [85.5]	11,330 [78.2]
			Heat Cured	18,795 [129.6]	15,830 [109.1]
Mixture 0.145 w/cm – 50FA/50SF – 1500 lb sand					
1	9.50 [241]	16.3 [414]	Ambient	13,190 [90.9]	12,700 [87.6]
			Heat Cured	20,310 [140.0]	18,000 [124.1]
1.5	8.00 [203]	11.9 [302]	Ambient	12,160 [83.9]	12,850 [88.6]
			Heat Cured	23,540 [162.3]	20,920 [144.2]
2	8.75 [222]	12.8 [325]	Ambient	13,590 [93.7]	14,230 [98.1]
			Heat Cured	24,700 [170.3]	20,330 [140.1]
3	6.50 [165]	10.5 [267]	Ambient	-	-
			Heat Cured	25.830 [178.1]	21,300 [146.9]

Table 3.9. Flexural strength results when varying steel fiber content (UHPC Phase IV, Table 4.6)

Batch No.	Fiber Percent (%)	Avg. Moment, lb-in [N-m]	Avg. MOR, psi [MPa]
1	1	12,860 [1454]	1610 [11.1]
2	1.5	14,380 [1625]	1800 [12.4]
3	2	14,760 [1668]	1850 [12.7]
4	3	14,550 [1644]	1820 [12.5]

3.5.2 Polyethylene Fibers

Polyethylene fibers, a poly-based alternative to steel fibers, were investigated as a partial replacement for steel fibers.

Methodology

Two fiber lengths were used:

- 2 in. polyethylene fibers with a specific gravity of 0.92
- 0.5 in. polyethylene fibers with a specific gravity of 0.91

Three mixtures were tested using 1.5% total fiber content (steel/polyethylene fibers):

- First mixture: 0.75% by volume of 0.5 in. steel fibers and 0.75% of 2 in. polyethylene fibers
- Second mixture: 0.75% by volume of 0.5 in. steel fibers and 0.75% of 0.5 in. polyethylene fibers
- Third mixture: 1.5% polyethylene fibers (0.5 in.) only

The evaluation included:

- Workability tests: Slump and spread tests
- Compressive strength tests: Conducted at 7 and 28 days on 4 in. cube specimens
- Flexural strength tests

Results

- Heat curing at 203°F was applied for all compressive strength tests

- Slump and spread values decreased as the percentage of polyethylene fibers increased (Table 3.10)

Table 3.10. Workability and Compressive Strength Tests

Fiber Combination	Slump (in.)	Spread (in.)	7-Day Compressive Strength (psi)	28-Day Compressive Strength (psi)
50% steel fibers + 50% 2-in. polyethylene fibers	4.0 – 5.0	9.5 – 11.0	19,500	18,640
50% steel fibers + 50% 0.5-in. polyethylene fibers	3.5 – 4.25	9.0 – 9.67	18,800	19,330
100% polyethylene fibers (1.5%)	2.25 – 2.75	8.42 – 9.0	17,330	17,100

Flexural Strength (Modulus of Rupture - MOR)

- Flexural testing was conducted on specimens after 28 days under ambient curing

- Greatest flexural strength: 1,590 psi, achieved with 50% steel fibers and 50% 2 in. polyethylene fibers (Table 3.11)

- Lowest flexural strength: 1,300 psi, recorded when using 100% polyethylene fibers

Table 3.11. Flexural Strength Results for Ambient Polyethylene Fiber Reinforced UHPC (UHPC Phase IV, Table 4.8)

	Mixture	Polyethylene Fiber Length, in. [mm]	Avg. Moment, lb-in [N-m]	Avg. MOR, psi [MPa]
1	50stl/50poly	2.0 [51]	12,720 [1438]	1590 [11.0]
2	50stl/50poly	0.5 [13]	11,090 [1253]	1390 [9.56]
3	All Poly	0.5 [13]	10,410 [1176]	1300 [8.97]
4	All Steel	0.5 [13]	11,930 [1348]	1490 [10.3]

3.5.3 USA-made Steel Fibers/ Steel Fibers – U

Before using the non-proprietary UHPC for the overlay project in UHPC Phase V, NMDOT enforced the Buy America (49 U.S. Code § 5323[j]) requirement. This regulation mandated that steel fibers purchased for the implementation project must be produced in the United States (UHPC Phase V, page 62). The steel fibers provided by Bekaert Corporation, which were no longer produced in the US and were only available internationally, were used for preliminary mixture proportioning for the UHPC overlay. Steel fibers – U, supplied by Concrete Fiber Solutions (CFS), have the same length as the previously used fibers, (0.5 in.) with a length-to-diameter aspect ratio of 22.

Methodology

The performance of Steel Fibers – U was evaluated through workability, compressive strength, and flexural strength tests. Slump and spread tests were performed. Compressive strength was measured at 1, 3, 7, 14, 21, and 28 days using different mixtures:

- 0.15 w/cm – 50SF/50FA – 1,700 lb sand
- 0.14 w/cm – 50SF/50FA – 1,700 lb sand
- 0.16 w/cm – 50SF/50FA – 1,700 lb sand

Two curing regimens were investigated:

Ambient curing:

- Specimens were initially cured at room temperature (68°F) for 24 hours before demolding
- They were then stored under ambient laboratory conditions (68°F, 30% relative humidity) until their designated testing age

Heat curing:

- Specimens were water-cured at 203°F for four days, followed by dry curing at the same temperature for two days, resulting in a total curing period of seven days
- After completing the seven-day curing process, samples were stored in a wet room at 100% relative humidity for further strength testing

Results

- The 0.5 in. Steel Fibers – U increased workability but reduced the compressive strength of UHPC
- None of the mixtures achieved the target compressive strengths of 14,000 psi at seven days and 17,000 psi at 28 days required by NMDOT based on ASTM C1856

A key difference between the Bekaert used and Steel fibers – U was their aspect ratio:

- Bekaert Corporation's 0.5 in. straight steel fibers had a length-to-diameter aspect ratio of 65
- The Steel Fibers – U used in this study had an aspect ratio of 22

Compared to the new fibers, the Bekaert steel fibers were slimmer, allowing for a greater number of fibers to be incorporated at the same volume, which likely contributed to the greater compressive strength observed in previous mixtures.

3.5.4 Modified Steel Fibers - U

During the mock-up overlay slab tests, modified steel fibers – U were used to achieve the target compressive strengths of 17,000 psi (UHPC Phase V, Page 86).

These new steel fibers have dimensions of 0.012 in. x 0.51 in. with a length-to-diameter aspect ratio of 43 and a tensile strength that meets the requirements of ASTM A820 (2021).

Methodology

The 0.145-37.5/62.5-1600 mixture with 1.75% of the modified steel fibers was used to evaluate workability and compressive strength, using 3.94-in. cubes.

Two re-evaluations were conducted:

- First re-evaluation: No ice was added to control the mixing temperature
- Second re-evaluation: Ice was added to reduce mixing temperature

Results

First Re-evaluation (No Ice Added)

- Slump: 6 in.
- Spread: 10.1 in.
- Mixing temperature: 94.3°F
- 7-day compressive strength: 19,640 psi

Second Re-evaluation (With Ice Added)

- Slump: 5 in.
- Spread: 9.83 in.
- Mixing temperature: 89.3°F
- 28-day compressive strength: 18,300 psi

Both mixtures exceeded the minimum required 7- and 28-day compressive strength of 14,000 and 17,000 psi, respectively, as specified by ASTM C1856 (2017) (UHPC Phase V, page 86).

3.6 Admixture Type

According to the optimized UHPC mixture proportions, using a larger aggregate top size and greater sand content can decrease workability. Additionally, while a low w/cm ratio is typically used in UHPC to achieve greater compressive strength, it may further reduce workability (Iman Talebinejad, 2004). To mitigate this, an admixture was introduced to enhance flowability and improve workability.

This study investigated the effect of three different admixtures on workability and compressive strength:

- Rheomac – A viscosity-modifying admixture that enhances microstructure density and promotes the formation of secondary calcium silicate hydrates in UHPC (UHPC Phase II)
- Navitas 33 – A rheology-modifying admixture tested at varying dosages in different mixture proportions (UHPC Phase II)
- Master Glenium Products – Additional polycarboxylate-based HRWRAs were explored, as the baseline mixture already included Glenium 3030 NS from BASF Chemicals (UHPC Phase IV)

None of the tested admixtures were able to maintain or improve workability or strength. Consequently, they were not included in the final mixture design. The examination of these admixtures is described below.

3.6.1 Viscosity Modifying

Using Rheomac, three batches were prepared with minimum, intermediate and maximum recommended dosages. The workability of the mixtures was evaluated based on visual inspection and ease of placement, classified as poor, fair, good, or very good. Additionally, 2 in. and 4 in. cube specimens were tested for 7-day compressive strength. The testing results are listed below (Table 3.12).

Workability Results:

- Minimum and intermediate dosages resulted in poor workability
- Maximum dosage was evaluated as good

Compressive Strength Results:

- The greatest compressive strength of 24,540 psi was achieved with the intermediate dosage when testing a 2 in. cube
- The lowest compressive strength of 21,590 psi was recorded when testing a 4 in. cube

Table 3.12. Effect of Rheomac on compressive strength and workability (UHPC Phase II, Table 13.5)

Dosage	Compressive strength, psi (MPa)		Workability description
	2 in. (50 mm) Cubes	4 in. (100 mm) Cubes	
minimum	22,170 (152.9)	22,380 (154.3)	poor
intermediate	24,540 (169.2)	21,590 (148.9)	poor
maximum	23,700 (163.4)	22,660 (156.2)	good

3.6.2 Rheology Modifying Admixture

Three batches were prepared using the minimum, intermediate and maximum recommended dosages. Workability was again evaluated based on visual inspection and ease of placement, classified as poor, fair, good or very good. Additionally, compressive strength was tested. The testing results are shown below (Table 3.13).

Workability Results:

- Minimum dosage: Poor
- Intermediate dosage: Fair
- Maximum dosage: Good

Compressive Strength Results:

- The greatest compressive strength of 23,360 psi was achieved with the minimum dosage when testing a 2 in. cube
- The lowest compressive strength of 20,530 psi was recorded when testing a 4 in. cube

Table 3.13. Effect of Navitas 33 on compressive strength and workability (UHPC Phase II, Table13.6)

Dosage	Compressive strength, psi (MPa)		Workability description
	2 in. (50 mm) Cubes	4 in. (100 mm) Cubes	
minimum	23,360 (161.1)	21,380 (147.4)	poor
intermediate	23,320 (160.8)	20,530 (141.5)	fair
maximum	23,950 (165.1)	21,060 (145.2)	good

3.6.3 High Range Water Reducing Admixtures

During UHPC Phase IV three additional chemical admixtures were analyzed:

- Master Glenium 7700 (HRWRA)
- Master Glenium 7920 (HRWRA)
- MasterSet DELVO (water-reducing and retarding admixture)

Methodology

The mixture proportions used for these tests were 0.15 w/cm – 50FA/50SF – 1700 lb sand which means that 0.15 w/cm ratio was used with a combination of 50% fly ash and 50% silica fume and 1700 lb of sand. The Master Glenium admixtures dosage was 86.8 fl. oz. per 100 lb of cement, and the DELVO admixture dosage was 1 fl. oz. per 100 lb of cement. (UHPC Phase IV, page 335).

Compressive strength tests were performed in 2 in. and 4 in. cubes tested at 1, 3, 7, and 28 days of ambient curing.

Results

The greatest compressive strength was achieved using 9 gal/yd^3 of Master Glenium 7700 HRWRA on the 28-day test, with a value of 16,190 psi (Table 3.14). However, this value does not meet the minimum requirement of 17,000 psi required by ASTM C1856.

Table 3.14. Effect of chemical admixtures on compressive strength and workability (UHPC Phase IV, Table 4.4)

Chemical Admixture and Dosage	Specimens	Avg. Compressive Strength, psi [MPa]			
		1-Day	3-Day	7-Day	28-Day
7700 HRWRA (9.0 gal/yd^3) [44.6 L/m^3]	2-in. (51-mm)	4340 [29.9]	10,650 [73.4]	12,930 [89.9]	16,190 [111.6]
	3.94-in. (100-mm)	3960 [27.3]	10,130 [69.8]	12,450 [85.9]	14,430 [99.5]
7700 HRWRA (7.5 gal/yd^3) [37.1 L/m^3]	2-in. (51-mm)	5400 [37.3]	10,640 [73.4]	12,500 [86.2]	15,650 [1] [107.9] [1]
	3.94-in. (100-mm)	4890 [33.7]	10,370 [71.5]	11,120 [76.7]	13,990 [1] [96.5] [1]
7920 HRWRA (9.0 gal/yd^3) [44.6 L/m^3]	2-in. (51-mm)	664 [4.57]	6630 [45.7]	9050 [62.4]	12,200 [2] [84.1] [2]
	3.94-in. (100-mm)	329 [2.26]	6520 [45.0]	9780 [67.4]	12,650 [2] [87.2] [2]
7700 HRWRA (9.0 gal/yd^3) [44.6 L/m^3] + DELVO	2-in. (51-mm)	4800 [33.1]	10,500 [72.4]	12,600 [86.9]	14,730 [101.5]
	3.94-in. (100-mm)	5030 [34.7]	10,090 [69.6]	12,240 [84.4]	14,290 [98.5]

[1] 32 – day compressive strength
[2] 24 – day compresseive strength

3.7 Mixing Process

Aggregate Preparation

Prior to mixing, the fine aggregates were scalped through the No. 4 sieve to remove the large particles and washed through a No. 200 sieve to remove the fine particles. To remove the moisture, the aggregates were oven-dried at 239 °F for 24 hours.

Mixing Procedure at NMSU's Structural Systems and Material Testing Laboratory (SSMTL)

The mixing process at NMSU's SSMTL consisted of the following steps (UHPC Phase III, page 87):

1) Dry mixing - sand, cement, fly ash and silica fume were added in order of decreasing particle size and mixed
2) Initial water addition- half of the water was added while mixing continued
3) Remaining water and HRWRA - the remaining water and HRWRA were added, and mixing continued until the desired consistency was reached
4) Steel fibers were incorporated into the mixture as the final step

UHPC Overlay Mixing Process

For UHPC overlay preparation, mixing times range from 16 to 30 minutes, with an average of 21 minutes (UHPC Phase V, page 53):

1) Dry Mixing lasted approximately 30 seconds
2) Once all the water was added and the desired consistency was reached, the mixer was reversed for 3 minutes to ensure thorough mixing
3) Steel fibers were then added, and mixing continued for an additional 3 minutes

3.8 Curing Regimen and Case Studies

A heat curing regimen enhances compressive strength and improves durability properties. Wet curing reduces early-age shrinkage and increases water retention compared to other curing methods. Additionally, an extended curing period results in lower shrinkage (UHPC Phase III, page 42).

It is essential that this regimen is both economical and readily available for precast plants. To adapt the concrete mixture to the specific conditions and limitations of New Mexico, a curing regimen using the highest achievable temperature in the state was investigated. According to the local precast plant, the maximum attainable temperature within their facilities was 203°F.

3.8.1 Curing Regimen

Two curing regimens were designed and tested with compression tests of 2 in. and 4 in. cubes.

Option 1:

- 24 hours at room temperature, 70 °F
- Then, 4 days in water bath at 203 °F
- Finally, 2 days dry cured 203 °F

Option 2:

- 24 hours at room temperature, 70 °F
- Then, 4 days in water bath 122 °F
- Finally, 2 days dry cured at 392 °F

The findings are shown below:

- Samples cured using Option 1 experienced a 24.1% reduction in compressive strength compared to Option 2
- However, Option 2 was not economically feasible in New Mexico, as the maximum achievable temperature at local precast plants was 203°F
- Therefore, Option 1 is recommended (UHPC Phase II, page 195)
- This curing regimen was further validated in UHPC Phase III (page 87)

Time-Dependent Strength Gain and Ambient Curing

During UHPC Phase IV, an ambient curing regimen was evaluated to assess time-dependent strength gain in non-proprietary UHPC.

Ambient Curing Process:

- 24 hours at ambient temperature
- demolding after 24 hours
- moist cured in a wet room for 72 hours

This curing period was chosen as a compromise between a conservative laboratory approach and a cost-effective field approach (UHPC Phase IV, page 391).

Results (UHPC Phase IV, page 425):

- Thermal curing achieved greater strength compared to ambient curing
- However, results demonstrated that ambient curing still allowed for time-dependent strength gain
- Over time, strength values for ambient curing began approaching those of thermal curing
- Rapid early-age strength gain was exhibited with the initiation of elevated thermal curing 24 hours after casting
- In contrast, ambient cured (AC) specimens exhibited a gradual strength gain, resulting in lower 7-day compressive strengths (Table 3.15) when compared to the results from thermal curing (Figure 3.1) (UHPC Phase IV, page 438)
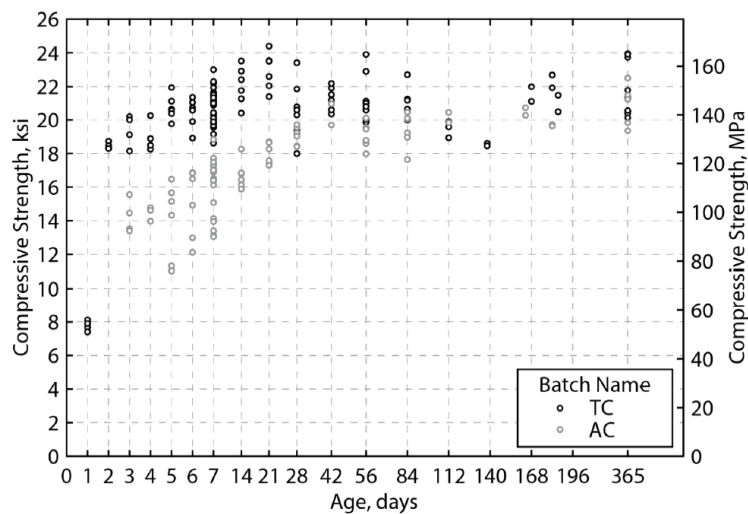
Figure 3.1. Comparison of compressive strength results for thermal and ambient curing regimes on 4 in. cube specimens (UHPC Phase IV, Figure 4.30)

Table 3.15. Summary of compressive strength results for UHPC produced using ambient curing regime (UHPC Phase IV, Table 4.14)

Age days	Specimen Count	$f_{c,avg}$ ksi (MPa)	Std. Dev. ksi (MPa)
3	4	14.2 (98.2)	1.00 (6.89)
4	4	14.5 (100)	0.37 (2.57)
5	6	14.0 (96.5)	2.29 (15.8)
6	6	15.0 (104)	2.07 (14.2)
7	20	16.1 (111)	1.71 (11.8)
14	6	16.7 (115)	0.84 (5.77)
21	6	18.0 (124)	0.63 (4.36)
28	6	19.1 (131)	0.55 (3.82)
42	2	20.3 (140)	0.89 (6.15)
56	6	19.1 (132)	0.77 (5.31)
84	6	19.4 (134)	1.04 (7.16)
112	2	20.1 (139)	0.43 (2.96)
164	2	20.5 (141)	0.32 (2.20)
182	2	19.7 (136)	0.07 (0.47)
365	5	20.9 (144)	1.29 (8.88)

NOTE: Results based on 4.0 in. (100 mm) cube specimens.

3.8.2 Case Studies

Joint Application

During UHPC Phase IV, UHPC applications were studied at NMSU. Specifically, joints were tested using a slab-joint-slab system (more detail in Chapter 6.1 of this document).

Specimens were cured at room temperature for the first 24 hours, then demolded and wet-cured for the first 7 days. After that, they were stored at room temperature until testing.

Compressive and flexural strengths were measured after 14 days of curing using 4 in. cube specimens and 3 x 4 x 16 in. prism specimens, respectively. Results showed that the compressive strength varied from 13.1 to 17.1 ksi. Additionally, results from flexure tests showed a range of 10.2 to 12.1 ksi (UHPC Phase IV, page 472).

Shear Keys

Shear keys for concrete bridges were tested on full-scale, 25-foot-long (7.62 m) reinforced concrete channel girders at NMSU (more details in chapter 6.2 of this document).

All specimens were formed using the following steel molds: 4 in. cubes and 4 by 8 in. cylinders. Specimens were cured under room temperature (30% humidity) for 24 hours. They were then removed from the steel molds and placed in a moist curing environment for 7 or 28 days. Lastly, specimens were taken out just before the 7-day and 28-day strength tests. Results showed that 28-day compressive strength varied from 17.2 to 19.9 ksi. Additionally, 7-day flexure strength varied from 13.2 to 14.9 ksi and 28-day flexural strength varied from 15.9 to 17.7 ksi (UHPC Phase IV, page 570).

4. MATERIAL PROPERTIES OF OPTIMIZED UHPC

Since the primary responsibility of concrete is to provide compressive strength in structures, when optimizing a new mixture, strength tests are essential to verify whether performance expectations are met. Several factors influence the ultimate strength of concrete, including particle packing, chemical interactions, activation from cementitious materials, w/cm ratio, and the type and number of fibers.

Unit weight is also a significant factor in structural design, as it affects the total weight of the structure. The goal is to develop the lightest yet strongest material possible.

The compressive strength test is the most commonly performed test, as concrete primarily resists compression forces within a structure. It is crucial to ensure that this strength is at least not reduced when optimizing the mixture proportions using readily available and cost-effective materials. The compressive strength objective for the UHPC mixture developed in this work was to exceed 20,000 psi.

Another critical property is the modulus of elasticity, which measures the extent to which concrete can stretch before cracking. Similarly, the modulus of rupture evaluates the maximum stress the concrete can withstand before breaking or yielding.

However, long-term properties such as creep and shrinkage introduce additional complexities. Creep refers to the gradual deformation of concrete under sustained loads, while shrinkage is the reduction in volume as concrete dries. These properties are challenging to measure accurately in short-term laboratory tests, as they typically manifest over extended periods. Creep increases proportionally with both time and the length of the span subjected to loads. The longer the span and the duration under stress, the greater the potential for creep, making it difficult to anticipate fully during early testing phases.

Accurate prediction of these long-term effects is crucial for ensuring the stability and durability of the structure throughout its lifespan.

4.1 Unit Weight

The unit weight of UHPC was quantified using the 4.0 in. cube specimens produced for evaluation of compressive strength. The cube specimen molds were designed in accordance with British Standards, using the nominal dimension of 4.0 in. (UHPC Phase IV, page 9). The mixture proportions used for this test are provided in Table A-4 (Appendix A) from this document, which represents a batch of 1.25 ft^3.

Regardless of specimen age at testing or curing regimen used, the unit weight ranged between 145 lb/ft^3 to 153 lb/ft^3. The average for all batches of tests using ambient and thermal curing regimens were equal to 149.8 lb/ft^3 and 150.1 lb/ft^3.

It was observed that the unit weight was below the predicted value from the AASHTO equation representative for values between 5 ksi and 15 ksi. (UHPC Phase IV, page 430)

Furthermore, based on the results of UHPC Phase IV, it was recommended that 155 lb/ft^3 should be considered as the unit weight of UHPC. When accounting for steel reinforcement, this value should be conservatively increased to 160 lb/ft^3. (UHPC Phase IV, page 430).

4.2 Factors Impacting Compressive Strength

Compressive strength is the most commonly assumed mechanical property of concrete. Therefore, during the development of locally produced UHPC, compressive strength testing was the primary focus.

The first set of tests examined whether the inclusion of steel fibers would increase compressive strength. Subsequently, the effects of different fiber types on compressive strength were analyzed. Further comparisons were made regarding w/cm ratio and aggregate content in the mixture.

After finalizing the optimized mixture, tests were performed for real-world applications, beginning with laboratory tests in the initial phase, followed by field tests.

Compressive strength was evaluated in accordance with the British Standards Institution (BSI) specification BS 1881: Part 116, using 4 in. cube specimens. Cube specimens were chosen due to the significantly high compressive strengths exhibited by UHPC and to help eliminate the challenges associated with preparing cylinder specimen ends.

Specifically, the use of unbonded neoprene end caps, as outlined in ASTM C1231 (2015), is restricted to concretes with lower compressive strengths. Similarly, sulfur capping, as specified in ASTM C617 (2015), proves ineffective for compressive strengths exceeding 18 ksi (UHPC Phase IV, page 7).

4.2.1 Steel Fibers

In preliminary tests of UHPC in Phase II of the study, two mixture proportions were proposed:

- Plain UHPC, meaning that it contains 0% steel fibers
- Fiber-reinforced UHPC

These mixtures were tested to investigate the advantages of incorporating steel fibers. During Phase II, the optimal amount of steel fiber in the mixture was investigated. Additionally, the effects of substituting steel fibers with alternative fibers possessing enhanced properties were analyzed for their impact on compressive strength.

Zero Steel fibers

Specimens were prepared in the form of:

- 2 in. and 4 in. cubes for compressive strength testing.
- 3 x 4 x 16 in. beams to test flexural strength, measured in terms of the modulus of rupture (MOR).

The curing regimen used was Option 2 (Chapter 3.8 of this document), which involves (UHPC Phase V, Table 2.5) :

- 24 hours of ambient curing
- Followed by water curing at 122 °F (50 °C)
- Then, dry curing at 392 °F (200 °C)

At 28 days, the compressive strength of plain UHPC reached 23.19 ksi. These results confirm that the strength of locally produced UHPC was comparable to commercially available products. The lowest recorded strength, 18.90 ksi, was observed by not incorporating steel fibers in the mixture during the 7-day test on 4 in. cubes. The maximum 7-day compressive strength was seen on the fiber reinforced specimen when testing on a 2 in. cube specimen, 22.21 ksi. A similar trend was observed from 28-day compressive strength tests. The minimum compressive strength was seen on the 4 in. cube without steel fibers, 20.48 ksi. The maximum strength was seen for the fiber reinforced 2 in. cube, 24.7 ksi. (Table 4.1) (UHPC Phase V, page 18).

Table 4.1 Compressive and flexural strength with and without steel fibers (UHPC Phase V, Table 2.6)

Mixture	w/cm ratio	Curing Regimen	7-day Compressive Strength, psi [MPa]		28-day Compressive Strength, psi [MPa]		7-day MOR, psi [MPa]
			2 in. (50 mm)	4 in. (100 mm)	2 in. (50 mm)	4 in. (100 mm)	3x4x16 in. (75x100x400 mm)
Plain	0.20	OV	21,240 [146.5]	18,900 [130.3]	23,190 [159.9]	20,480 [141.2]	1580 [10.9]
Fiber Reinforced	0.20	OV	22,210 [153.2]	19,850 [136.9]	24,700 [170.3]	21,680 [149.5]	2650 [18.3]

Original Steel Fibers

Specimens were prepared in the following forms:

- 2 in. and 4 in. cubes for compressive strength testing
- 3 x 4 x 16 in. beams to test flexural strength, measured in terms of modulus of rupture (MOR)

The curing regimen used was Option 2 (Chapter 3.8 of this document), which involves (UHPC Phase V, page 18, Table 2.5) :

- 24 hours of ambient curing
- Followed by water curing at 122 °F
- Then, dry curing at 392 °F

At 28 days, the compressive strength of the fiber-reinforced UHPC achieved 24.7 ksi. Compressive strengths exceeded 19.0 ksi when steel fibers were incorporated. The greatest strength, 24.70 ksi, was achieved with fiber reinforcement on the 28-day test (UHPC Phase V, page 18).

Nycon-SF Type I Fibers

At the beginning of UHPC Phase III, Nycon-SF Type I fibers were introduced as a replacement for the traditional steel fibers. The fibers were tested using:

- Eight 2 in. cube specimens
- Eight 4 in. cube specimens

Compressive strength tests show that for the 2 in. specimens, strength increased from 17.9 ksi (specimen 1) to 26.7 ksi (specimen 8) (Table 4.2), showing a notable improvement across the samples. In contrast, the 4 in. specimens exhibited more consistent results, with compressive strengths ranging from 21.2 ksi to 23.4 ksi.

According to the compressive strength tests performed on 2 and the 4 in. cube, the steel fibers met the requirements, enhancing the compressive strength of the mixture. However, these steel fibers were not used further in the study. New USA-made steel fibers were introduced in UHPC Phase IV.

Table 4.2. Compressive strength test results using Nycon-SF Type I fibers (UHPC Phase III, Table 2.1)

Compressive Strength, psi (MPa)		
Specimen No.	2 in. (50 mm) Cubes	4 in. (100 mm) Cubes
1	17,950 (123.8)	22,080 (152.2)
2	20,230 (139.5)	22,160 (152.8)
3	23,200 (160.0)	22,160 (152.8)
4	22,500 (155.1)	22,080 (152.2)
5	26,855 (185.2)	21,220 (146.3)
6	25,423 (175.3)	23,470 (161.8)
7	27,955 (192.7)	22,260 (153.5)
8	26,730 (184.3)	21,780 (150.2)
Average	*23,860 (164.5)*	*22,150 (152.7)*

4.2.2 Water to Cementitious Ratio

Methodology

During UHPC Phase II, the water-to-cementitious material (w/cm) ratio was gradually reduced from 0.2 to 0.14. Additionally, a new curing regimen (identified as Option 2 in Chapter 3.6 of this document) was implemented.

Seven-day compressive strength tests were conducted using 2 in. and 4 in. cube specimens.

Results

- Reducing the w/cm ratio significantly increased compressive strength (Table 4.3)
- When the w/cm ratio was 0.20, the compressive strength was 19.12 ksi
- Lowering the w/cm ratio to 0.14 increased compressive strength to 25 ksi (UHPC Phase V, page 18)

Based on these compressive strength results and improved workability, mixture proportions with w/cm ratio of 0.14 were selected for further optimization. (UHPC Phase II, page 188).

Table 4.3. Compressive strength at reduced w/cm ratios (UHPC Phase II, Table 13.1)

w/cm ratio	Curing Regimen	Avg. 7-Day Compressive Strength, psi [MPa]	
		2-in. (50-mm) cubes	4-in. (100-mm) cubes
0.20	95/95	19,120 [131.8]	17,820 [122.8]
0.18	95/95	23,020 [158.7]	18,410 [126.9]
0.15	95/95	25,070 [172.8]	20,050 [138.2]
0.14	95/95	25,080 [172.9]	20,470 [141.1]

4.2.3 Fine Aggregate

Methodology

Tests on aggregate content were conducted using 2 in. and 4 in. cube specimens, maintaining consistent mixture proportions with a w/cm ratio of 0.14 for all samples. The study evaluated the seven-day compressive strength in relation to (UHPC Phase V, page 20):

- Sand contents ranging from 1500 to 2100 lb/yd³,
- Effects of varying the aggregate top size

Results (UHPC Phase V, page 21, Figure 2.3)

- Increasing the sand content in the mixture yielded positive outcomes in terms of compressive strength by maintaining it while reducing the cementitious materials, which have a higher cost.
- At 1,500 lb/yd³ of sand, the seven-day compressive strength reached 22.5 ksi.
- Increasing the sand content to 1,700 lb/yd³ resulted in a slight decrease of compressive strength to approximately 21 ksi.
- Further increasing the sand content to 1,900 lb/yd³ yielded a compressive strength of 20.5 ksi.
- Similarly, when the aggregate top size was increased from sieve No. 30 to No. 4, the seven-day compressive strength remained between 20.5 ksi and 22.5 ksi.
- Aggregate content ranging between 1,900 and 2,100 lb/yd³ was selected for future work.

4.3 Modulus of Elasticity

Three approaches were tested to measure the modulus of elasticity:

- First approach: Used 4 in. cube specimens but was found to be unreliable due to small specimen size.
- Second approach: Used 4 × 8 in. cylinder specimens subjected to thermal curing.
- Third approach: Used 4 × 8 in. cylinder specimens but cured under ambient conditions.

All tests were conducted in accordance with ASTM C469 (2014). The mixture proportions for this test are detailed in Table A-3 of this document, representing a batch size of 1.25 ft³. The testing process and results of the three approaches are described below.

First Approach: 4 in. Cube Specimens

Six 4 in. cube specimens were produced using mixture proportions that included steel fibers with an ultimate tensile strength of 375 ksi. The specimens were subjected to thermal curing and instrumented with surface-bonded strain gauges to monitor strain development under compressive loading.

At an ultimate strain value of 0.0035, the following results were obtained:

- Average modulus of elasticity: 5,845 ksi
- Average compressive strength: 22.4 ksi

However, it was determined that further testing was necessary due to limitations in specimen size (UHPC Phase IV, page 347).

Second Approach: Long-Term Modulus of Elasticity (Thermal Curing)

The long-term modulus of elasticity of thermally cured UHPC was evaluated using 4 by 8 in. cylinder specimens, tested at various intervals over one year: 7, 14, 21, 28, 42, 56, 84, 112, 168, and 365 days.

- The minimum modulus of elasticity was recorded at 84 days with a value of 5,727 ksi
- The maximum modulus of elasticity was recorded at 168 days with a value of 6,441 ksi
- The average modulus of elasticity over all test intervals was 5,998 ksi

Results indicate that the modulus of elasticity for thermal-cured (TC) specimens remained relatively consistent, with only slight increases in strength over time (Table 4.4). 168 days after casting, the average modulus of elasticity for TC specimens was within 10% of the 7-day value (UHPC Phase IV, page 434).

Table 4.4. Summary of Modulus of Elasticity results for UHPC produced using thermal curing (UHPC Phase IV, Table 4.17)

Age days	Specimen Count	$E_{c,avg}$ ksi (GPa)	Std. Dev. ksi (GPa)
7	4	5853 (40.4)	78.6 (0.54)
14	2	5830 (40.2)	154 (1.06)
21	2	5835 (40.2)	78.0 (0.54)
28	2	5899 (40.7)	237 (1.63)
42	2	6069 (41.8)	333 (2.29)
56	2	6021 (41.5)	160 (1.10)
84	2	5727 (39.5)	206 (1.42)
112	2	6101 (42.1)	360 (2.48)
168	2	6441 (44.4)	646 (4.46)
365	3	6207 (42.8)	234 (1.61)

NOTE: Results based on 4.0 x 8.0 in. (102 x 203 mm) cylinder specimens.

Third Approach: Long-Term Modulus of Elasticity (Ambient Curing)

The long-term modulus of elasticity of UHPC produced with ambient curing was determined by testing 4 by 8 in. cylinder specimens. The specimens were tested over one year at the same intervals used for thermal curing. (Table 4.5).

- Minimum modulus of elasticity: 5,176 ksi, recorded at 14 days
- Maximum modulus of elasticity: 6,782 ksi, recorded at 112 days
- Average modulus of elasticity: 5,975 ksi.

Table 4.5. Summary of Modulus of Elasticity results for UHPC produced using ambient curing (UHPC Phase IV, Table 4.66)

Age days	Specimen Count	$E_{c,avg}$ ksi (GPa)	Std. Dev. ksi (GPa)
7	4	5382 (37.1)	364 (2.51)
14	2	5176 (35.7)	253 (1.75)
21	2	5492 (37.9)	1.91 (0.01)
28	2	6175 (42.6)	871 (6.00)
42	2	6318 (43.6)	103 (0.71)
56	2	5952 (41.0)	144 (0.99)
84	2	6548 (45.1)	860 (5.93)
112	2	6782 (46.8)	959 (6.61)
164	2	5834 (40.2)	289 (2.00)
365	4	6100 (42.1)	235 (1.62)

NOTE: Results based on 4.0 x 8.0 in. (102 x 203 mm) cylinder specimens.

These results indicate that elevated thermal curing is not critical for the development of early-age modulus of elasticity. However, according to Phase IV, a much larger specimen volume is necessary to obtain a more accurate representation of this behavior (UHPC Phase IV, page 434).

4.4 Modulus of Rupture

Modulus of rupture strength is defined as the flexural stress corresponding to the first crack. It is evaluated by testing small-scale beam specimens in four-point bending test, conducted in accordance with ASTM C1609. Specifically:

Specimen dimensions: 16 in. in length with a 3 x 4 in. cross section (UHPC Phase IV, page 10).

Mixture proportions: The proportions used for this test are detailed in Table A-3 of this document, representing a batch size of 1.25 ft^3.

Curing methods: specimens were cured using two curing regimens. Specifically, the thermal curing regimen was used, which is Option 1 in Chapter 3.8.1 from this document. Additionally, ambient curing was performed on the specimens demolded after 24 hours of setting and moist cured in a wet room for 72 hours. After that, the specimens remained in ambient condition until testing.

Unlike the modulus of elasticity, the modulus of rupture is significantly affected by the curing regimen, similar to compressive strength. Results are shown below:

7-day MOR results:

- Thermal cured (TC) specimens: 1,203 psi
- Ambient cured (AC) specimens: 656 psi

Thermal-Cured (TC) Specimens:

- MOR values increased rapidly after elevated thermal curing, reaching approximately 90% of 7-day strength within 48 to 72 hours after casting
- After reaching this level of strength, the MOR remained constant with increasing age

Ambient Cured (AC) Specimens: (UHPC Phase IV, page 431)

- MOR values were significantly lower than those of TC specimens
- Strength gain was more gradual, continuing to increase for up to a year after casting, with average MOR surpassing 900 psi

Furthermore, in UHPC Phase IV, during the review of the application of UHPC as an overlay material, 16 x 3 x 4 in. beam specimens were evaluated and tested at 28 days and the average modulus of rupture was 2,440 psi (UHPC Phase IV, Table 5.27). Additionally, the effect of steel fiber content on MOR is shown below (Table 4.6):

- 1.5% steel fibers: Highest MOR recorded: 2,569 psi
- 2.0% steel fibers: MOR decreased to 2,327 psi
- 3.0% steel fibers: Lowest MOR recorded: 2,320 psi

Table 4.6. Flexural performance and Modulus of Rupture for UHPC and NSC specimens (UHPC Phase IV, Table 5.27)

| | | Flexural Performance | | | | Modulus of Rupture | |
| | | Ultimate Load | | First Peak Load | | | |
		(lb)	(N)	(lb)	(N)	(psi)	(MPa)
NSC	Specimen 1	3,270	14,546	3,270	14,546	1090	7.52
	Specimen 2	2,970	13,211	2,970	13,211	990	6.83
	Average	3,120	13,879	3,120	13,879	1,040	7.17
	Standard Deviation	212	944	212	944	71	0.50
UHPC	Slab 1 (1.5% fibers)	8,990	39,990	7,636	33,967	2,545	17.55
	Slab 3 (1.5% fibers)	-	-	-	-	-	-
	Slab 4 (1.5% fibers)	-	-	-	-	-	-
	Slab 5 (1.5% fibers)	-	-	-	-	-	-
	Slab 6 (2.0% fibers)	10,570	47018	6,981	31,053	2,327	16.04
	Slab 7 (1.5% fibers)	-	-	-	-	-	-
	Slab 8 (1.5% fibers)	8,970	39,901	7,706	34,278	2,569	17.71
	Slab 9 (3.0% fibers)	9,760	43,415	6,960	30,960	2,320	16.00
	Average	9,573	42,581	7,321	32,565	2,440	16.83
	Standard Deviation	760	3,380	406	1,804	135	0.93

4.5 Durability

The durability of the UHPC is established by studying resistance to freezing and thawing, alkali-silica reaction, and delayed ettringite formation (DEF). Specifically, these tests were performed when the original steel fibers were replaced by the Nycon-SF Type I (UHPC Phase III, page 29). Furthermore:

- Freezing and thawing resistance: UHPC produced with optimized mixture proportions and curing methods was tested in accordance with ASTM C666 (AASHTO T161)
- Alkali-silica reaction (ASR) resistance: Assessed using the mortar bar method (ASTM C1260)
- Delayed ettringite formation (DEF): investigated by evaluating the chemical composition of the cementitious materials

As shown in Table 4.7, replacing steel fibers with Nycon-SF Type I fibers does not result in significant change in durability factors. The required limit of durability factors is 95, with values greater than 100 indicating excellent resistance to freezing and thawing.

The ASTM expansion limit for ASR tests was 0.1%, results show the greatest expansion to be 0.025 %.

Specimens cured at temperatures exceeding 158°F exhibited an increased risk of Delayed Ettringite Formation (DEF) expansion. Since these specimens were cured at 203°F (Option 1, Chapter 3.8.1) to achieve high compressive strength, DEF was specifically addressed in UHPC Phase II, Section 15.3. Existing research on DEF suggests that DEF expansion is more influenced by the SO_3/Al_2O_3 ratio of the cementitious materials used in the mixture. As the SO_3/Al_2O_3 ratio in the UHPC mixture remained below the critical threshold of 0.7, DEF expansion was not a concern in this study.

Table 4.7. Durability factors for UHPC mixtures with different fiber types (UHPC Phase III, Table 2.2)

Percent Fly Ash, %		37.5	50	37.5	50	37.5	50
Fiber Type		-	-	Original	Original	Nycon-SF Type I	Nycon-SF Type I
Specimen	1	100.1	100.3	99.9	100.1	100.7	100.6
	2	100.7	100.4	100.2	100.0	100.4	100.6
	3	100.3	100.3	99.8	100.2	100.5	100.7
	AVG	100.4	100.3	100.0	100.1	100.5	100.7

- no fibers

4.6 Creep and Shrinkage

Two different UHPC mixtures were prepared for this test (Table 4.8). The primary differences between the mixtures are the silica fume and fly ash contents, as well as the amount of water.

For each mixture, four specimens of 3 x 4 x 16 in. were cast. Since creep is a function of time and stress, creep strains were measured while specimens were subjected to a compressive load for 90 days. Tests were conducted at 0.5 f'c, 0.4 f'c, and 0.3 f'c, comparing the drying phase and the basic phase of creep. All measurements were taken using a Whittemore gauge (UHPC Phase III, page 56).

Table 4.8. Mixture proportions for creep and shrinkage tests (UHPC Phase III, Table 5.1)

Fly ash content	50%	37.5%
Group Number	1	2
Cement [lb/yd^3 (kg/m^3)]	1264 (750)	1264 (750)
Silica fume [lb/yd^3 (kg/m^3)]	158 (94)	198 (117)
Fly ash [lb/yd^3 (kg/m^3)]	158 (94)	119 (70)
Sand [lb/yd^3 (kg/m^3)]	1866 (1107)	1866 (1107)
HRWRA [gal/yd^3 (l/m^3)]	9 (44.6)	9 (44.6)
Water [lb/yd^3 (kg/m^3)]	246 (146)	226 (134)
Steel Fibers [lb/yd^3 (kg/m^3)]	200 (119)	200 (119)

Generally, drying creep strain is greater than the basic creep strain due to the additional effect of shrinkage. On average, basic creep is 4% lower than drying creep.

Comparing the creep and shrinkage results for mixtures where 50% or 37.5% of silica fume was replaced by fly ash, no significant effect on creep behavior was observed (Table 4.9). As expected, creep strain decreases as the stress level decreases. Additionally, the stress level (stress/strength) has significant influence on creep (UHPC Phase III, page 62). Specifically, when the stress level ratio was 0.3 in the mixture with 37.5% fly ash, the elastic strain was measured at 942 με, and the creep strain was 223 με, resulting in a creep coefficient of 0.24. When the ratio increased to 0.5, the elastic strain increased to 1517 με, the creep strain to 408 με, and the creep coefficient to 0.27.

Table 4.9. Creep results (UHPC Phase III, Table 6.2)

Percent fly ash	Type of Creep	Strength psi (MPa)	Stress level (Stress / Strength)	Elastic Strain (με)	Creep Strain (με)	Creep Coefficient, c_c
37.5	Drying	21,270 (147)	0.5	1517	408	0.27
		22,350 (154)	0.4	1297	303	0.23
		21,350 (147)	0.3	942	223	0.24
	Basic	21,270 (147)	0.5	1482	336	0.23
		22,350 (154)	0.4	1317	280	0.21
		21,350 (147)	0.3	920	224	0.24
50	Drying	21,220 (146)	0.5	1482	392	0.26
		21,500 (148)	0.4	1350	320	0.24
		21,950 (151)	0.3	1072	273	0.27
	Basic	21,220 (146)	0.5	1465	382	0.26
		21,500 (148)	0.4	1375	302	0.22
		21,950 (151)	0.3	1052	258	0.27

The creep results obtained from the experimental work were compared to existing creep models, including AASHTO 2004 and 2012, ACI 209R-92, AFGC/SETRA, and CEB-FIP MC90. Comparison of these models is crucial, as an accurate creep prediction model is essential for estimating creep with acceptable precision, allowing for reasonable predictions of losses due to creep in prestressed girders. (UHPC Phase III, page 72: comparison between models).

The comparison of the creep results with standard models (Figure 4.1) is presented below:

- The AASHTO 2012 model failed on day 27, producing an infinite value, which resulted in expansion strain instead of shortening. Consequently, the AASHTO 2012 model is not suitable for UHPC
- The AASHTO 2004, ACI 209R-92, and CEB-FIP MC90 models overestimated creep by 300% to 500% across all mixtures tested
- The AFGC/SÉTRA model underestimated creep for all UHPC mixtures evaluated.
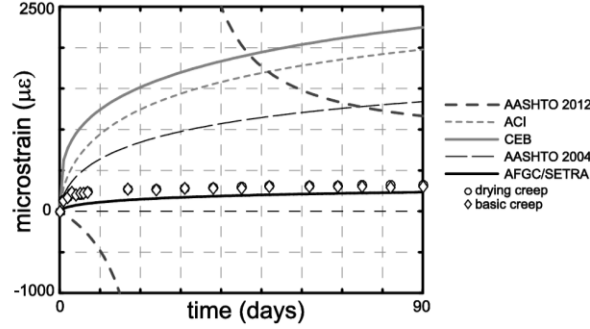
Figure 4.1. UHPC creep results vs. predicted values (UHPC Phase III, Figure 6.8)

Due to the discrepancies between each model, a modified equation was developed from the AASHTO 2004 equation to provide more accurate creep predictions, the equation is presented below. (UHPC Phase III, Equation 6.11).

The AASHTO 2004 model equation is:

$$\Psi(t, t_i) = 3.5 k_c k_f k_h t_i^{-0.118} \left(\frac{(t - t_i)^{0.6}}{10 + (t - t_i)^{0.65}} \right)$$

The time factor was developed to represent creep development for normal strength concrete. Creep in normal concrete is greater than the creep in UHPC at similar stress to strength ratio. Using this factor to predict UHPC creep tends to overestimate creep values. To modify this factor, a computer program was developed to find the best expression that may replace the existing expression in the denominator of the time factor.

The creep results from the resulting equation showed significant increases in creep when the stress level was increased. Therefore, a stress level factor was developed to describe the effect of the stress level on creep. The resulting model equation is listed below.

$$\Psi(t, t_i) = 3.5 k_c k_f k_h k_s t_i^{-0.118} \left(\frac{(t, t_i)^{0.6}}{4 \times (4 + (t, t_i)^{0.65})} \right)$$

Where,

$k_s = 1.25 S_L^2 - 0.225 S_L + 0.8975$;

$ks = stress\ level\ factor$;

$SL = stress\ level\ in\ a\ creep\ test = applied\ stress/strength\ of\ concrete$;

$k_c = 1.45 - 0.13 \frac{V}{S} \geq 1.0, \frac{V}{S} = volume\ to\ surface\ ratio\ in\ mm$;

$k_f = \frac{35}{7 + f'_{ci}}, f'_{ci} = the\ compressive\ strength\ of\ concrete\ at\ time\ of\ prestressing$;

$k_h = 1.56 - 0.008H = relative\ humidity\ in\ \%$; and

$t_i = the\ age\ of\ concrete\ in\ days\ at\ the\ time\ of\ loading$.

5. COMPARISON BETWEEN UHPC AND HPC

A structurally deficient bridge was examined for repair by using both UHPC and HPC materials. This presented an opportunity to evaluate the performance of UHPC and HPC at a structural level. Bridge 5296, located on NM-186, consisted of two simply supported spans. According to the bridge inspection report, Bridge 5296 exhibited severe deterioration due to the following issues:

- Drainage problems, lack of protective wearing surfaces, and overhangs
- Exposed grouted shear keys, leading to weathering, vehicular wear, and drainage issues, which cause leaching, delamination, and spalling
- Exposed rebar shows moderate to heavy corrosion
- Locked roller bearings at the center pier restricted joint movement, leading to significant cracking and connection failure
- Stress concentrations around transversely threaded rods caused vertical cracks and leaching
- Nesting swallows worsened the deterioration
- Substandard Railings
- Significant rust, delamination, and spalling in the piles under the center pier and abutments, with corroded rebar

As a result, the two spans of the bridge were replaced with one span made of HPC and another of UHPC, ensuring that both spans were tested under real conditions, including environmental factors and traffic loads. (Table A-2). Due to UHPC's superior strength, each span was designed with specific dimensions, described in the sections below. The optimized mixture proportions were tested at structural level, using both laboratory and field tests. The objective was to determine whether the same girder design could be used for both HPC and UHPC.

The girders were designed using the CONSPAN software with varying depths (12.5 in. to 15 in.) and web widths (6 in. to 7 in.). The optimized dimensions for the UHPC (Figure 5.1) section are:

- Effective width = 48 in.
- Depth = 12.5 in.
- Flange depth = 4 in.
- Web width = 6 in.

Compressive strengths at release ranged between 11 ksi and 14 ksi depending on the number of strands per web.

- For 4 strands per web, the compressive strength at release was 14,000 psi
- For 6 strands per web, the compressive strength at release was 11,000 psi
- The required number of strands per web was 6 for exterior girders, and 4 for interior girders
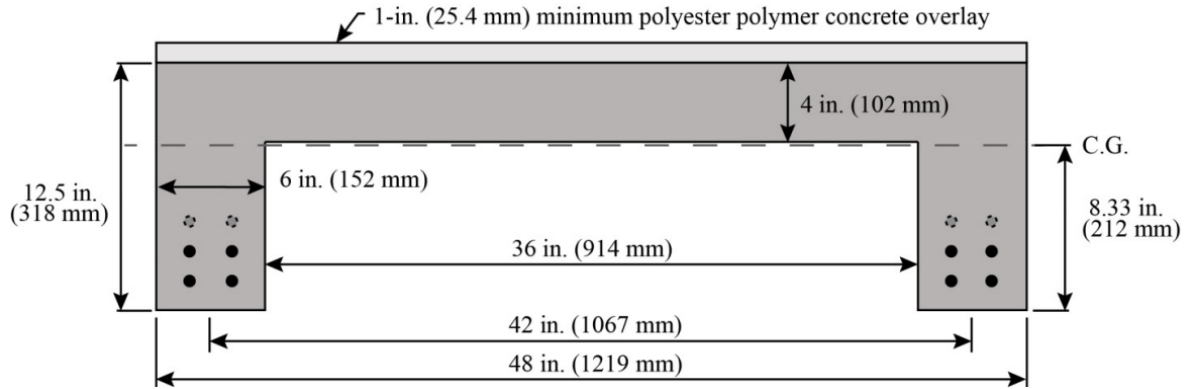
Figure 5.1. Preliminary cross section of UHPC girder design (UHPC Phase III, Figure 8.24a)

The compressive strength limitations of HPC restrict the design feasibility. Specifically, with HPC's release strength of 7 ksi and 28-day strength of 9.5 ksi, the optimized UHPC girder geometry is unsuitable for HPC. HPC required additional prestressing strands to satisfy both serviceability and strength limit states. However, this increased the prestressing force beyond allowable compressive strength at release. As a result, the girder size had to be increased to meet both service and strength requirements. Specifically, depth was increased by 2.5 in, web width was increased by 1.0 in, and cross-sectional area was increased by 52 in² compared to the UHPC girder.

The girders were designed using the CONSPAN software with different depths (12.5 in. to 15 in.) and web widths (6 in. to 7 in.). The optimized dimensions for the HPC section (Figure 5.2) are:

- Effective width = 48 in.
- Depth = 15 in.
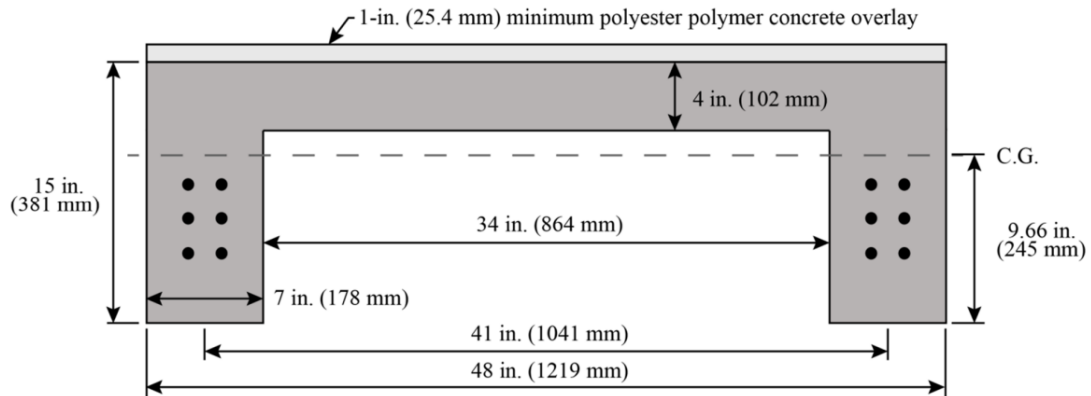- Flange depth = 4 in.
- Web width = 7 in.

Figure 5.2. Preliminary cross section of HPC girder design (UHPC Phase III, Figure 8.26a)

Additionally, the results above validate the discussion in Chapter 2.1, where numerical analysis using structural software demonstrates that implementing UHPC in bridges can lead to significant concrete volume savings compared to HPC.

Each girder was reinforced in accordance with AASHTO LRFD requirements, using a total of 0.6 in. diameter low-relaxation prestressing strands (UHPC Phase III, page 113). To monitor the behavior of prestressing strands, mild reinforcing steel, concrete, and internal temperature variations throughout the curing process, various types of instrumentation were embedded in the girder before casting. This instrumentation is designed to capture key structural behavior, including prestressing/release forces and stresses, temperature fluctuations, creep, shrinkage, and loading response. (UHPC Phase III, page 116).

5.1 Laboratory Mechanical Analysis

Before replacing the girders on Bridge 5296, four large-scale prestressed concrete girder specimens were cast at Coreslab Structures (Albuquerque) Inc. These specimens were then transported to NMSU's Structural Systems and Materials Testing Laboratory (SSMTL) for testing (UHPC Phase III, page 124). After arrival at the SSMTL, longitudinal and transverse flexural tests were performed. The details are shown in the following section.

5.1.1 Longitudinal Flexural Test

Bridge girders primarily resist bending moments and shear forces caused by traffic loads, dead loads, and environmental effects. The longitudinal flexural test replicated these bending stresses, providing insights into the girder's performance under actual service conditions.

The test determined the maximum load the girder could withstand before failure, which is crucial for ensuring that the bridge can safely support expected traffic loads.

Methodology

The flexural test setup (Figure 5.3) involved positioning two hydraulic actuators attached to steel structural frames, spaced 24 in. apart along the centerline of the girder. Each actuator was positioned 12 in. from midspan. The load from each actuator was distributed via steel spreader beams and transferred through cylindrical steel load cells and half-cylinder load points positioned above each stem. The girder was supported on four reinforced concrete short columns, each equipped with a steel column cap and a cylindrical roller support. (UHPC Phase III, Page 124).

Each girder was instrumented with 25–30 strain gauges and 2–4 embedded vibrating wire strain gauges (VWSGs), along with external instrumentation to monitor various structural responses. Specifically, string potentiometers measure vertical deflections at quarter points, midspan, and offset midspan. Linear variable differential transducers (LVDTs) recorded tension and compression at midspan, including extreme tensile strain at the stem's bottom, and compressive strain above the west stem (allowing for neutral axis tracking during loading). Electronic clinometers captured end rotations at all supports.

All instruments, except the VWSGs, were connected to a data acquisition system for real-time monitoring of load, deflection, moment, neutral axis depth, and strain. The first test was conducted on the HPC specimen, followed by testing of the UHPC specimen. Load was applied to induce a

0.1 in. increment at an initial rate of 0.05 in./min. load rate and was then increased to induce deflection at a rate of 0.1 in./min.
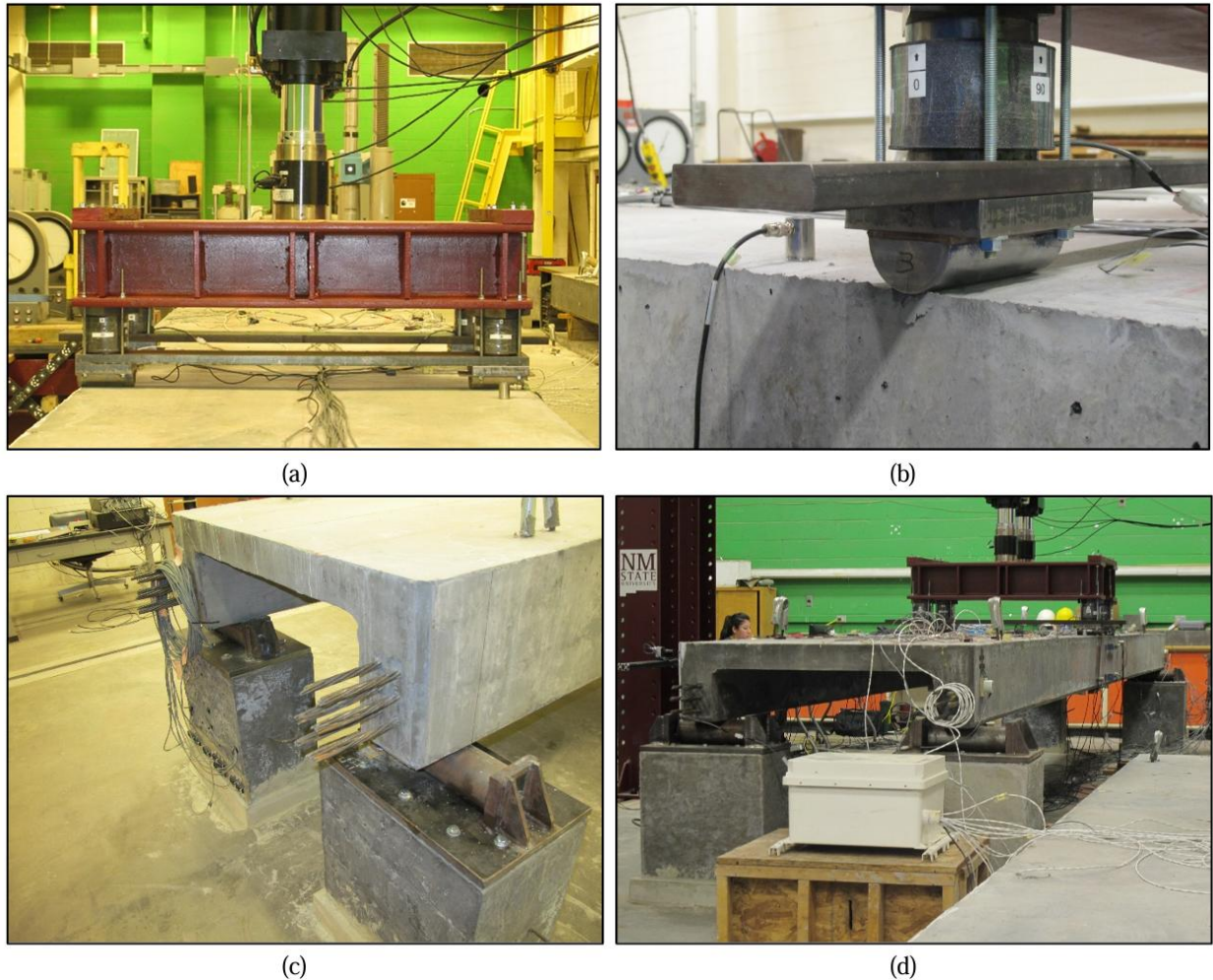
Figure 5.3. Test set up - a) hydraulic actuators and spreader beam assembly; b) load cells and loading point; c) reinforced concrete short columns with steel cap and roller support; d) fully instrumented girder test set up; (UHPC Phase III, Figure 8.34)

Results

The HPC girder experienced initial cracking in the east stem at a load of approximately 36.8 kips, identifying the cracking moment as 202 kip-ft. In comparison, the UHPC girder exhibited its first crack at a load of 49 kips with a moment of 270 kip-ft, occurring in the west stem.

The UHPC girder demonstrated a cracking moment nearly 70 kip-ft greater than that of the HPC specimen. This increase in cracking resistance is primarily attributed to the higher matrix strength of UHPC, while the high-strength steel fibers contribute to enhancing the post-cracking performance. The ultimate moment capacities were 463 kip-ft for the UHPC specimen and 419 kip-ft for the HPC specimen. (Figure 5.4) (UHPC Phase III, page 131).
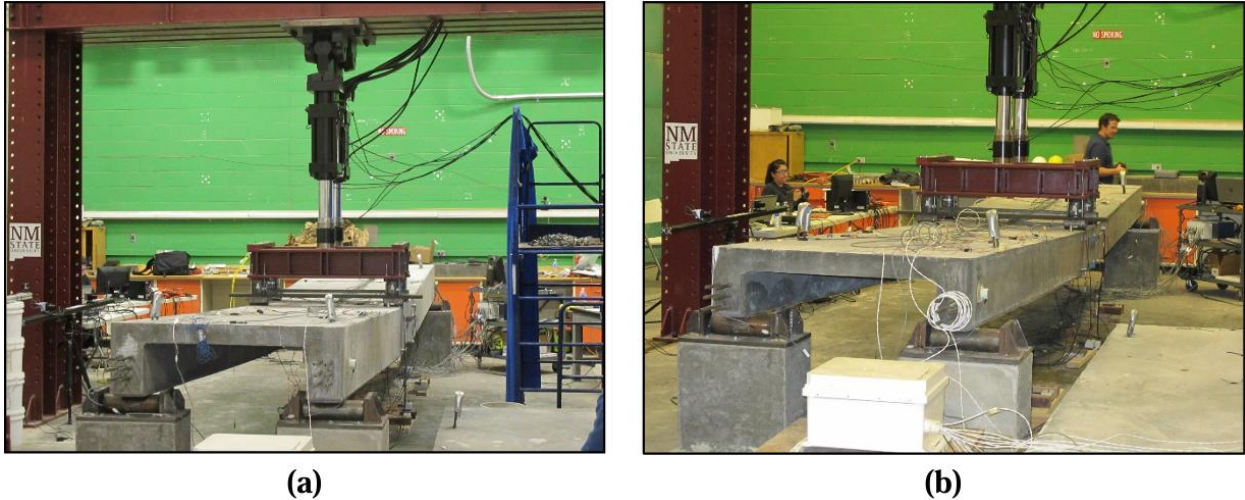
Figure 5.4. Test approaching to failure point - a) HPC girder; b)UHPC girder; (UHPC Phase III, Figure 8.42)

The HPC specimen exhibited near-linear elastic behavior until softening and initial cracking occurred at approximately 37,000 lb, with a deflection of about 0.75 in. Hairline cracks began to propagate and became increasingly visible as the beam's deflection grew. Post-cracking strength increased steadily, peaking at around 76,000 lb with a deflection of approximately 7 in. That marked the end of the test, after which the beam was gradually unloaded. Upon full unloading, the beam showed a residual midspan deflection of about 1.08 in. while still retaining some camber (UHPC Phase III, page 127).

The UHPC specimen exhibited linear elastic behavior up to approximately 40,000 lb, with significantly slower propagation of hairline cracks compared to the HPC specimen. The peak load of the HPC specimen was reached at a deflection of about 3.4 in. At the same deflection, the UHPC girder continued to gain post-cracking strength, reaching approximately 84,000 lb before significant softening began. As deflection approached 6.5 in. and cracks formed along the deck (flange) surface, the test was stopped. The girder retained a residual deflection of approximately 1.3 in. (UHPC Phase III, page 129).

5.1.2 Transverse Flexural Tests

While longitudinal flexural tests assessed the bending resistance of a girder, transverse flexural tests evaluated its ability to resist lateral bending and shear stresses induced by non-uniform loads. These loads may result from side impacts, differential settlements, or asymmetric live loads.
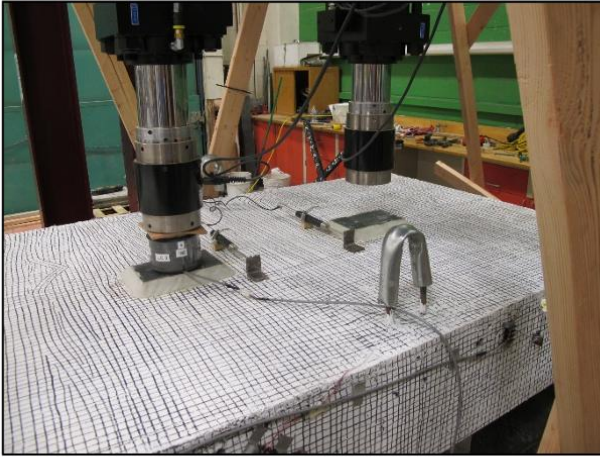
| (a) | (b) |

Figure 5.5. Transverse flexural load application - a) single location loading; b) dual loading; (UHPC Phase III, Figure 8.48)

Methodology

Structural testing frames and actuators were positioned at 24 in. and 48 in. from the end of the girder, designated as Load Point A and Load Point B, respectively (UHPC Phase III, page 138). The specimens were tested under three loading configurations.

In the first two configurations, a single actuator applied a load at the transverse midspan at each of the two locations (Figure 5.5), designated as Transverse A and Transverse B, respectively. In the third configuration, both actuators applied load simultaneously, referred to as Transverse AB.

The load was transferred to the girder surface at the transverse midspan using 1.0 in. thick steel plates measuring 5.0 in. by 7.0 in. These plates were centered beneath the hydraulic actuators and secured to the surface with high-strength, non-shrink mortar (Figure 5.6) (UHPC Phase III, page 138). Transverse loading of the full-scale specimens was applied in displacement-controlled increments of 0.025 in. at a load rate of 0.05 in./min.

(a)   **(b)**

(c)   **(d)**
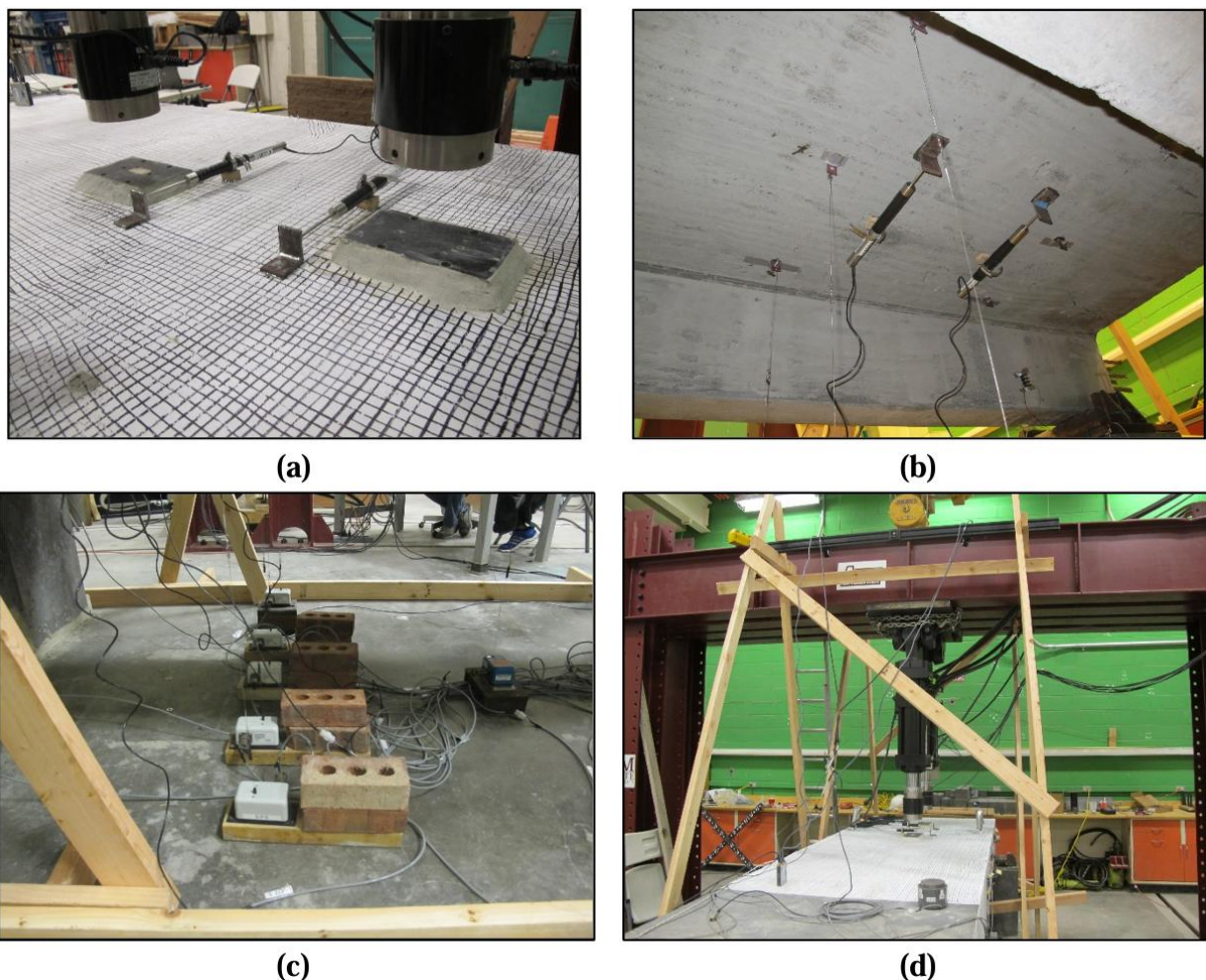
Figure 5.6. Transverse flexural testing instrumentation - LVDTs attached to the surface; a) top face; b) bottom face; c) string potentiometers placed along transverse section below load point; d) simple timber frame for DIC; (UHPC Phase III, Figure 8.49)

Results

The UHPC girder reached a cracking load of 23.2 kips near transverse A with a deflection of 0.07 in, compared to the HPC girder, which exhibits a cracking load of 12.9 kips near transverse A with a deflection of 0.05 in. This represents an approximately 57% increase in cracking load for UHPC over HPC.

Transverse A testing showed that HPC carried a maximum load of 42.1 kips with a deflection of 0.24 in, while UHPC carried a load of 50.9 kips with a deflection of 0.15 in. (UHPC Phase III, page 140, Table 8.6).

Transverse B testing revealed the HPC surface of the girder failed due to punching shear at a load of 77.9 kips, whereas the UHPC surface sustained up to 101 kips before the test was halted, demonstrating superior shear resistance.

Due to this performance disparity, only the UHPC girder was tested in the Transverse AB dual configuration. According to the test, the UHPC girder achieves an ultimate load of 144 kips with a transverse midspan deflection of 0.20 in. At this point, full-depth cracking develops at the girder end near the transverse midspan, extending longitudinally along the surface for approximately one-third of the girder's length (Figure 5.7) (UHPC Phase III, page 139).
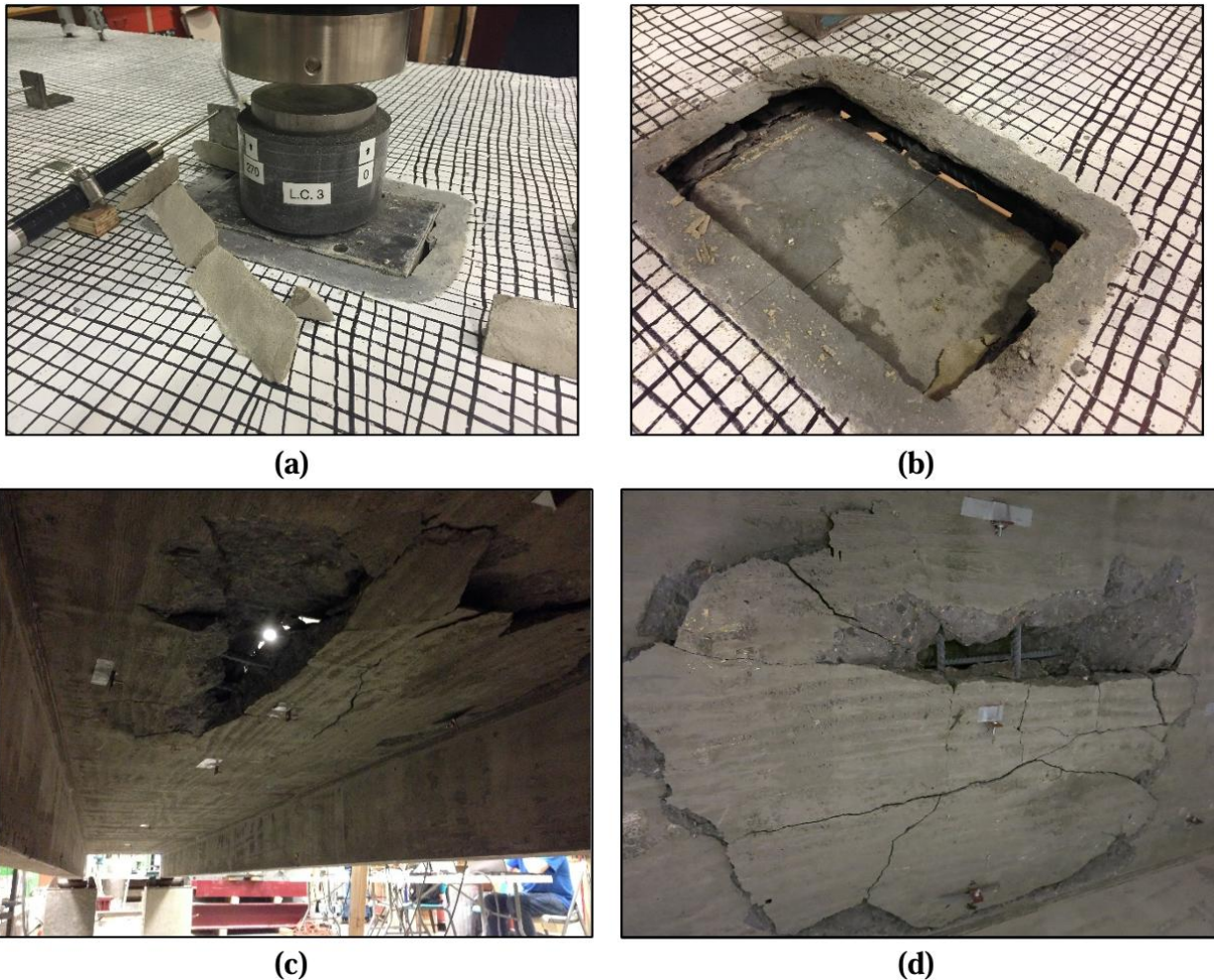
Figure 5.7. HPC specimen failure fur to punching shear - a,b) top of girder; c,d) bottom of girder; (UHPC Phase III, Figure 8.51)

5.2 Field Mechanical Analysis

The field testing was conducted at bridge 9706, formerly the location of Bridge 5296 before it was replaced with UHPC and HPC girders. During casting, auxiliary compressive strength tests were performed on specimens from each batch. Additionally, to monitor behavior and investigate the long-term performance of the UHPC bridge, it was instrumented with internal and external gauges for long-term structural monitoring.

5.2.1 Auxiliary Compressive Strength Tests

During the UHPC Phase III study, eight UHPC full-scale prestressed concrete girders were cast at Coreslab Structures (Albuquerque) Inc. The mixture proportions used for casting are provided in Table A-2 in Appendix A.

Compressive strength tests were conducted on 4 in. cube specimens at 7 and 28 days using four different batches. The girders U-6 and U-7 came from the first batch of UHPC. Similarly, the girders U-2 and U-5 come from the second batch, girders U-1 and U-4 come from the third batch and finally, the girders U-3 and U-8 come from the fourth batch. The results are as follows (UHPC Phase III, Page 176):

- First batch, an average compressive strength of 18 ksi at 7 days and 21.7 ksi at 28 days was recorded (Table 5.1)
- Second batch, only 28-day compressive strength results were recorded, with an average of 20.7 ksi (Table 5.2)
- Third batch, the average 7-day compressive strength was recorded as 20.1 psi (Table 5.3)
- Fourth batch, the average 7-day compressive strength was recorded as 20.5 psi. (Table 5.4)

Table 5.1. Compressive strength results for U-6 and U-7 (UHPC Phase III, Table 10.3)

Specimen No.	Age, days (hours)	4.0 in. (100 mm) cubes Compressive Strength, ksi (MPa)	
		Specimen	Average
CS1	7 (168)	16.7 (268)	
CS2	7 (168)	20.2 (324)	
1	7 (168)	16.3 (261)	18.0 (289)
2	7 (168)	19.5 (312)	
3	7 (168)	17.4 (278)	
4	28 (672)	20.6 (330)	21.7 (347)
5	28 (672)	22.7 (364)	

Table 5.2. Compressive strength results for U-2 and U-5 (UHPC Phase III, Table 10.6)

Specimen No.	Age, days (hours)	4.0 in. (100 mm) cubes Compressive Strength, ksi (MPa)	
		Specimen	Average
1	7 (168)	NA	NA
2	7 (168)	NA	
3	28 (672)	20.9 (335)	20.7 (5363)
4	28 (672)	20.4 (327)	

Table 5.3. Compressive strength results for U-1 and U-4 (UHPC Phase III, Table 10.9)

Specimen No.	Age, days (hours)	4.0 in. (100 mm) cubes Compressive Strength, ksi (MPa)	
		Specimen	Average
1	7 (168)	20.3 (325)	20.1 (5209)
2	7 (168)	19.9 (319)	
3	28 (672)	TBD	TBD
4	28 (672)	TBD	

Table 5.4. Compressive strength results for U-3 and U-8 (UHPC Phase III, Table 10.12)

Specimen No.	Age, days (hours)	4.0 in. (100 mm) cubes Compressive Strength, ksi (MPa)	
		Specimen	Average
1	11 (264)	20.6 (330)	20.5 (5286)
2	11 (264)	20.4 (327)	
3	28 (672)	TBD	TBD
4	28 (672)	TBD	

5.2.2 Instrumentation Plan

The initial instrumentation plan included a total of 324 gauges, distributed as follows:

- 192 gauges - externally located along the depth of each stem at every quarter point of each beam, with 2 gauges per stem (4 per beam)
- 96 gauges - internally located atop each stem at every quarter point of each beam, with 1 gauge per stem (2 per beam)
- 36 gauges - internally located along the flange of every quarter point of beams 1 and 2 (an interior and exterior beam), 3 gauges per beam

Due to high initial costs, a reduced instrumentation plan was implemented. Three options were analyzed to eliminate gauges, as shown below:

- Removing internal gauges
- Eliminating distant quarter point gauges
- Alternating quarter point gauges (selected)

The alternating placement of gauges at quarter points was chosen to minimize cable length while still maintaining effective data collection. Additionally, the number of gauges internally located along the flanges of beams 2 and 3 was reduced from 5 to 3. Figures 5.8 and 5.9 illustrate the cross-sectional layout of the gauge locations, and Figure 5.10 provides the plan view.
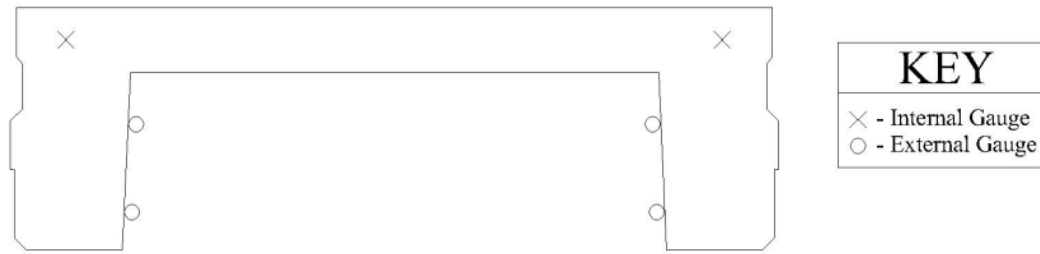
Figure 5.8. Cross section at A (UHPC Phase III, Figure 9.2)

Figure 5.9. Cross section at D (UHPC Phase III, Figure 9.8)
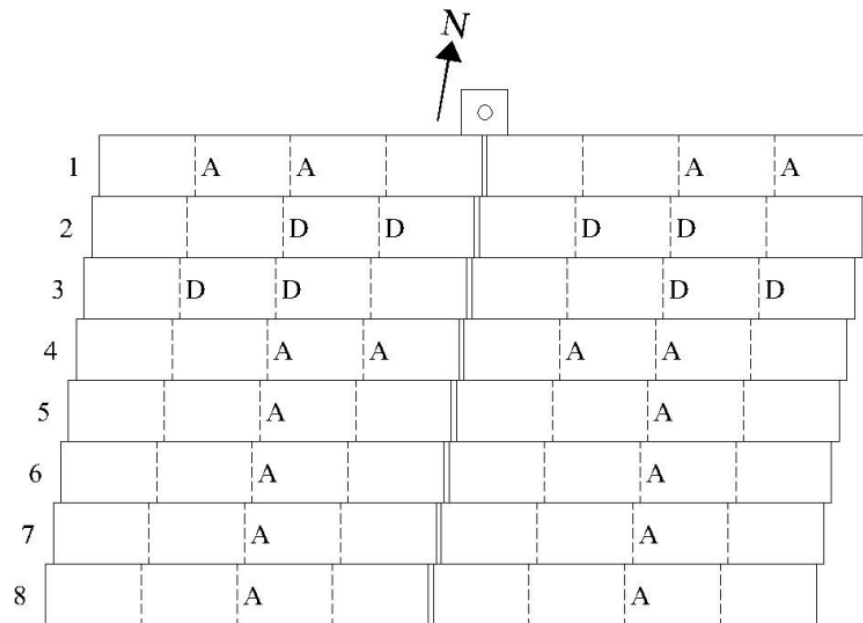
Figure 5.10. Plan view of instrumentation plan (UHPC Phase III, Figure 9.9)

5.2.3 Monitoring bridge 9706

Field testing was conducted to assess the structural response of NM Bridge No. 9706 under various load conditions and to compare the performance of the UHPC and HPC spans. A diagnostic test was performed to identify critical load paths. Proof tests were conducted using trucks loaded to their maximum allowable weight to evaluate the structure's capacity, identify critical load paths, and induce peak strains.

Methodology

Field testing was conducted using NMDOT standard 10 yd³ dump trucks with an average weight of 63.4 kips (UHPC Phase IV, Page 42). Between one and four trucks were used to create the following load configurations: single truck (ST), double trucks side-by-side (DT), triple trucks side-by-side (TT), single truck back-to-back (STBB), and double trucks back-to-back (DTBB).

A total of ten truck paths were employed: ST and STBB were used for paths 1–6, DT and DTBB were used for paths 7–9, and TT was used for path 10. Testing included various velocities: 5 mph for slow-moving loads, 45–55 mph for fast-moving loads, and incremental loading with increasing speeds. (UHPC Phase IV, Page 43).

Estimations of bridge capacity, and an analysis of expected behavior for the UHPC and HPC girders ensured that the diagnostic and proof tests did not damage the bridge and that their responses were accurately predicted. (UHPC Phase V, page 49).

Diagnostic test

A pre-test was conducted with slow-moving truck load paths to calibrate the BDI strain transducers and verify that strain values closely matched the expected values calculated beforehand. A total of nine truck load paths were designed, and each path was repeated twice to confirm consistent behavior.

The total applied truck load was intentionally kept below the target proof load due to uncertainties in the bridge response. The truck load paths were designed not to maximize load, but to compare strain behavior, ensure effective load distribution among adjacent girders, and evaluate the initial behavioral response of the UHPC and HPC spans, both designed with comparable flexural capacities.

Proof test 1

The objective was to apply the greatest possible load to the bridge without exceeding the available moment capacity. The testing procedure included:

1) Preliminary slow-moving and incremental truck load paths were conducted to calibrate the BDI Strain Transducers. These preliminary loads were conducted at the beginning of each of the three proof testing days.
2) A repeat of all diagnostic load paths.
3) Sequence 1: Preliminary Testing:
    *   Sequence 1.A consisted of applying a single 10 yd³ truck as a slow-moving load sequentially through three preliminary single truck load paths
    *   Sequence 1.B consisted of applying a slow-moving load through three preliminary double truck load paths
    *   All three paths were repeated during the proof test for redundancy
4) Sequence 2: Diagnostic Test Repetition:
    *   Sequence 2.A. Applied single slow-moving truck loads
    *   Sequence 2.B. Applied double slow-moving truck loads

- Purpose: Directly compared strain behavior and results between the diagnostic and proof test

5) Sequence 3: Incremental Loading:
   - Sequence 3.A: Applied a single 10 yd³ truck as an incremental load through six single truck load paths
   - Sequence 3.B: Applied an incremental double truck load for three double truck load paths
   - Sequence 3.C: Applied an incremental triple truck load for one triple truck load path

6) Sequence 4: Back-to-Back Truck Loading
   - Single and double truck loads were applied back-to-back
   - Load trucks were positioned so that:
     - Each truck's back axles were approximately 3 ft (0.91 m) apart
     - The back-to-back distance between truck ends was less than 6 in.
     - Each truck's end extends 1.5 ft (0.46 m) past the back axle

Results

During the diagnostic test, strains were continuously monitored and recorded with 36 BDI strain transducers.

- For the UHPC single moving truck load, the maximum strain recorded was 87.9 με (path 1), while for the HPC single moving truck load, the maximum strain recorded was 78 με (path 1)
- For the UHPC double moving truck load, the maximum strain recorded was 113.5 με (path 7), and for the HPC double moving truck load, the maximum strain recorded was 125.6 με (path 8)
- In the incremental single truck load tests, the maximum recorded strains for the UHPC span were 102.5 με (paths 1) and 89 με (path 6). For the HPC span, the maximum recorded strains were 84.5 με (paths 1) and 84.2 με (path 4)
- Finally, in the incremental moving truck load tests, the maximum recorded strain for the UHPC span was 116 με (path 7). For the HPC span, the maximum recorded strain was 142 με (path 8)

The expected strain values were generally greater than the measured strain values. (UHPC Phase IV, Page 93).

Proof Test 1 Results (UHPC Phase III, page 113):

Single Moving Truck Load Tests (Sequences 1.A and 2.A):

- UHPC: Maximum strains: 97.5 με (Path 6), 86.5 με (Path 1)
- HPC: Maximum strains: 90.7 με (Path 1), 89.2 με (Path 4)

Double Moving Truck Load Tests (Sequences 1.B and 2.B):

- UHPC: Maximum strains: 120 με (Path 8), 113 με (Path 7)
- HPC: Maximum strains: 125 με (Path 8), 118 με (Path 7)

Incremental Single Truck Load Tests (Sequence 3.A):

- UHPC: Maximum strains: 99 με (Path 6), 97 με (Path 1)
- HPC: Maximum strains: 96 με (Path 4), 94 με (Path 6)

Incremental Double Truck Load Tests (Sequence 3.B):

- UHPC: Maximum strains: 126 με (Path 8), 109 με (Path 7)
- HPC: Maximum strains: 152 με (Path 8), 134 με (Path 7)

Incremental Triple Truck Load (Sequence 3.C):

- UHPC: Maximum strain recorded: 127.5 με (Path 10)
- HPC: Maximum strain recorded: 152.3 με (Path 10)

Incremental Back-to-Back Single Truck Load Tests (Sequence 4.A):

- UHPC: Maximum strains: 120 με (Path 6), 110 με (Path 1)
- HPC: Maximum strains: 112.5 με, 103.2 με

Incremental Back-to-Back Double Truck Load Tests (Sequence 4.B):

- UHPC: Maximum strains: 146.5 με (Path 7), 153.6 με (Path 8)
- HPC: Maximum strains: 166 με (Path 8), 145 με (Path 9)

(Refer to UHPC Phase IV, Page 116 for a comparison between calculated and expected strains).

From Proof Test 3 Results (UHPC Phase III, Page 138):

Single Truck Moving Load:

- UHPC: Maximum strain recorded: 121 με
- HPC: Maximum strain recorded: 122 με

(Both recorded at Path 1 on the exterior girders, as expected)

Single Truck Incremental Moving Load:

- UHPC: Maximum strain recorded: 123 με
- HPC: Maximum strain recorded: 124 με

(Both recorded at Path 1 on the exterior girders, as expected)

Single Back-to-Back Incremental Moving Load:

- UHPC: Maximum strain recorded: 132 με
- HPC: Maximum strain recorded: 173 με

Double Back-to-Back Incremental Moving Load:

- UHPC: Maximum strain recorded: 179 με
- HPC: Maximum strain recorded: 194 με

Triple Trucks Side-by-Side Incremental Moving Load:

- UHPC: Maximum strain recorded: 147 με
- HPC: Maximum strain recorded: 182 με

5.3 Discussion and Findings

- The results (UHPC Phase III, page 135) reveal that the maximum strains developed near midspan
- According to lab tests, a difference in strain magnitude was observed, with HPC reaching approximately 1300 με and UHPC reaching only 1025 με
- According to field tests, strain measurements were significantly lower than those recorded in laboratory tests. This discrepancy arises because laboratory tests push materials to ultimate limits to determine their full performance capacity. In contrast, field tests focus on ensuring the safety and serviceability of the structure under real-world conditions rather than testing its ultimate failure limits

6. EXPLORATION OF UHPC IN NEW MEXICO

Besides the application in bridge girder, UHPC has the potential for broader use in various structural elements. To complement the previously reviewed tests, additional UHPC applications were explored, including joint applications; UHPC shear keys in concrete bridges, composite beams made with normal strength concrete (NSC), and UHPC and UHPC overlays on bridge decks.

6.1 Joint Applications

When placing box beams, it is essential to connect the sections using joints. However, joints often represent the weakest part of the structure due to limitations in bonding between the components, since they are responsible for transferring loads from one beam to another. To address this issue, UHPC can become an excellent candidate for joint filling, offering superior tensile strength, excellent bonding capabilities, and enhanced reinforcement of vulnerable areas.

Methodology

A slab-joint-slab system was designed to simulate the behavior of box girders (Figure 6.1-6.3) to investigate the behavior of UHPC developed at NMSU for joint applications. The system was loaded on one side of the specimen to force load transfer through the joint. The joint was filled with UHPC, while the slab-joint-slab system was constructed with normal-weight concrete.

The specimen was instrumented with sensors to measure its behavior under the applied loads. The system was subjected to load–unload cycles, with the weight incrementally increasing until failure occurred. Additionally, non-shrink grout, typically used by the NMDOT, was tested for comparison with UHPC to evaluate performance differences (UHPC Phase IV, page 455).

The slab-joint-slab system in this study was based on standard NMDOT (2018) shapes, with minor modifications to accommodate the geometric features of the joint. The compressive strength of the slab concrete was tested at 28 days following ASTM C39 standards. Time-dependent tests were conducted on the joint material, evaluating compressive strength (ASTM C39) and flexural tensile strength (ASTM C78) at 7, 14, and 28 days.
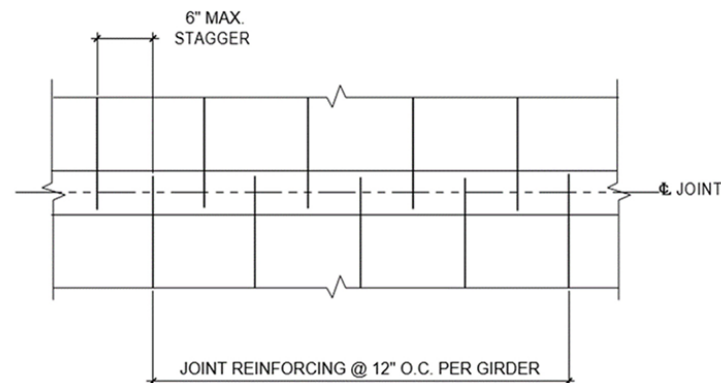
Figure 6.1. Typical NMDOT staggered bar lap detail (UHPC Phase IV, Figure 5.3)
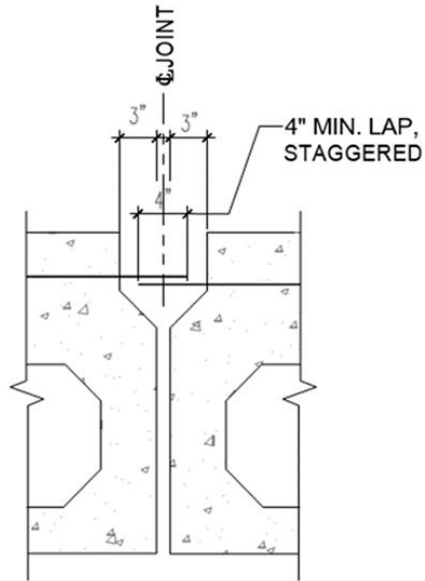
Figure 6.2. NMDOT box girder joint lap splice cross section (UHPC Phase IV, Figure 5.4)
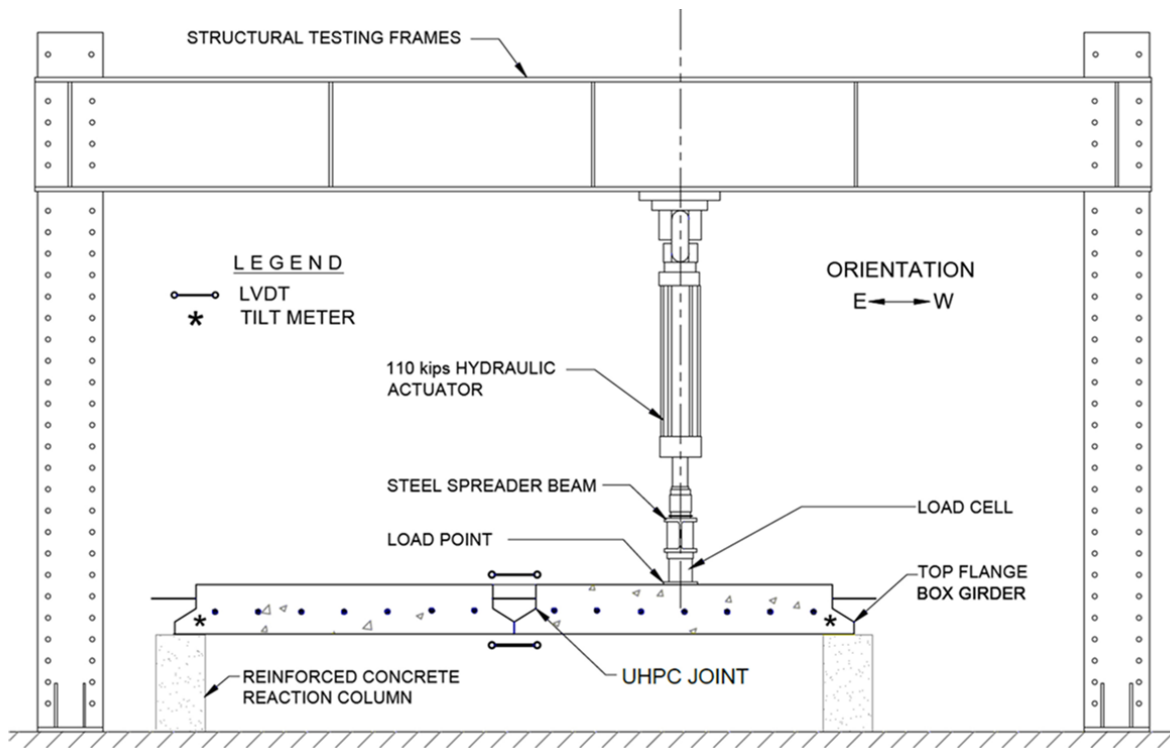
Figure 6.3. North view of test set up (UHPC Phase IV, Figure 5.7)
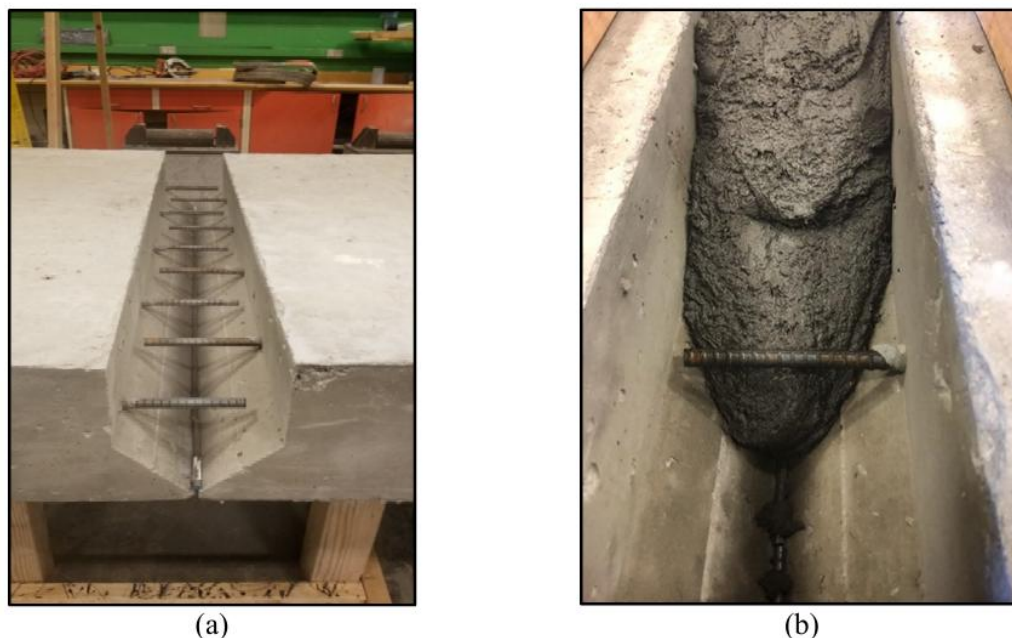
Figure 6.4. View of experimental joint - a) prior to casting; b) during casting; (UHPC Phase IV, Figure 5.13)

Materials

The mixture was proportioned using sand from Socorro, New Mexico; commercially available Rio Grande Type I/II portland cement; Class F fly ash; and Rheomac SF 100 silica fume. Additionally, the mixture included HRWRA Master Glenium 3030 NS, and 1.5% by volume of 0.5 in. straight steel fibers. The cementitious materials consisted of 80% portland cement, with 20% SCMs composed of silica fume and fly ash in a 50/50 ratio (10% each). The sand content was 1,700 lb/yd³, and the water-to-cementitious material (w/cm) ratio was 0.15, with the addition of the HRWRA. The detailed mixture proportions are provided by Table A-5, in Appendix A.

Results

As expected, UHPC joints significantly outperformed traditional grout joints, demonstrating superior strength and load capacity. During cyclic loading, UHPC joints (Figure 6.4) exhibited minimal separation, enabling them to sustain greater loads with less deflection. The joint system's performance was notably influenced by the number, size, and spacing of the rebar. Specimens with a greater amount or larger diameter of rebar exhibited greater strength with reduced vertical displacement under load.

During testing, three distinct failure modes were observed (Figure 6.5-6.8): separation between the joint and slabs, crushing of the weaker joint material due to flexural stresses, and diagonal cracking in the concrete slab along the rebar path (UHPC Phase IV, page 543).

Figure 6.5. Specimen No. 1 - failure at north face; (UHPC Phase IV, Figure 5.38)

Figure 6.6. Specimen No. 2 - initial separation at bond point; (UHPC Phase IV, Figure 5.59)
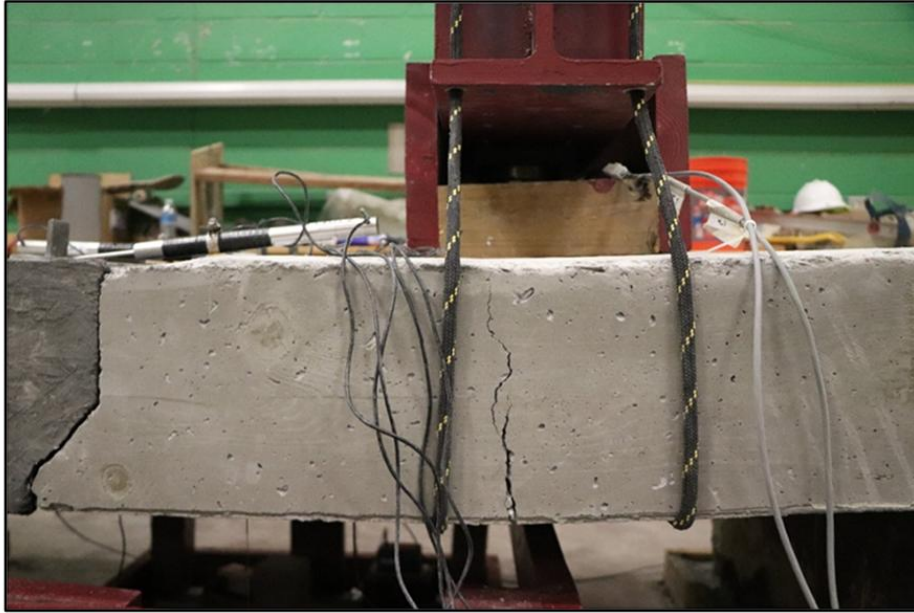
Figure 6.7. Specimen No. 3 - failure at south face; (UHPC Phase IV, Figure 5.67)

Figure 6.8. Specimen N0. 4 - failure of system; (UHPC Phase IV, Figure 5.87)

Limitations

A literature review referencing the Idaho Department of Transportation identified key limitations associated with UHPC applications (Ebrahimpour et al., 2018). Their extensive use of UHPC for connections in precast bridge decks revealed several challenges:

- Proper installation requires rigorous preparation, which can sometimes be difficult to achieve
- The material had a fast setting time, necessitating batching in small quantities

- Specialized portable field mixing equipment is required, making the process labor-intensive.
- Due to its "watery" consistency, placing UHPC on steep grades presents challenges.

6.2 Shear Keys in Concrete Bridges

Non-proprietary UHPC shear keys were compared to a non-shrink grout shear key commonly used by the NMDOT. Given UHPC's superior strength, it was expected to offer improved performance over the standard material. The objective of this comparison was to evaluate whether UHPC provided a more effective bond with precast concrete girders. The mixture proportions are presented under Table A-6, in Appendix A.

The inclusion of steel fibers in the UHPC enhanced its performance by bridging micro-cracks that are otherwise unavoidable. This feature increased the durability and sustainability of the shear key when UHPC was implemented.
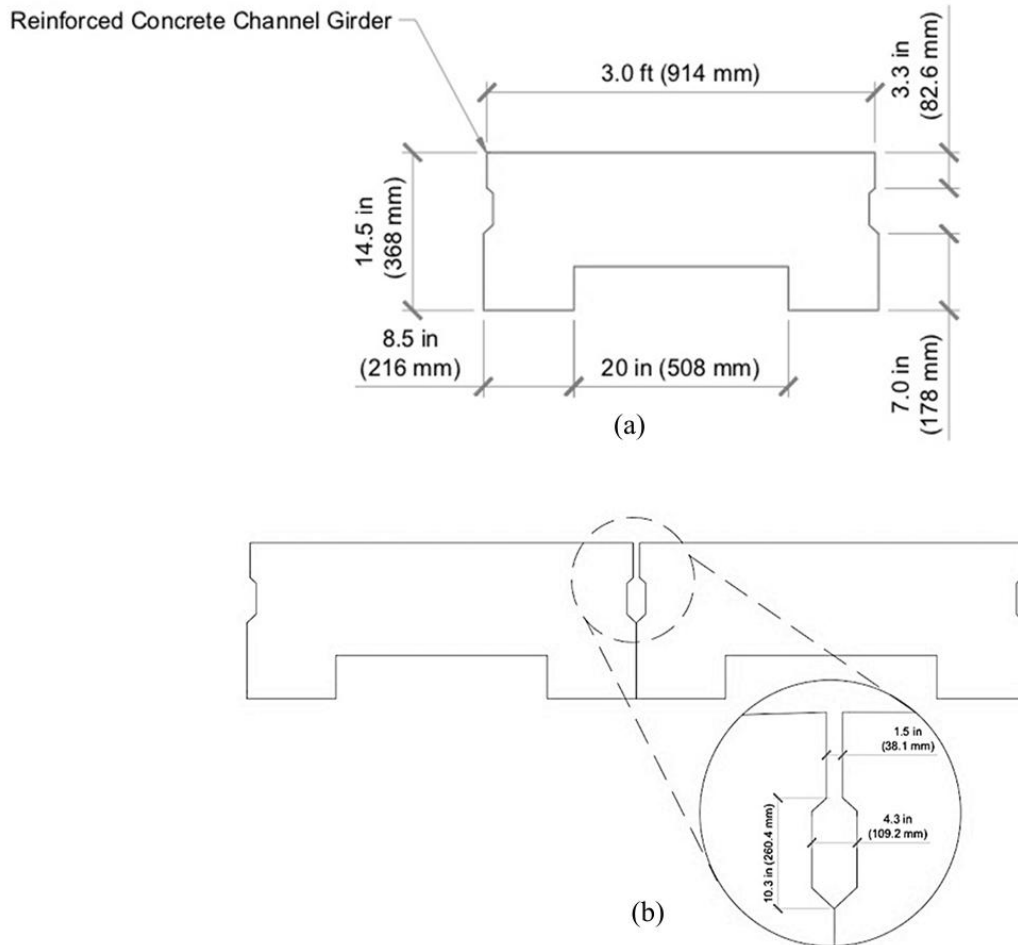
Figure 6.9. Bridge 5296 girder cross section - a) reinforced concrete channel girder cross-section; b) shear key detail; (UHPC Phase IV, Figure 5.109)

93

Methodology

To evaluate the behavior of the shear keys and the two different grouting materials, six tests were conducted on full-scale, 25-foot-long (7.62 m) reinforced concrete channel girders (Figure 6.9). The tests varied based on whether UHPC or non-shrink grout was used as the grouting material.

Four flexural tests (Figure 6.10) were performed on the jointed girders using a four-point loading configuration, with the load applied at the mid-span of the eastern girder. Additionally, two shear tests were conducted using a four-point loading configuration, with the load applied approximately 12 in. from the edge of the girder support on the eastern girder.

By applying the load exclusively to the eastern girder, the load transfer through the shear key was more effectively observed. Flexural testing of the girders included 1,000 load–unload cycles to achieve an estimated service-load deflection of 0.40 in. (UHPC Phase IV, Page 546). The cyclic loading criteria were determined based on deflection limits specified in the AASHTO LRFD Bridge Design Specifications (UHPC Phase IV, Page 545).
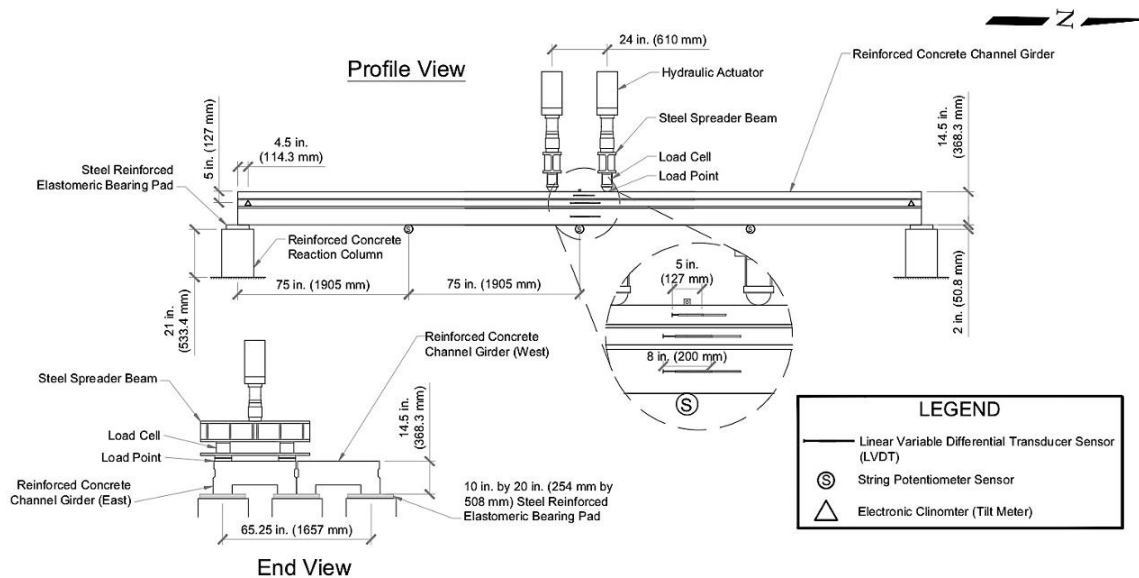
Figure 6.10. Profile view of two-girder system flexural test set up and instrumentation (UHPC Phase IV, Figure 1.110)

Results

UHPC met expectations and proved to be an excellent candidate for replacing the non-shrink grout shear key currently used by the NMDOT. In flexural tests, UHPC demonstrated effective bonding with concrete girders, even when the grout was poorly bonded due to lack of pre-wetting. It successfully transferred loads without requiring additional post-tensioning or lateral compression. Furthermore, UHPC exhibited less variation in the moment distribution factor across load cycles compared to non-shrink grout, indicating superior long-term performance.

In shear tests, UHPC showed no joint opening during load transfer, further demonstrating its superior performance over non-shrink grout (UHPC Phase IV, Page 622).

94

6.3 Composite Beams

Fabricating composite beams strengthens critical areas rather than fully replacing them with UHPC. A comparative study was conducted between reinforced and unreinforced beams made of UHPC and normal strength concrete (NSC). Variations include using a single or multiple layers of UHPC combined with NSC in the remaining cross-section, with UHPC specifically incorporated into the shear region of the beams. The mixture proportions are listed under Table A-7, in Appendix A.

Several specimens were tested with different UHPC layer placements (Figures 6.11 to 6.18), including top, bottom, or both, with or without reinforcement. The study aimed to determine the optimal UHPC placement for enhancing structural performance. (UHPC Phase IV, page 625).
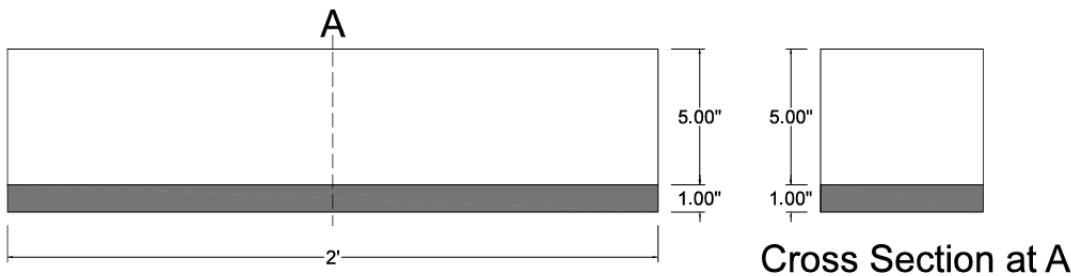
Figure 6.11. Composite beam design with UHPC at the bottom point (UHPC Phase IV, Figure 5.152)
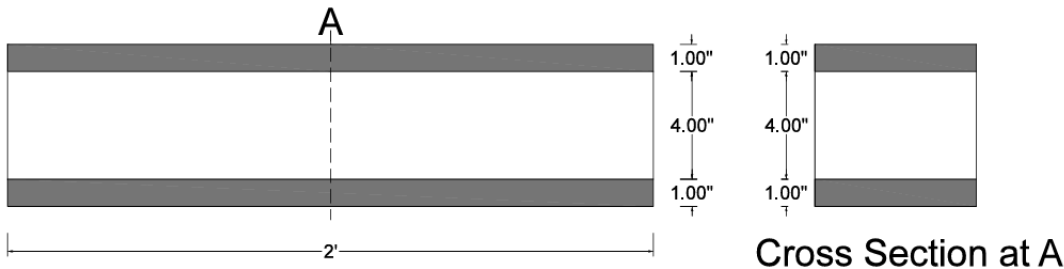
Figure 6.12. Composite beam design with UHPC at the top and bottom points (UHPC Phase IV, Figure 5.153)
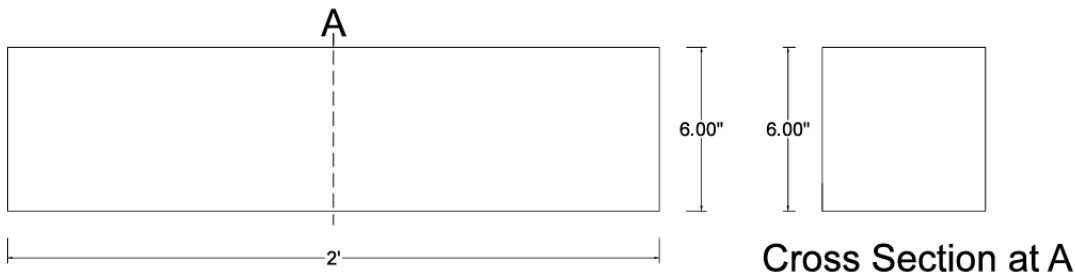
Figure 6.13. NSC beam design (UHPC Phase IV, Figure 5.154)
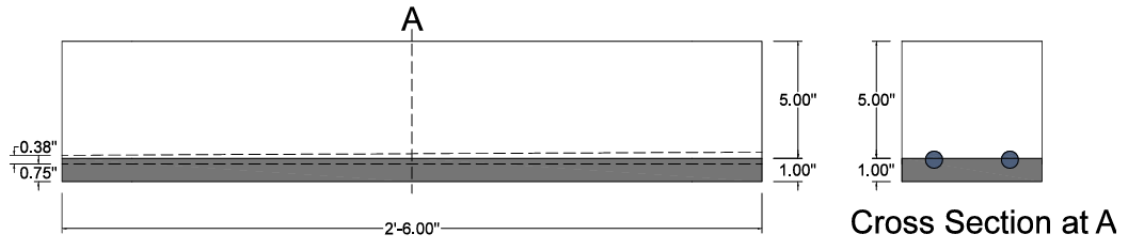
Figure 6.14. Composite beam design with UHPC at the bottom point and 2 #3 bars near the interface (UHPC Phase IV, Figure 5.155)
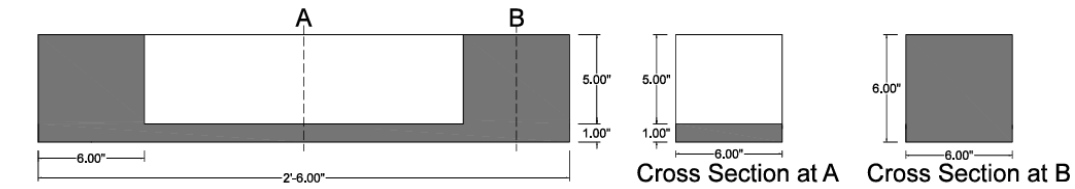
Figure 6.15. Composite beam design with UHPC at the bottom point and at the end points (UHPC Phase IV, Figure 5.156)
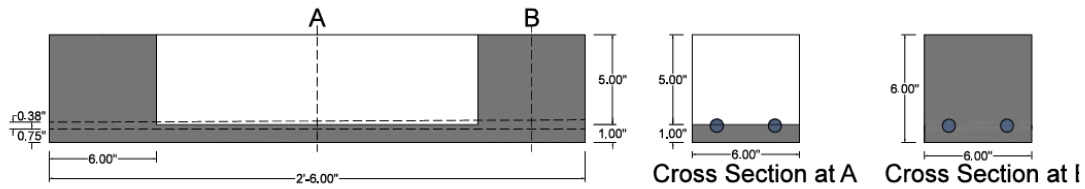
Figure 6.16. Composite beam design with UHPC at the bottom and at the end points with 2#3 bars near the interface (UHPC Phase IV, Figure 5.157)
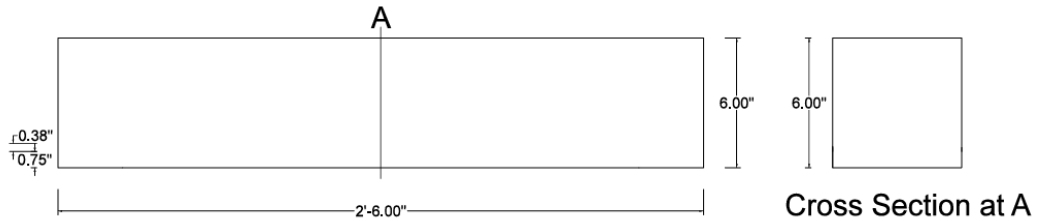
Figure 6.17. NSC beam design (UHPC Phase IV, Figure 5.158)

Figure 6.18. NSC beam design with reinforcement (UHPC Phase IV, Figure 5.159)

Methodology

Tests (Figures 6.19 and 6.20) were conducted on beams measuring 6 in. by 6 in., with lengths of 24 and 30 in. Each test included three specimens: one beam with a concrete cross-section and two beams with composite cross-sections. To ensure a strong bond between UHPC and NSC, the materials were mixed and cast simultaneously.

At the interface, rodding was performed to a depth of 0.5 in., followed by vibration using a vibrating table to further enhance bond integrity (UHPC Phase IV, Page 625).

The specimens were cast and cured with sensors installed to monitor their behavior. They were then subjected to loading at the beam midpoints, while linear displacements were recorded (UHPC Phase IV, Page 628).

String potentiometers were placed at midspan, both at the top and bottom of the beam. Load cells were positioned at the center below both supports. In addition to these sensors, LabView software was used for real-time data recording, allowing continuous observation of the specimen behavior during testing and ensuring accurate data collection for future analysis (UHPC Phase IV, page 628 for details on the test setups).
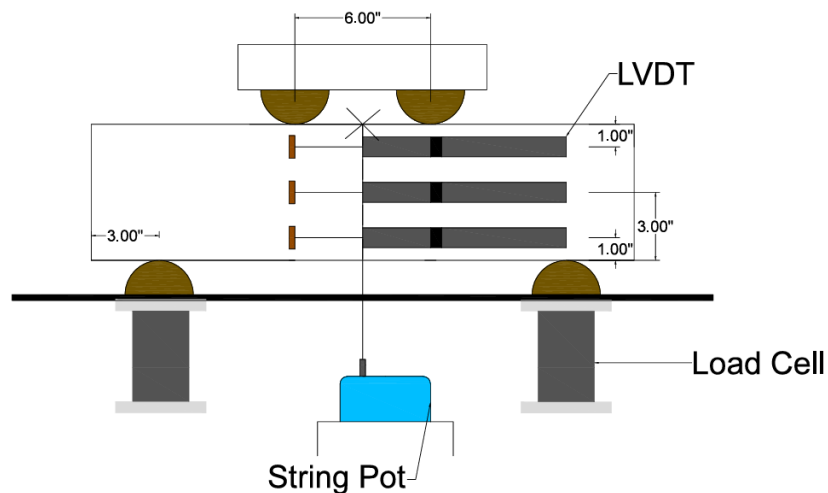
Figure 6.19. Instrumentation set up for NSC beams (UHPC Phase IV, Figure 5.160)

Figure 6.20. Test set up for beams with 1 in. of UHPC at the bottom and at the top (UHPC Phase IV, Figure 5.165)

Results

The NSC beam achieved a maximum load of just over 6,000 lb. However, adding a 1in. UHPC layer to the bottom increased the maximum load to over 11,000 lb. Further increasing the thickness of the UHPC layer on the compression face resulted in ultimate loads approaching 15,000 lb (UHPC Phase IV, Page 632).

The presence of UHPC in the cross-section of beams significantly influenced their load-deflection behavior. Beams with UHPC layers demonstrated substantially greater ultimate load capacities compared to those constructed entirely of NSC. Additionally, the inclusion of UHPC reduced the maximum deflection before failure, enhancing the overall stiffness and performance of the composite beams.

6.4 Thin-Bonded Overlay on Deteriorated Bridge Decks

After conducting structural-level field tests on UHPC, NMSU began exploring its broader applications. One promising use is strengthening bridge decks, where UHPC serves as an overlay material to enhance load capacity and extend service life. Results from loading tests (UHPC Phase IV, Page 671) confirm that UHPC can effectively function as an overlay material, provided that proper surface preparation is performed.

Building on this concept, UHPC was used to rehabilitate the bridge deck of Bridge 7032 in Socorro, NM. The following sections detail the mock slab placements, field implementation, and monitoring of a non-proprietary UHPC overlay applied to the concrete deck of Bridge 7032.

6.4.1 UHPC Overlay Mock Slab

Three mock-up placements were initially conducted. However, since the 2020 construction season ended before the UHPC overlay could be placed, the contractor scheduled a fourth mock-up placement in April 2021 to reacquaint the construction crew with UHPC practices and ensure a smooth implementation. UHPC overlay mock slab placements were conducted at A1 Quality Ready Mix in Socorro, NM. The mixture design is detailed in Chapter 3.9 of this document, with parameters used shown in Table A-8.

The first three batches served to determine the optimal volume for the high-energy pan mixers used. Specifically, during the first mock-up placement, a batch with three bags of silica fume (75.0 lbs.) was used, which resulted in a total volume of 0.385 yd^3. However, due to mixing difficulty in the pan mixers, the volume was reduced to two (50.0 lbs.) and one (25.0 lbs.) silica fume bags for the second mock-up, resulting in a total volume of 0.256 yd^3 and 0.128 yd^3, respectively. During the third mock-up placement, all batches consisted of 0.200 yd^3, which was found to be an optimal volume for the high-energy pan mixers.

During the first mock-up placement, ADVA 198 was used as the HRWRA, which prevented the UHPC from setting after seven days of curing. As a result, samples from the first mock-up could not be properly tested. For the second and third mock-ups, MasterGlenium 3030 was used as the HRWRA.

Methodology

The High-Performance Deck (HPD), a 20 ft. × 20 ft. unreinforced deck, was cast (Figure 6.21) in forms with a minimum average textured depth of 0.25 in. to ensure optimal bonding with the UHPC overlay, and then field-cured for eight days before the UHPC application (UHPC Phase V, Page 79).

Figure 6.21. HPD surface preparation (UHPC Phase V, Figure 4.1)

Mixing Process

The mixing process began with the simultaneous addition of dry materials (sand, cement, and fly ash) from the volumetric truck into the mixer, followed by the separate addition of silica fume. Dry mixing was performed for 30 seconds to 1 minute, after which approximately 80% of the total water was added, followed by the HRWRA. The remaining 20% of water was added gradually to account for extra moisture in the sand and to prevent exceeding the desired consistency of the UHPC. Mixing continued until the desired workability was achieved, at which point the steel fibers were added, and mixing continued for an additional two minutes. Total mixing time varied between 10 to 15 minutes.

Specimen Preparation

After the mixing process, temperature, slump, and spread of the UHPC were measured. A total of five batches were produced and used for sample testing in both the second and third mock-up placements.

After obtaining slump and slump-flow measurements, 4 in. cube specimens and prismatic specimens measuring (3 x 4 x 16 in.) were cast in steel molds. Across all mock-up placements, a total of 24 cube samples and eight prismatic specimens were cast.

Curing Regimen

After transporting the samples to NMSU, the cube samples were cured under two different conditions:

1) Half were kept under ambient conditions of 68°F and 30% Relative Humidity.
2) Half were cured in a wet room at 100% Relative Humidity.

The prismatic samples were cured in a wet room for seven days and then maintained under ambient conditions until testing.

Testing

Various tests were conducted, including slump, slump-flow, compression, and flexural tests. Slump and slump-flow tests were performed for each batch, targeting values of 7 in. and 10 in., respectively. Compression tests were conducted on 24 cube samples at intervals of 2, 4, 7, 14, 28, and 56 days, with target compressive strengths of 10,000 psi at 7 days and 17,000 psi at 28 days. Flexural tests were conducted on eight prismatic samples at 7, 14, 28, and 56 days.

Direct tension pull-off (Figure 6.22) tests were performed after mock-ups 2 and 3. These tests involve drilling 1.875 in. holes to a depth of approximately 3 in. into the concrete. Steel plates were then attached to the core samples using epoxy, and a total of 15 pull-off tests were attempted (UHPC Phase V, Page 88).
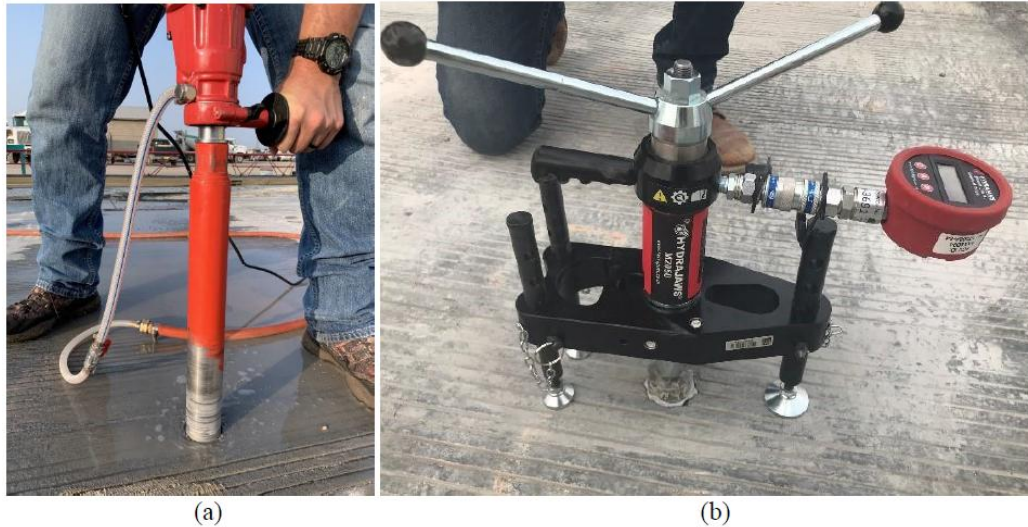
Figure 6.22. Pull-off test - a) core drilling; b) set up; (UHPC Phase V, Figure 4.7)

Additional pull-off tests were conducted on a 25-ft. long high-performance concrete (HPC) girder located in the materials laboratory at NMSU. The girder featured a 1 in. thick overlay, and eight core samples were successfully tested using the same methodology.

Results

Mock-up 1 Test Results

During the first mock-up placement, ADVA 198 was used as the HRWRA which did not allow the UHPC to set after seven days of curing. Therefore, samples from the first mock-up could not be properly tested.

Mock-up 2 Test Results

Mock-up 2 consisted of five batches. During the slump and spread tests, it was observed that batch 2, which was mixed for a longer time, exhibited a drier and stiffer consistency. While mixing time was not recorded for Mock-up 2, it was documented for Mock-up 3 after it was noted that mixing time significantly influenced the dryness and stiffness of the mixture.

In Mock-up 2, the slump for the first batch was 8 in., with a spread of 13 in. The second batch exhibited a slump of 2 in. and a spread of 8.25 in. The remaining three batches recorded slumps of 6.75 in., 4.75 in., and 8.25 in., with corresponding spreads of 12.7 in., 10.1 in., and 12.3 in., respectively (UHPC Phase V, Page 82).

Mock-up 3 Test Results

In Mock-up 3, the mixing times for the five batches varied from 11.5 to 14.5 minutes. The amount of water added to the mixture was adjusted in the first three batches to achieve the desired workability, targeting the slump values stated in the methodology. The slump values for these batches were 10.3 in., 10 in., and 9 in., respectively. The final two batches were within the target range, with slumps of 8.5 in. and 8.75 in.

Only Mock-up 3 achieved the target compressive strength of 10,530 psi at 7 days. However, neither of the mock-ups met the 56-day target strength of 17,000 psi, as specified by ASTM C1856 (2017), with Mock-up 2 coming closest at 13,820 psi.

The modulus of rupture (MOR) values for both mock-ups were comparable at 14 and 28 days, measuring 970 psi at 14 days and 1,060 psi at 28 days. However, Mock-up 3 demonstrated superior MOR at 7 and 56 days, with values of 1,260 psi and 1,250 psi, respectively.

Pull-off Bound Strength Test Results

Of the 15 pull-off test attempts, the first eight resulted in zero-strength readings, as the overlay debonded from the concrete substrate during core drilling. However, six tests were successfully completed.

The recommended tensile bond strength was 150 psi, with 250 psi indicating excellent bond strength. The six successfully tested samples average a bond strength of 230 psi. Two samples did not pass the test, resulting bond strengths of 100 psi each. The remaining four samples achieve bond strengths of 462 psi, 199 psi, 263 psi, and 254 psi, with three samples exhibiting excellent bond strength. These results highlight the importance of surface preparation, especially maintaining saturated surface-dry (SSD) conditions, in ensuring a strong bond between the overlay and substrate materials.

For the channel girder pull-off tests conducted in the laboratory, bond strengths across the eight core samples varied, with values ranging from 45.3 psi to 317 psi. While some individual samples fell below the ACI-recommended bond strength of 150 psi, the average bond strength across all eight samples was 171 psi, exceeding the recommended threshold.

Modified steel fibers for achieving the required compressive strength

Since neither Mock-up 2 nor Mock-up 3 met the required 56-day compressive strength (17 ksi), a modified steel fiber, designated as Fiber-U (Figure 6.23), was investigated. The UHPC mixture, after modifications, used (0.145-37.5/62.5-1600) included 1.75% steel fibers by volume, with dimensions of 0.012 in. x 0.51 in.

Figure 6.23. Previously utilized Steel Fiber - U vs. Modified Steel Fiber - U (UHPC Phase V, Figure 4.5)

Two re-evaluation mixtures were tested, with and without ice to manage the mixture temperature. Using ice reduced the mixture temperature by 5 °F. The slump decreased from 6 in. in the first mixture to 5 in. in the second. The compressive strengths at 7 days were 16,030 psi for the first mixture and 16,920 psi for the second. At 28 days, the compressive strengths were 17,560 psi and 18,300 psi, respectively, under ambient curing conditions.

Heat curing was applied only to the first re-evaluation mixture, resulting in a 7-day compressive strength of 19,640 psi and a 28-day compressive strength of 18,210 psi.

Mock-up Test 4

Although only about six months had passed since the third mock-up, the placement occurred in a different calendar year. Therefore, the objective of the fourth mock-up placement was to refresh the crew's UHPC construction knowledge. This placement was conducted on April 5, 2021, at A1 Quality Ready Mix in Socorro, NM.

Methodology

As with the previous mock-ups, a 20 ft. by 20 ft. High-Performance Deck (HPD) was cast. After seven days of curing, the surface was shot-blasted to slightly expose the aggregates and texturize the surface (Figure 6.24). Before placing the UHPC, the HPD was kept wet to saturate the surface conditions.

Figure 6.24. Mock up No. 4 - HPD surface preparation (UHPC Phase V, Figure 4.11)

Three batches of UHPC were produced. The first batch exceeded the mixer's capacity, so mixing was not performed. During placement, Confilm®, an evaporation retarder from BASF, was applied to reduce surface moisture evaporation. However, the UHPC overlay was not immediately covered with a plastic tarp after finishing. As a result, cracks become visible within 15 minutes. The overlay was then covered and kept wet until pull-off testing was conducted.

Cube specimens tested at 2, 4, and 7 days were cured under ambient laboratory conditions (68 °F and relative humidity of 30%). The remaining samples, tested at 14, 28, and 56 days, were cured in a wet room at 100% relative humidity. All prismatic specimens were cured in the wet room for seven days, then stored under ambient conditions until their respective testing days.

For the pull-off tests, nine core drillings were attempted, but only five samples were successfully extracted. The same issue observed in previous mock-ups occurred, where the overlay debonded from the slab during drilling. Of the nine attempts, the first three debonded during drilling. To address this, a handmade wooden core drilling base was used to provide greater stability. With the base in place, six additional attempts were made, and only one more sample debonded.

Results

After measuring the workability of batch number 2, which achieved a slump of 8.5 in. (within the target range of 7 to 10 in.), a decrease in slump was intentionally attempted for batch number 3 by increasing the mixing time from 14 minutes to 20.5 minutes. However, this adjustment resulted in a greater-than-desired decrease, with a slump measurement of only 4 in.

The target 7-day compressive strength of 11,090 psi was successfully achieved, but the 56-day compressive strength target of 17,000 psi was not met, with an average strength of 13,370 psi. Flexural strengths range from 743 psi to 898 psi, which were lower than those recorded in previous mock-ups.

For the direct tension pull-off test, five core samples were prepared. One sample was accidentally detached while setting up the pull-off tester. The remaining four samples recorded bond strengths of 54.3 psi, 72.4 psi, 154 psi, and 226 psi. Only two of the nine initial attempts met the required minimum bond strength. The average bond strength of the four successfully tested samples was 127 psi (Figure 6.25). The lower bond strength results in this mock-up may be partially attributed to the fact that saturated surface-dry conditions were not maintained for 24 hours prior to overlay placement, potentially compromising bond performance.

6.4.2 Non-proprietary UHPC Overlay in the Field

Bridge No. 7032 (Figure 6.25), a four-span, two-lane bridge with traffic lanes separated by a center median, measures approximately 300 ft. in length and 54 ft. in width. Located off Exit 150 in Socorro, NM, the bridge was selected for an overlay using non-proprietary UHPC. As part of the rehabilitation, deteriorated concrete from the deck was removed and replaced with a High-Performance Deck (HPD), followed by the application of a 1-inch UHPC overlay.

Figure 6.25. Bridge No. 7032 - a) plan view; b) bottom of multicell box girder superstructure; (UHPC Phase V, Figure 5.1)

The HPD was placed in two stages: the first on November 30, 2020, and the second on March 1, 2021. Before applying the UHPC overlay, the HPD was kept saturated until placement. The UHPC overlay was installed through four production placements from April 10, 2021, to April 27, 2021. Tests for slump, slump-flow, compressive strength, and flexural strength were conducted (UHPC Phase V, page 103).

Methodology

Before installing the overlay, the HPD surface was prepared by providing a roughened texture and ensuring saturated surface conditions. Surface texturing was achieved using a ceramic bead blaster, and the HPD was kept saturated until the UHPC overlay was placed.

(a)

(b)

Figure 6.26. UHPC production placements 3 and 4 - a) overlay casting; b) surface finish; (UHPC Phase V, Figure 5.8)

The mixing procedure followed the same methodology as described for the previous mock-ups in Chapter 6.4.1 of this document. A total of 110 batches were mixed; however, only 105 were accepted and placed on the bridge deck. Five batches were rejected for not meeting the desired consistency (either too wet or too dry). The batches were divided into four production placements, with two placements per lane. As in Mock-Up 4, Confilm® was used as an evaporation retarder during the placements.

For each production batch (Figure 6.26), a minimum of four 4.0 in. cube samples and two prismatic 3x4x16 in. specimens were cast in steel molds. After 24 hours at ambient temperature and a 2-hour transport to the laboratory, the specimens were demolded. Half of the specimens were cured under ambient laboratory conditions (68°F and relative humidity of 30%) for early strength testing at 2, 4, and 7 days. The remaining specimens were cured in a moist room (73°F and relative humidity of 98%) for testing at 14, 28, and 56 days. Prismatic specimens were cured in the moist room for seven days, then under ambient conditions until their respective testing days.

Compressive strength testing was conducted at 2, 4, 7, 14, 28, and 56 days, while flexural testing was performed at 7, 14, 28, and 56 days.

The target compressive strength was 10,000 psi at seven days and 17,000 psi at 56 days. Slump tests aimed for values between 8.5 in. and 10 in., with an acceptable slump-flow range of 12 to 19.5 in.

Results

Production Placement 1 exhibited visible cracking (Figure 6.27). The UHPC overlay was not covered with plastic sheets and wet burlap immediately after surface finishing. As a result, isolated cracks appeared when the plastic sheets and burlap were removed.

Figure 6.27. Overlay cracking from production placement 1 (UHPC Phase V, Figure 5.9)

The average slump was 9.25 in, and the spread tests had an average of 15.8 in. (UHPC Phase V, Page 114).

All production placements met the compressive strength target of 10,000 psi at seven days, with the following results: 10,870 psi, 11,150 psi, 11,730 psi, and 11,770 psi for the four placements. However, no production placement met the target compressive strength of 17,000 psi at 56 days. Production Placement 1 had an average 56-day compressive strength of 12,780 psi, Production Placement 2 reached 13,630 psi, Placement 3 achieved 14,060 psi, and Placement 4 recorded 14,040 psi.

MOR strengths significantly decreased after 7 days of moist curing. Production Placement 3, which had the greatest average 7-day value of 1,570 psi, dropped to 869 psi in the 14-day test,

which was the lowest recorded value. The 28-day test measured 913 psi, and the 56-day test recorded 985 psi.

Bonding tests

To avoid causing damage to the bridge, Non-Destructive Testing (NDT) was performed, which included physical tests such as hammer sounding and chain dragging. Additional NDT methods, such as ground penetrating radar (GPR) and infrared thermal imaging, were used to assess the integrity of the overlay. Additionally, the strength of the overlay-substrate bond and verification of delaminated areas were directly evaluated through pull-off tests.

Methodology

The physical test relies on the interpretation of the inspector. The chain drag method is an acoustic technique in which a mop-like tool with several chains attached to a handle is dragged across the bridge's overlay. Areas in good condition produce a distinct high-pitched sound, while delaminated areas emit a hollow sound.

Two of the most suitable techniques for evaluating delamination in concrete bridge decks are GPR and thermal imaging.

- GPR typically consists of a transmitter, an antenna, a receiver antenna, and a control computer. The transmitter sends short electromagnetic pulses (EMPs) through the concrete deck. These pulses were then reflected at interfaces between materials with different electrical properties, primarily from the top steel reinforcement and the concrete interface within the deck.
- Infrared thermal imaging (Figure 6.28) detects internal anomalies using electromagnetic surface radiation. Special infrared cameras capture the emitted thermal radiation from surface materials. The concept behind using infrared thermal imaging in concrete bridge deck evaluations is that defects such as voids, cracks, and delamination disrupt heat transfer through the concrete. As a result, the surface area above a delamination heats up faster (during high temperatures) than an area where the concrete is intact.
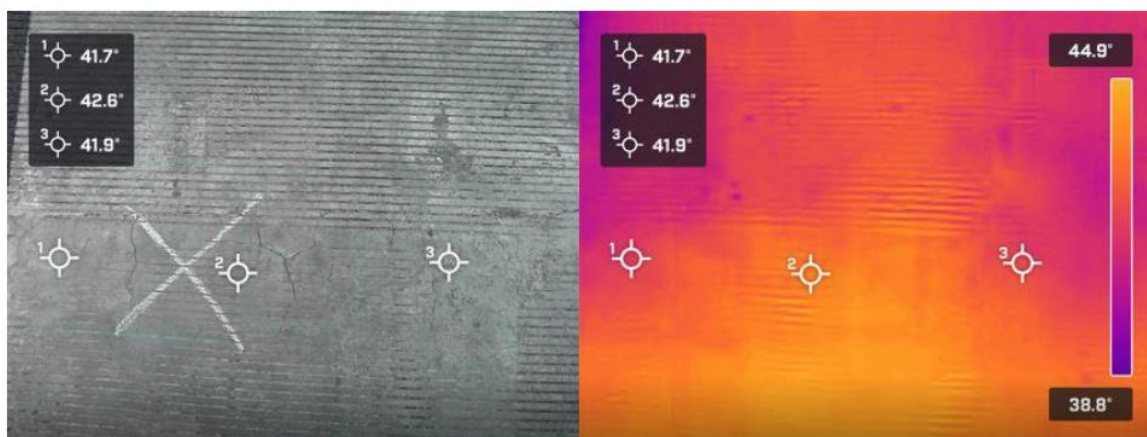
Figure 6.28. Infrared thermal imaging on potential delamination No. 1 (UHPC Phase V, Figure 6.95)

Pull-off testing (Figures 6.29 and 6.30) was conducted on August 10, 2021. Core drilling, test setup, and pull-off tests were performed similarly to the mock-up tests, with the only difference being the use of a different epoxy.

A total of ten core drillings were attempted, five on each lane. Core Sample No. 1 was drilled in a possible delaminated area, and Core Sample No. 4 was drilled in another suspected delaminated area. Core Sample No. 1 was successfully cored and tested. However, Core Sample No. 4 could not be tested because the overlay portion of the core debonded from the concrete substrate during drilling, resulting in a zero-strength location. The remaining core samples were successfully drilled and tested.

(a)

(b)

(c)

Figure 6.29. Pull-off testing procedure on Bridge 7032 - a) core drilling; b) epoxying of steel plates; c) testing set up; (UHPC Phase V, Figure 6.99)

Results

From the chain drag test, no potential delamination was found on the westbound lane, while four potential delamination areas were identified on the eastbound lane.

In the GPR tests, limitations were encountered due to the UHPC overlay composition (primarily steel fibers). The signals were scattered, preventing accurate interpretation of possible delamination.

In the infrared thermal imaging tests, two potentially delaminated areas were identified. Further pull-off testing confirmed that some of the areas identified by both chain dragging and thermal imaging were indeed actual delamination.

Three core samples did not meet the ACI-recommended bond strength of 150 psi, with values ranging from 72.4 psi to 145 psi. However, four core samples exceeded the ACI 546 (2014) "excellent" bond strength threshold of 250 psi, with the values ranging from 308 psi to 407 psi.

Figure 6.30. Core sample No. 6 from pull-off testing on the bridge (UHPC Phase V, Figure 6.101)

The UHPC overlay placement began on the eastbound lane; therefore, better handling, placement, consolidation, finishing, and overall production practices were implemented for the westbound lane. The average tensile strength for the eastbound lane was 174 psi, while the average tensile strength for the westbound lane was 291 psi. The total average bond strength of the ten core samples was 239 psi.

<u>Monitoring of Bridge No. 7032</u>

A total of 156 steel and concrete strain gauges and 24 thermocouples were installed on the bridge. Strain gauges were used to measure compressive and tensile deformations, while thermocouples were installed to measure the temperature near the strain gauge locations. Half of the sensors were installed on the westbound lane and the other half on the eastbound lane.

Sensors were installed after midspan NO. 1, pier NO. 1, and at midspan NO. 2 (Figure 6.31). All sensors were positioned in the second and fourth girders only (central girders). The first and second

sets of sensors consisted of strain gauges longitudinally separated at quarter points from diaphragm to diaphragm. The third set of sensors had strain gauges longitudinally separated at sixth points from diaphragm to diaphragm. The last set of sensors had strain gauges transversally separated at quarter points from stem to stem of the box girder.

At each strain gauge location, two strain gauges were positioned: one in the longitudinal direction and one in the transverse direction. Figures 6.31 and 6.32 provide more detail. The gauges were installed near the piers and near the midspan of the bridge, where maximum shear forces and bending moments occur.
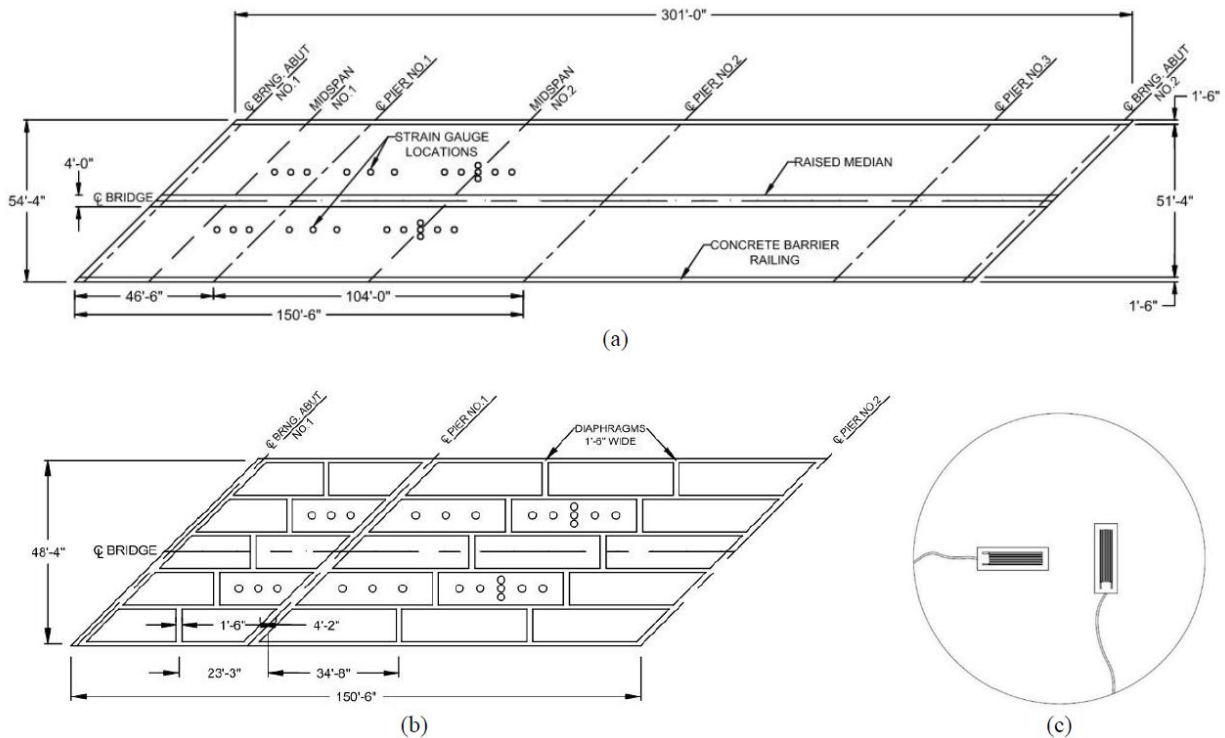
Figure 6.31. Strain gauge location layout - a) plan view; b) west side plan view; c) strain gauge location; (UHPC Phase V, Figure 6.7)
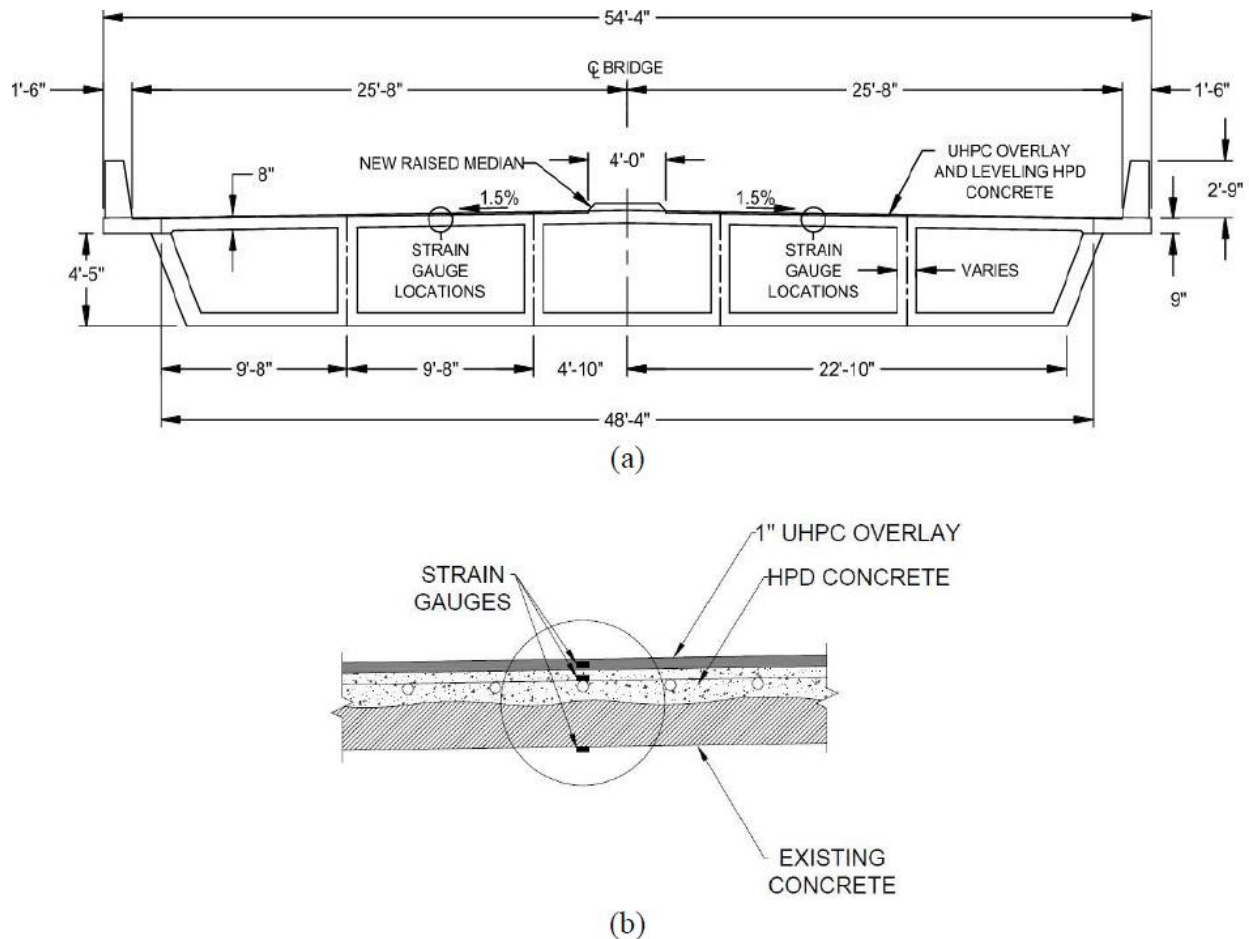
Figure 6.32. Strain gauge location layout - a) cross section; b) profile pattern; (UHPC Phase V, Figure 6.8)

Sensor Monitoring and Data Collection

Sensors began recording strain and temperature data on November 30, 2020, when the placement of the first HPD began. The rest of the sensors started collecting data on March 1, during the second placement. Sensors embedded in UHPC began monitoring on April 10, 2021. Approximately 9 gauges were damaged after casting UHPC placements 1 and 2.

The measured strain responses generally ranged between 200 and 250 µstrain. This small range (less than 1000 µstrain) for the daily cycle can be attributed to the restraint provided by the concrete superstructure (substrate). Thermocouples inside the UHPC overlay exhibited greater fluctuations between high and low temperatures compared to those in the multi-cell box girder or HPD. The overlay protects the deck and is directly exposed to external weather conditions.

Rising daily temperatures resulted in increasing strain magnitudes, while decreasing temperatures caused strain reduction. For example, from April 16, 2021, to April 20, 2021, a trend of decreasing daily temperatures coincide with a multi-day decline in strain across all properly functioning strain gauges.

113

More data was collected from UHPC placements 3 and 4 due to fewer sensors being damaged during overlay placement.

Longer-term data collection of the bridge involved collecting strain and temperature data from an overlay age of 28 days until December 15, 2021. Over a one-year period, the overlay exhibited greater temperature oscillations due to its direct exposure to ambient weather. The temperature differential between the UHPC and HPD range from 20–52 °F due to thermal effects, while the temperature differential between the HPD and the box girder range from 30–40 °F. Seasonal thermal cycles were evident throughout two years of data collection, with low-temperature daily cycles observed from October to March and high-temperature daily cycles from April to September in both 2021 and 2022.

Strain and Temperature Behavior

Strain decreases on rainy days. An initial strain reduction was observed in sensor UE22L (UHPC) on June 5 during a rainy day. Following this event, rain was again present on the bridge from June 27–30 and July 6–7. After these three rain events, the strain data behavior from sensor UE22L returned to a pattern similar to sensors CE22L and HE22L (girder and HPD) (UHPC Phase V, Page 269).

Data anomalies were primarily observed on rainy days. While it is possible that these anomalies were due to sensor malfunctions; every anomaly detected results in a strain decrease (compressive behavior) rather than a strain increase (tensile behavior). This suggests that temperature oscillations influenced strain behavior.

Over the two-year monitoring period, strain-temperature observations generally indicated that as temperature increased, strain also increased, and vice versa. The most consistent data came from sensors placed lower on the structure, such as those in the girders, while the most anomalies were detected in sensors embedded in UHPC, which were affected by rain, snow, and humidity (UHPC Phase V, Page 292).

Yearly cycles from working sensors with no anomalies show that strain varied by approximately 9000 µstrain (from -4000 to 5000 µstrain) in the first two bays, a wider range than the last bay, where strain variation was 7000 µstrain.

Data from properly functioning strain gauges revealed a high strain peak during the first yearly cycle (2021–2022) from June through August, and a low strain minimum from December through February; a high strain peak during the second yearly cycle (2022–2023) from June through August, with a low strain minimum from November through February. The second year of data collection showed longer compressive deformations, as seen mainly in November.

Comparison of Yearly Strain Cycles

Strain responses in the girder concrete ceiling during July (the second year) were 500–600 µstrain greater than during the first yearly cycle (UHPC Phase V, Page 263).

6.4.3 Recommendations

Substrate surface preparation should begin with the removal of any debris, followed by sandblasting or shot blasting to achieve an acceptable surface texture. A proper substrate surface texture was obtained by removing the surface paste and exposing the fine aggregate. The minimum required surface texture should be a "light sandblasted texture," as specified by ACI 303 (2012). A second surface cleaning is crucial to remove any remaining debris from prepared surface. To ensure maximum bonding, the surface should be maintained under saturated surface conditions for 24 hours before placing the UHPC overlay.

For UHPC, it is critical to achieve the correct water-to-cementitious materials (w/cm) ratio to ensure the required workability and strength. To achieve this,

- Cementitious materials and aggregates should be stored separately in sealed containers
- Aggregate water content must be determined before mixing
- Excess moisture on the deck should be removed by sweeping or sponging

Contractors should confirm the maximum volume capacity of the UHPC that can be safely mixed in the selected mixers. Due to the extreme stiffness of UHPC during mixing, materials may not be effectively mixed at the rated capacity of the mixer.

When finishing the overlay, a curing compound should be applied, and the overlay should be immediately covered with plastic sheets to minimize evaporation and prevent related cracking (UHPC Phase V, Page 397).

7. ROADMAP

7.1 Early Developments (Pre-1980s to Early 1980s)

The evolution of UHPC can be traced back to advancements in concrete technology beginning in the 1930s. During this period, Eugene Freyssinet demonstrated that applying pressure to fresh concrete during setting could enhance its strength (Xercavins et al., 2008). In the 1960s, the introduction of superplasticizers enabled a reduction in the water-to-binder ratio, significantly improving both the strength and durability of concrete. At that time, concrete with a compressive strength of 5,950 – 7,250 psi (41–50 MPa) was classified as high-strength concrete. By the 1970s, this threshold had increased to 8,990 psi (62 MPa).

The early 1980s marked the emergence of UHPC, initially in experimental settings that relied on vacuum mixing and heat curing techniques (Azmee & Shafiq, 2018). During the same period, significant advancements in high-strength concrete (HSC) and high-performance concrete (HPC) were achieved, with compressive strengths ranging from approximately 7,250 – 17,400 psi (50 to 120 MPa) (Blais et al., 1999). HSC focuses on achieving compressive strength above 5,950 psi (41 MPa) whereas HPC aims for enhanced durability, workability, and resistance to environmental factors rather than being limited to strength only. UHPC surpasses both HSC and HPC in terms of high compressive strength, ductility and durability. A key breakthrough in the early 1980s was the introduction of micro-defect-free (MDF) cement, which facilitated the production of ultra-high strength concrete exceeding 29,010 psi (200 MPa). However, its high production costs and complex manufacturing processes limited its widespread application.

Further advancements in UHPC occurred in Denmark with the development of dense silica particle (DSP) cement, which improved particle packing density and simplified production, allowing concrete to reach strengths of up to 50,050 psi (345 MPa) (Bache, 1981). By the mid-1980s, the brittle nature of high-strength concrete was addressed with the introduction of steel fibers, leading to the development of slurry-infiltrated fiber concrete (SIFCON). This material incorporated up to 20% steel fibers, significantly enhancing tensile strength, though workability challenges remain unchanged (Lankard, 1984).

Despite its improved material properties, UHPC's adoption in the 1980s remained limited due to high material costs, complex production requirements and compatibility issues with traditional construction practices.

7.2 Advancements in the 1990s

The 1990s marked a significant period for the development and application of UHPC. While research on UHPC material had begun more than two decades earlier, it was introduced in the early 1990s as Reactive Powder Concrete (RPC), recognized for its exceptional compressive strength and durability. These enhanced properties were achieved through the use of fine powders, superplasticizers, and steel fibers (Richard & Cheyrezy, 1995). The first structural applications of UHPC followed toward the end of the decade, marking a major milestone in its advancement.

By 1995, RPC had been fully developed based on the following fundamental principles:

- Enhancement of homogeneity by elimination of coarse aggregates
- Optimization of particle packing through a well-graded granular mixture, and application of pressure before and during setting
- Improvement of microstructure via post-set heat treatment
- Improvement of ductility by incorporating small-sized steel fibers
- Adaptation to existing practices by maintaining conventional mixing and casting procedures

The unique formulation and high-performance characteristics of RPC made it suitable for a wide range of construction applications where strength, durability, and reduced permeability were critical requirements. Based on its fundamental principles, two variants of RPC were developed: RPC 200 and RPC 800. Both were composed of fine quartz sand aggregate, low-C_3A cement, crushed quartz, and silica fume. The primary differences between them lay in compacting pressure and heat treatment temperature. Table 7.1 presents a comparison of the characteristics of RPC 200 and RPC 800.

Table 7.1. Comparison of RPC 200 and RPC 800 characteristics

	RPC 200	RPC 800
Compacting Pressure	-	50 MPa
Heat Treatment	20-90 C	250-400 C
Compressive Strength	170-230MPa	490-810MPa
Flexural Strength	30-60MPa	45-141MPa
Modulus of Elasticity	50-60 GPa	65- 75 GPa

7.3 Post-2000 Developments

By the early 2000s, UHPC became commercially available in the United States, prompting various state departments of transportation to explore its use in infrastructure projects. From the mid-2000s, extensive research focused on optimizing the UHPC's mixture design and its performance across different structural applications. This following review includes material-level optimization, improvements in mechanical properties, and assessments of UHPC's environmental and economic viability. Additionally, new formulations were developed to expand its applicability in diverse structural systems, further advancing its role in modern construction.

7.3.1 Optimization of Mixture Proportions of UHPC

Supplementary Cementitious Materials (SCMs) and Limestone powder (LP)

In recent years, research has focused on optimizing UHPC by incorporating SCMs such as silica fume and fly ash to enhance mechanical performance, durability, and cost efficiency.

Alkaysi et al. (2016) evaluated the effects of silica powder on the durability of UHPC. The study assessed durability by examining resistance to freeze-thaw cycles, chloride ingress, and the presence and distribution of air voids. Mixtures with silica powder proportions varying from 0% to 25% of the cement weight were tested. Results indicated that all specimens exhibited mass loss well below the acceptable limit after more than 60 freeze-thaw cycles. Concrete containing 25% silica powder demonstrated slightly higher ion permeability than those with 15% silica powder, while mixtures with 0% silica powder exhibited the lowest permeability. Particle size distribution analysis revealed that while variations in silica powder content affected packing density across the particle size range, the overall distributions remained close to the optimal particle packing density. These findings suggest that silica powder has minimal impact on UHPC durability and could potentially be eliminated from the mixtures to reduce material costs without significantly compromising performance.

To reduce the cost of UHPC, Alsalman et al. (2017) developed a UHPC mixture using local sand, silica fume, and fly ash. The study investigated the effects of sand gradation, binder type and content, and curing regimes on the compressive strength of UHPC. Binder content varied between 55.56 lb/ft³ (890 kg/m³) and 85.07 lb/ft³ (1363 kg/m³), with silica fume content ranging from 0% to 21% and fly ash content between 0% and 40%. Only one mixture included 3% steel fibers. The results showed that the highest compressive strength of 22,510 psi (155 MPa) was achieved with a mixture containing sand particles sized between 300 μm and 600 μm, along with 5% silica fume. A similar mixture incorporating the same sand size, 5% silica fume, and 20% fly ash closely followed, reaching a compressive strength of 22,060 psi (152 MPa). The study demonstrated that the effect of silica fume on compressive strength was minimal when used at replacement rates greater than 10% of the binder. Additionally, the findings confirmed that compressive strength increased with higher total binder content, regardless of silica fume content or sand type.

Wang et al. (2019) optimized the of UHPC mixture proportions using the D-optimal method to enhance compressive strength, wet packing density, and pore structure. The study introduced Limestone Powder (LP) as a partial replacement for cement and silica fume, with substitution

ratios ranging from 0 to 0.2. The silica fume content varied between 0.025 and 0.1, while cement content ranged from 0.2 to 0.5. Using a mathematical optimization model, the researchers identified an optimal UHPC mixture consisting of 24.97 lb/ft³ (400 kg/m³) of cement, 6.24 lb/ft³ (100 kg/m³) of silica fume, 24.97 lb/ft³ (400 kg/m³) of limestone powder, and 2.37 lb/ft³ (38 kg/m³) of superplasticizer. This mixture proportions achieved a wet packing density of 0.7734, a maximum compressive strength of 19.13 ksi (131.9 MPa) and had a total of 3802 air bubbles (pore entry radius<10 nm), demonstrating improved particle packing efficiency while maintaining high mechanical performance.

The study concluded that incorporating powdered limestone improved cost efficiency and sustainability by reducing cement consumption without compromising UHPC properties. Due to its high replacement ratio, powdered limestone was identified as an eco-efficient alternative that promotes sustainable construction practices while maintaining structural integrity and durability.

Li et al. (2020) investigated the effects of steel slag powder (SSP) and hybrid expansive agents (EA) on the hydration characteristics and shrinkage behavior of UHPC. The research aimed to determine how variations in SSP and EA content influenced hydration heat, compressive strength, and shrinkage over time. The results demonstrated that incorporating steel slag powder effectively reduced shrinkage, with specimens containing 20% SSP exhibiting 15% less shrinkage compared to the control mixture without SSP. Additionally, the inclusion of 5% hybrid EA significantly reduced the total shrinkage, achieving a 40% reduction compared to mixtures without EA.

Aggregate

The role of aggregate in UHPC has been extensively studied, with a focus on optimizing particle size, gradation, and alternative materials to enhance mechanical properties and durability. Research has examined the effects of coarse aggregates, sand gradation, alternative aggregates, and their influence on UHPC performance.

Effects of Coarse Aggregates on UHPC Performance

J. Ma et al. (2004) investigated the effect of incorporating coarse aggregate in UHPC by comparing two mixtures. The first mixture, classified as Reactive Powder Concrete (RPC), contained only quartz sand with a particle size of 0.0118–0.0315 in. (0.3–0.8 mm). The second mixture incorporated crushed basalt with a size range of 0.0787–0.196 in. (2–5 mm) as a coarse aggregate. The study found that aggregate size had no significant impact on compressive strength. However, UHPC containing coarse aggregates required a shorter mixing time, had a lower cementitious paste volume, and exhibited reduced autogenous shrinkage compared to RPC with quartz sand.

A study by Liu et al. (2016), examined the effects of coarse aggregate (0%, 15%, 25%, and 35%) and fiber properties on UHPC's tensile behavior. The results showed that increasing the coarse aggregate content negatively impacts workability, with spread and slump values declining around 37% and 56%, respectively for 35% aggregate replacement. The highest tensile strength was achieved in UHPC without coarse aggregate, highlighting the importance of matrix homogeneity in UHPC mixtures. Furthermore, increasing fiber dosage from 1% to 2.5% reduced fiber utilization efficiency due to interlocking effects between fibers and aggregates.

Li et al. (2018) investigated UHPC with coarse basalt aggregates having maximum particle size of 0.63 in. (16 mm). The study found that as the aggregate size increased from 0.118 to 0.63 in (3 mm to 16 mm), UHPC maintained 7-day compressive strength around 17,695 psi (122 MPa) for all sizes, but at 28-day compressive strength decreased from 20,885 psi to 19,145 psi (144 MPa to 132 MPa). Additionally, tensile strength was also found declined from 1,421 psi to 1,189 psi (9.8 MPa to 8.2 MPa). The findings demonstrate that coarser aggregates may negatively impact UHPC's tensile properties.

Influence of Sand Gradation on UHPC Strength

Ji et al. (2011) analyzed the effects of river sand particle size and gradation on the strength of reactive powder concrete. Four different sand gradations were tested, with particle size ranges from 0.049 – 0.098 in. (1.25–2.5 mm), 0.0248 – 0.049 in. (0.63–1.25 mm), and 0.00315 – 0.0063 in. (0.08–0.16 mm). The results showed that higher packing density improved overall concrete performance, but the highest compressive strength 28,280 psi (195 MPa) was achieved with a maximum grain size of 0.0248 in (0.63mm).

Alsalman et al. (2017) studied the effect of locally sourced Arkansas River sand with three different gradations to examine the effect of sand gradation, binder type and content, and curing regimes on the concrete's compressive strength. Sand-1 had a natural gradation ranging from the No. 4 [0.187 in (4.75 mm)] sieve to the No. 200 (75 µm) sieve. Sand-2 had a smaller particle size, passing the No. 30 (600 µm) sieve and being retained on the No. 50 (300 µm) sieve and Sand-3, which passed the No. 200 (75 µm) sieve had the smallest particle size. These sands were used to evaluate the effect of four curing regimes on concrete compressive strength. The results showed that UHPC made with sand particles (<75 µm), exhibited the maximum compressive strength of 25,960 psi (179 MPa), demonstrating the significance of optimized sand gradation in UHPC formulations. The curing regimen for this result involved two days of curing at 140°F (60°C) followed by an additional three days at 194°F (90°C). Additionally, with the increase in binder content from 890 kg/m3 to 1009 kg/m3, compressive strength at 90 days increased from 16,550 psi (114 MPa) to 20,200 psi (140 MPa) for an ambient curing condition.

Later, Pyo et al. (2017) investigated coarser fine aggregates with a maximum size of 0.196 in. (5 mm) and their effects on mechanical properties and shrinkage of UHPC. The highest compressive strength of 25,530 psi (176 MPa) was achieved in mixtures containing only sand and 1.5% steel fibers, while mixtures incorporating basalt aggregates exhibited lower compressive strength. This study indicated that coarser fine aggregates could negatively impact compressive and tensile strength in UHPC due to reduced packing efficiency and aggregate-paste interactions.

Alternative Aggregate Materials in UHPC

In the review of this section, studies were found to explore alternative aggregates, such as iron ore tailings, lightweight sand, and rock dust, to enhance UHPC sustainability and performance.

Zhao et al. (2014) investigated the feasibility of using iron ore tailings as a replacement for natural aggregate in UHPC. The results showed that the highest compressive strength, 21,760 psi (150 MPa at 90 days), was achieved with 30–40% replacement of natural aggregate. However, full

replacement (100%) led to a significantly lower compressive strength of 13,050 psi (90 MPa). Additionally, the study found that flexural strength was highest in mixtures with 0% replacement, reaching 3,260 psi (23 MPa at 90 days), but gradually declined as the proportion of iron ore tailings increased.

Meng and Khayat (2017) explored the replacement of sand with pre-saturated lightweight sand (LWS) to improve internal curing and reduce autogenous shrinkage. LWS replacement levels ranged from 0% to 75%. The results demonstrated that incorporating LWS effectively decelerated and minimized the drop in internal relative humidity and autogenous shrinkage. Analyses using isothermal calorimetry and thermal gravimetry indicated that LWS enhanced cement hydration, particularly after 28 days of curing. Further investigation through mercury intrusion porosimetry (MIP) and scanning electron microscopy (SEM) analyses revealed the reduced porosity and improved interfacial properties between the sand and cement matrix when LWS was used. Among the replacement levels tested, a 25% LWS replacement ratio yielded the highest compressive strength of 24,370 psi (168 MPa).

Yang et al. (2020) investigated quartz sand replacement with recycled rock dust in UHPC, with replacement levels of 20%, 40%, 60%, 80%, and 100%. The results showed that a higher rock dust content slightly reduced flowability. At replacement level of 40%, mixtures exhibited the highest flowability. At 90 days, mixtures with 20% and 100% replacement achieved the highest compressive strength of 18,860 psi (130 MPa). Moreover, Microstructural analysis indicated that rock dust improved the interfacial transition zone (ITZ), enhancing bond strength between aggregates and cement paste.

Summary of Aggregate Influence on UHPC Performance

The abovementioned studies reviewed the critical role of aggregate type, size, gradation, and alternative materials in UHPC performance. Key findings include:

- Smaller aggregate sizes and optimized gradation contribute to higher compressive strength by improving particle packing
- The inclusion of coarse aggregates can reduce workability and tensile strength, emphasizing the importance of a homogeneous matrix
- Alternative aggregates such as iron ore tailings, lightweight sand, and rock dust provide sustainable solutions while maintaining structural integrity
- Proper selection of aggregate materials significantly impacts shrinkage behavior, durability, and mechanical properties, making it a crucial factor in UHPC mixture design

Steel fibers

Steel fibers play a crucial role in enhancing the mechanical properties, ductility, and durability of UHPC. Extensive research has been conducted to investigate the influence of fiber type, content, distribution, and alignment on the behavior of UHPC under various loading conditions.

Deeb et al. (2012) examined self-compacting high-performance concrete (SCHPC) and UHPC, both with and without steel fibers. UHPC mixtures incorporated 6% fiber by volume, consisting of 5% short fibers 0.236 in. long, 0.0059 in. diameter (6 mm long, 0.15 mm diameter) and 1%

longer fibers of 0.51 in. long and 0.0059 in. diameter (13 mm, 0.15 mm diameter). The results showed that fiber-free UHPC exhibited excellent flowability, demonstrating its potential for self-compacting applications. However, the addition of fibers compromised flowability, reducing the mixture's ability to flow smoothly through narrow gaps.

Gesoğlu et al. (2016) further explored the impact of different fiber types and dosages. Various types of fibers, including micro-steel fibers, hooked-end steel fibers, and micro-glass fibers at varying volume fractions (0.25%–2%) were tested. The study showed that increasing steel fiber content generally enhanced compressive and flexural strength for all cases. The highest compressive strength of 26,110 psi (180 MPa) was recorded in mixtures with 2% micro-steel fibers, while 2% hooked-end fibers significantly improved ductility and exhibited strain-hardening behavior. Additionally, flexural strength was highest in UHPC containing 2% hooked-end fibers 2,030 psi (14 MPa), demonstrating their superior performance in load-bearing applications

Wu et al. (2016) examined the effect of fiber shape (straight, corrugated, and hooked-end) and content (0%–3%) on UHPC performance. The results showed that flowability decreased with increasing fiber content across all fiber types. Mixtures incorporating straight steel fibers exhibited the highest flowability, measuring 8.46 in. (215 mm) at 0% fiber, which decreased to 5.31 in. (135 mm) at 3% fiber. Among the fiber types tested, hooked-end fibers resulted in the greatest reduction in workability. In contrast, both compressive and flexural strength increased as fiber content increased. The highest peak load, 4,270 lb (19,000 N), was recorded in mixtures containing 3% hooked-end fibers, which exhibited a deflection of 0.03 in. (0.8 mm). The study concluded that fiber shape significantly influences the flexural load-deflection behavior, with hooked-end fibers providing the greatest improvement in peak load and deflection capacity.

To mitigate autogenous shrinkage, Yoo et al. (2019) investigated the effects of calcium sulfoaluminate-based (CSA) expansive agents (EA) (0%–8%) in UHPC incorporating various steel fiber types, including straight (S-fiber), half-hooked (HH), and twisted (T) fibers. The study evaluated fiber pullout behavior and bond strength under static and dynamic loading conditions. According to results, T-fibers exhibited an average bond strength of 4,440 psi (31 MPa,) surpassing HH-fibers and S-fibers by a factor of 1.4 and 3.4, respectively. The highest recorded bond strength of 5,080 psi (35 MPa) was achieved in T-fiber specimens with 8% CSA EA, while S-fibers with 6% CSA EA had the lowest bond strength. Fiber inclination was also found to play a role, with aligned S-fibers showing lower bond strength than inclined ones, whereas HH- and T-fibers performed better in an aligned configuration.

Additionally, the study revealed that CSA EA improved bond strength but led to fiber rupture rather than pullout failure in HH- and T-fibers. Under dynamic loading, T-fibers maintained superior bond strength, though their advantage diminished under impact loading conditions relative to static conditions. The study highlighted that S-fibers were most effective for extreme loading conditions, such as impact and blast resistance, due to their high rate of sensitivity.

A study by Li et al. (2020), explored the development of functionally graded ultra-high performance cementitious composite beams (FGCB) by integrating UHPC, Two-Stage Concrete (TSC), and Slurry-Infiltrated Fibrous Concrete (SIFCON). The FGCB was fabricated with a

SIFCON bottom layer and a TSC top layer, aiming to optimize structural performance while reducing material costs. The study examined three steel fiber types and varying fiber contents. The results indicated that flexural strength increased from 1,310 psi (9.0 MPa) to 2,090 psi (14.5 MPa) with 1% addition of steel fiber content and reached 6,310 psi (43.5 MPa) with 3% fiber content. FGCB exhibited excellent energy absorption, impact resistance, and interfacial bonding compared to conventional UHPC beams, making it suitable for high-performance structural applications.

To enhance fiber orientation and dispersion, Zhang et al. (2020), developed a casting device for fiber alignment in layered UHPC. The study tested 2% and 3% steel fibers (straight and hooked end), analyzing their effects on flexural and tensile behavior. Results showed that aligned fibers significantly improved ultimate tensile and flexural strength, as well as cracking resistance and ductility. However, fiber alignment introduced anisotropy, increasing diagonal cracking under tension. The study also revealed that uneven fiber distribution at interlayer boundaries weakened localized regions due to propagation of diagonal and vertical cracks, underscoring the importance of uniform fiber dispersion in UHPC applications.

Summary of Steel Fiber Influence on UHPC Performance

Research findings abovementioned confirm that steel fiber type, content, and alignment significantly impact UHPC's mechanical properties:

- Higher steel fiber content (up to 3%) improves compressive and flexural strength but reduces flowability
- Hooked-end fibers enhance ductility and flexural strength better than straight or micro-steel fibers
- CSA EA (up to 8%) improve fiber bond strength, but excessive CSA EA can lead to fiber rupture rather than pullout
- Functionally graded UHPC (FGCB) exhibits superior flexural strength and impact resistance with optimized fiber distribution
- Aligned fibers enhance tensile and flexural strength but can cause localized weaknesses in layered UHPC

w/cm ratio

The water-to-cement (w/cm) ratio is a key parameter influencing the compressive strength, durability, and mechanical properties of UHPC. Several studies have examined the effects of varying w/cm ratios on strength development, elasticity, and tensile behavior in UHPC mixtures.

Talebinejad et al. (2004) investigated the effects of w/cm ratio, cement content, and silica fume percentage on UHPC compressive strength under four different curing conditions. A total of 38 mixture proportions were tested, with w/cm ratios ranging from 10% to 20%, cement contents varying between 81.16 lb/ft³ and 131.48 lb/ft³ (1300 and 2105 kg/m³), and silica fume percentages between 20% and 35%. The results showed that reducing the w/cm ratio from 20% to 11.5% led to a 46% increase in compressive strength, highlighting the significant impact of water content on UHPC performance.

A more recent study by Carey et al. (2020), further explored UHPC mixtures with w/cm ratios between 0.11 and 0.19. The study identified that the optimal w/cm ratio was 0.15, as the mixture attained the highest compressive strength 29,460 psi (203 MPa), highest elastic modulus 9,630 ksi (66 GPa), and highest indirect tensile strength 4,160 psi. (30 MPa).

The findings from these studies emphasize the critical role of w/cm ratio in determining the strength and durability of UHPC:

- Lowering the w/cm ratio enhances compressive strength, as observed in both studies
- A w/cm ratio around 0.15 optimizes mechanical properties, balancing workability and strength development
- Excessively low w/cm ratios may pose challenges in workability and require the use of advanced superplasticizers to maintain flowability

Shrinkage

Shrinkage in UHPC is a critical factor that influences long-term durability, dimensional stability, and cracking resistance. Research has extensively explored methods to minimize early-age shrinkage, autogenous shrinkage, and long-term shrinkage effects through various approaches, including the use of pozzolanic materials, shrinkage-reducing admixtures (SRA), expansive agents (EA), and alternative binders.

Shrinkage Mitigation Strategies in UHPC

Staquet and Espion (2004) studied the effect of partially replacing silica fume with fine fly ash and metakaolin on early-age shrinkage. Their findings showed that UHPC mixtures containing metakaolin exhibited the lowest autogenous shrinkage at early ages compared to other mixtures. Additionally, heat curing at 107.6 °F (42°C) for two days after casting significantly reduced thermal and autogenous shrinkage, particularly in mixtures containing metakaolin.

Further research by Soliman et al. (2014), explored the effectiveness of shrinkage-reducing admixtures (SRA) and wollastonite microfibers in limiting early-age shrinkage in UHPC. Nine UHPC mixtures were tested, incorporating wollastonite microfibers (0%, 4%, and 12%) as a partial cement replacement, along with SRA dosages of 1% and 2% by cement weight. The results showed that increasing wollastonite microfiber content from 4% to 12%, progressively increased total shrinkage reduction from 10% to 22%, at 7 days compared to the control mixture. The addition of SRA further reduced shrinkage but can result in a lower degree of hydration, indicating a potential trade-off between shrinkage mitigation and hydration development.

To address autogenous shrinkage, Yoo et al. (2019), evaluated the effectiveness of calcium sulfoaluminate-based (CSA) EA in UHPC. The study tested mixtures with CSA EA dosages ranging from 0% to 8% and found that shrinkage strain was effectively reduced when CSA EA content exceeded 6%. However, when the dosage was below 4%, shrinkage increased by 10–15%, indicating that suboptimal EA content may worsen shrinkage instead of mitigating it.

Similarly, Li et al. (2020), examined the combined effects of steel slag powder (SSP) and hybrid EA on UHPC shrinkage behavior. Their findings demonstrated that replacing cement with 10%,

15%, and 20% SSP reduced shrinkage by 7.1%, 10.8%, and 15%, respectively, compared to the control mixture. Additionally, incorporating 5% hybrid EA resulted in a 40% reduction in total shrinkage. The most effective shrinkage mitigation was achieved by combining 15% SSP with 5% EA, suggesting that a synergistic approach using both alternative binders and expansive agents significantly improves the dimensional stability of UHPC.

Monitoring Autogenous Shrinkage

Huang and Ye (2017) introduced a methodology for determining "time-zero", the point marking the onset of autogenous shrinkage in cement pastes. The study used a hygrometer-based technique to track changes in internal relative humidity (RH) starting one hour after casting. The results demonstrated that tracking RH drop provides a more precise indicator of autogenous shrinkage initiation compared to traditional methods that rely on final setting time or skeletal formation. Autogenous deformation measurements conducted following ASTM C1698-09 revealed a consistent shrinkage trend across multiple samples, with deviations of less than 50 microstrains. This real-time monitoring approach was found to enhance predictive modeling for long-term shrinkage behavior in UHPC and provides more accurate data for material optimization.

Numerical Modeling and Long-Term Shrinkage Behavior

Zhu et al. (2020), developed an ABAQUS user subroutine to simulate creep and shrinkage in UHPC and normal concrete (NC) using a numerical integration method. Long-term creep and shrinkage tests were conducted over 160 days, examining UHPC specimens at stress-to-strength ratios of 20%, 30%, and 40%. The results showed that creep was most significant between the 5th and 30th day, stabilizing after 90 days. The final shrinkage strain was measured at 145 με, while the final creep coefficient was 0.46 under the tested conditions.

Additionally, a finite element (FE) model was developed to simulate the long-term behavior of a prototype railway bridge, analyzing the impact of 1000 days of creep and shrinkage. The simulation revealed that UHPC significantly reduced long-term deflection, with the deflection amplification factor being 1.29 for UHPC beams, compared to 1.59 for NC beams. These findings indicate that UHPC exhibits superior dimensional stability over time, making it ideal for long span and high-performance structural applications.

Summary of Shrinkage Mitigation in UHPC

- Pozzolanic replacements such as metakaolin and heat curing at 108 °F (42°C) reduce early-age shrinkage
- Shrinkage-reducing admixtures (SRA) and wollastonite microfibers lower total shrinkage and delay shrinkage cracking but may reduce hydration degree
- CSA-EA effectively reduces autogenous shrinkage above 6% dosage, but lower amounts can exacerbate shrinkage
- Steel slag powder (SSP) combined with hybrid EA provides up to 40% total shrinkage reduction, demonstrating a synergistic mitigation effect
- Real-time hygrometer monitoring improves shrinkage prediction, leading to better material optimization

- Numerical modeling confirms UHPC's superior dimensional stability, reducing long-term creep and deflection, making it an ideal choice for long-span structures

Workability

Workability is a critical parameter in UHPC as it influences mixing, casting, and overall performance. Various factors, including w/cm, high-range water reducers (HRWR), superplasticizers (SP), cement type, and rheological modifiers, significantly impact the flowability, viscosity, and thixotropy of UHPC. Several studies have investigated optimal material combinations and admixture strategies to improve UHPC workability while maintaining its high compressive strength.

<u>Effect of Material Composition and Admixtures on Workability</u>

Wille et al. (2011) developed a UHPC mixture with a compressive strength exceeding 200 MPa using commercially available materials in the U.S. market. The study examined the impact of silica fume (0.18–0.25), high-range water reducer (HRWR) (1–8% of cement weight), glass powder (0.20–0.53), water-to-cement (w/cm) ratio (0.166–0.3), and water-to-binder (w/b) ratio (0.107–0.254) on compressive strength and spread values of UHPC mixtures.

A total of 38 different mixtures were evaluated. The initial mixtures required HRWR dosages up to 8% to achieve flowability; however, sufficient workability was achieved with as little as 1% HRWR when particle dispersion was optimized. The study found that minimizing HRWR content while maintaining adequate dispersion improved both flowability and compressive strength. Spread values varied between 6.3 in. (150 mm) and 14.4 in. (366 mm), with the lowest spread 5.9 in. (150 mm) achieved using a 1:0.25:0.30 cement-to-silica fume-to-glass powder ratio, resulting in 25,527 psi (176 MPa) compressive strength. In contrast, the highest spread 14.4 in. (366 mm) was recorded for a 1:0.20:0.40 mixture, which yielded 26,107 psi (180 MPa) compressive strength.

Dils et al. (2013) investigated the influence of cement type on the workability, rheology, and compressive strength of UHPC mortar UHPC. The study evaluated six Belgian cement types (labeled C1 to C6), each with distinct chemical and physical properties, including variations in tricalcium aluminate (C_3A) content, sulfate (SO_3) levels, alkali content (Na_2Oeq), and Blaine fineness. The researchers also assessed the effect of vacuum mixing on air content, microstructure, and strength development.

The results showed that cements with lower C_3A-specific surface area, defined as the product of C_3A content and Blaine fineness, performed better in terms of rheology and workability. Specifically, the three best-performing cements were:

- C2: 4.5% C_3A, 2.6% SO_3, 0.74% alkali content, 377 m²/kg Blaine fineness
- C3: 5.2% C_3A, 3.1% SO_3, 0.73% alkali content, 359 m²/kg Blaine fineness
- C4: 2.8% C_3A, 2.6% SO_3, 0.60% alkali content, 365 m²/kg Blaine fineness

These cements achieved the target slump flow of 11.8 ± 1.97 in. (30 ± 5 cm) using a constant dosage of superplasticizer, with C3 providing the highest slump flow of 13 in. (33 cm), indicating excellent dispersion and flow characteristics. In contrast, cements with higher C_3A-specific surface

126

area, such as C5, could not achieve the target slump flow even with increased superplasticizer content, suggesting poor rheological behavior and greater sensitivity to admixture dosage.

Impact of Water and Superplasticizer Addition Methods

Ferdosian and Camoes (2016) studied the effects of water and superplasticizer (SP) addition methods on UHPC fluidity. The study used Type I portland cement (42.5R and 52.5R) and a carboxylic ether polymer-based superplasticizer (18% solid content) with a w/cm ratio of 0.35. Three different methods of water and SP addition were tested. The optimal fluidizing effect was achieved after a total of 15 minutes of mixing. The specific order followed: adding 70% of the mixing water to the cementitious materials and mixing for 3 minutes, followed by adding the optimum dosage of SP and mixing for the next 6 minutes. Finally, mixing was completed by adding the remaining 30% of water and blending for an extra 6 minutes.

Use of Rheological Modifiers to Enhance Thixotropy

Teng et al. (2020) investigated the use of welan gum (WG) and nanoclay (NC) as rheological modifiers to enhance thixotropy in UHPC mixtures. The study tested five dosages of WG (0.045%–0.27% of binder mass) and NC (0.25%–1.5% of binder mass) while maintaining a fixed SP dosage.

The results indicated that both WG and NC enhanced thixotropy, improving the static yield stress and shape retention of UHPC mixtures. For mixtures with variable SP dosages, WG had a more significant impact on thixotropy, whereas NC had a limited effect. These findings suggest that WG is a more effective rheological modifier for enhancing the buildability of UHPC without compromising workability.

Summary of Workability Optimization in UHPC

Workability in UHPC is influenced by multiple factors, including HRWR content, cement type, superplasticizer addition and rheological modifiers. The key findings from these studies are:

- Optimized HRWR dosage (1%–8%) enhances flowability, with reduced content improving both dispersion and compressive strength
- Proper mixing procedures can increase fluidity and improve uniformity of UHPC
- Welan gum (WG) is more effective than nanoclay (NC) in enhancing thixotropy, particularly in mixtures with variable SP dosages
- Minimizing entrapped air during mixing improves rheology and overall workability, ensuring better consistency and performance in UHPC applications

Curing regime

Curing plays a crucial role in the mechanical properties, durability, and long-term performance of (UHPC). Various curing regimens have been investigated to optimize compressive strength, tensile behavior, shrinkage control, and overall microstructural development. Studies have evaluated different curing temperatures, durations, and moisture conditions to understand their impact on hydration, mechanical properties, and shrinkage rates in UHPC mixtures.

Effect of Curing on Strength Development

Talebinejad et al. (2004) examined the effects of different curing regimens on the compressive strength of UHPC, considering variations in w/cm ratio (10%–20%), cement content 81.16 – 131.48 lb/ft³ (1300–2105 kg/m³), and silica fume percentage (20%–35%). The study evaluated four curing conditions, where specimens were initially cured at ambient temperature for seven days before undergoing different post-curing treatments. The first curing regimen maintained the specimens at ambient temperature for full duration. The second involved wet curing at 90°C for two days, followed by ambient storage, while the third extended the wet curing at 90°C to four days before transitioning to ambient conditions. The fourth and most intensive regimen combined four days of wet curing at 90°C with an additional two days of dry curing at 200°C, after which specimens were returned to ambient conditions. Among these regimens, the second and third curing option produced higher ultimate compressive strength of 33,794 psi (233 MPa) and 36,114 psi (249 MPa) compared to the first curing regimen of 22,046 psi (152 MPa). However, the fourth option produced the highest compressive strength of 47,137 psi (325 MPa), demonstrating the beneficial effects of high-temperature curing on UHPC strength development.

Graybeal (2006) conducted an FHWA study to characterize UHPC, evaluating its compressive and tensile strength, durability, creep, and shrinkage behavior under four different curing regimens: steam curing, untreated curing, tempered steam curing, and delayed steam curing. Compressive strength tests followed ASTM C39 for cylinders (3 in. diameter) and ASTM C109 for cubes (2 and 4 in.), with nearly 1,000 specimens tested from 44 batches of UHPC. The study found that steam-cured specimens achieved an average compressive strength of 30,458 psi (210 MPa), whereas untreated specimens exhibited significantly lower strength of 21,610 psi (149 MPa). Similarly, split tensile strength increased from 20,595 psi (142 MPa) in untreated specimens to 29,878 psi (206 MPa) in steam-treated specimens. The study also revealed that UHPC exhibited ductile stress-strain behavior when left untreated within the first one to three days of curing, allowing it to sustain deformation before failure. However, when steam curing was applied early, UHPC displayed a brittle response, where compressive failure occurred suddenly upon reaching peak load.

Graybeal also observed that UHPC experienced significant early-age shrinkage. The steam treated specimens reached a shrinkage of 850 microstrain over one year, whereas the untreated specimens exhibited shrinkage beyond 790 microstrain at 40 days after casting (24 hours after setting shrinkage rate of 60 microstrain per hour were observed for steam cured specimens).

Alsalman et al. (2017) investigated the effects of curing conditions on a UHPC mixture developed using locally available materials from Arkansas. Four different curing regimens were tested by varying the curing period (5-90 days), the curing temperature 69.8°F, 140°F, 194°F (21°C, 60°C, 90°C) and relative humidity (50% and 100%). Among the tested curing regimens, the most effective approach was the curing regimen which involved two days of curing at 140°F (60°C) followed by an additional three days at 194°F (90°C), resulting in the highest compressive strength of 25,962 psi (179 MPa).

Effect of Curing on Strength and Durability

Carey et al. (2020) evaluated the impact of different curing regimes on the mechanical and thermal properties of UHPC, varying w/cm ratio (0.11–0.19), fa/cm ratio (0–0.90), and fiber/cement ratio (0–0.23). The study tested four distinct curing regimens. The first regimen involved six days of curing at 69.8 - 77°F (21–25°C) and 100% relative humidity, followed by an additional seven days in a 194°F (90°C) water bath. The second curing regimen maintained the specimens at 69.8 - 77°F (21–25°C) and 100% relative humidity for six days before testing. The third followed the same six-day initial curing period but included an additional seven days in a 122°F (50°C) water bath. The fourth simulated real-world curing conditions by allowing specimens to cure using their own heat of hydration within insulating blocks for three days, after which they were cooled to room temperature before testing.

The results indicated that Curing Regime 1, which included high-temperature water bath curing at 194°F (90°C), produced the highest compressive strength of 29,460 psi (203 MPa). This regimen also resulted in the highest indirect tensile strength, suggesting that controlled high-temperature curing enhances UHPC's microstructure and mechanical properties.

Summary of Curing Regime Optimization in UHPC

Curing in UHPC is influenced by multiple factors, including temperature, curing duration, moisture conditions, and curing sequence. The key findings from these studies are:

- Higher curing temperatures significantly enhance strength
- Steam curing improves compressive and tensile strength; however, it also increases brittleness
- Early-age shrinkage is significant, it can be up to 95% of total shrinkage within two months
- Multi-stage curing (such as 140°F (60°C) for two days followed by 194°F (90°C) for three days) can balance strength development and brittleness, improve overall durability
- Water bath curing following initial ambient curing achieves the highest compressive and tensile strength, optimizing hydration and microstructure

Temperature resistance

The temperature resistance of UHPC is crucial for ensuring durability and structural integrity under high-temperature exposure. Due to its dense microstructure, UHPC is particularly susceptible to explosive spalling, making it essential to explore strategies for improving thermal stability, residual strength, and fire resistance through optimized material selection, fiber reinforcement, and aggregate modifications.

Effect of High-Temperature Exposure on UHPC Strength

Lian et al. (2018) studied the effects of exposing UHPC to temperatures up to 1,832°F (1,000°C). Specifically, six UHPC mixtures were examined to evaluate strength loss while investigating the effects of aggregate type, fiber type, and heating rate. The mixtures with quartz sand (Q) and steel slag (S) were divided into series 1 and in series 2, respectively. The mixtures in series 1 were further divided into four categories based on fiber inclusion (Figure 7.1), they are no fiber (Q-0),

2 vol% steel fiber (Q-S), 2 vol% PP fiber (Q-PP) and combination of 1 vol% steel fiber and 2 vol% PP fiber(Q-SP). Similarly, the mixtures in series 2 were divided into two categories according to fiber inclusion, they are no fiber (S-0) or combination of 1 vol% steel fiber and 2 vol% PP(S-SP) fiber.

Figure 7.1. Steel fiber and PP fiber

A total of 144 specimens were tested for compressive strength at six target temperatures: 68°F (20°C), 392°F (200°C), 752°F (400°C), 1,112°F (600°C), 1,472°F (800°C), and 1,832°F (1,000°C). The heating rate was set at 7.2°F/min (4°C/min) according to ASTM E831, with additional tests conducted at 1.8 °F/min (1°C/min) and 14.4°F/min (8°C/min). In the study, the holding time for all specimens was consistently set at 2 h to ensure uniformly distributed temperatures.

The effect of heating rates on explosive spalling of heated UHPCs was investigated. For mixtures without PP fibers (Q-0, S-0, Q-S) effect of heating rate on explosive spalling was observed and compared under identical target temperature of 752°F (400°C) and heating rate of 39.2°F/min (4°C /min). All mixtures suffered explosive spalling when being heated to the target temperature of 752°F (400°C). PP fiber, which melts at approximately 329°F (165°C), helped release vapor pressure, reducing the risk of explosives. For mixtures including PP fibers, none of the specimens experienced explosive spalling at a target temperature of 392°F (200°C). At 752°F (400°C), half of the four S-SP specimens displayed mild spalling, while the remaining stayed intact. Spalling occurred in all specimens to some extent between 735.8°F (391°C) and 937.4°F (503°C) at temperatures of 1,112°F (600°C) and above. Compared to hybrid fiber mixtures, consisting of both steel and PP fibers, Q-P concrete, which only contained PP fibers, had more severe and frequent spalling among the mixtures under investigation. This indicates that steel fibers reduce the probability and intensity of spalling resulting from thermal stress and incompatibility between the aggregate and the cement paste. However, they are unable to prevent the occurrence of explosion resulting from built-up vapour pressure.

Additionally, the compressive strength results showed that for all mixtures, compressive strength increased for an increase in temperature up to 392°F (200°C), compared to the compressive strength of control specimen at 68°F (20°C). Due to explosive spalling, strength results were not recorded above 392°F (200°C) for mixtures without fiber inclusion. For the mixtures including fibers, strength gain was observed in all the mixtures, for a rise in temperature from 392°F (200°C) to 752°F (400°C). As the temperature rises from 752°F (400°C) to 1,112°F (600°C), only S-SP mixture exhibited a strength gain, reaching 1.28 times the strength at 68°F (20°C), while Q-P and

Q-SP mixture exhibited a decline in strength by 0.89 times and 0.95 times of the strength at 68°F (20°C), respectively. For a further rise in temperature up to 1,832°F (1,000°C), all the mixtures experienced further reductions in strength in comparison to control specimen strength.

Effects of Exposure Duration and Fiber Content

Ahmad et al. (2019) studied the effects of heat exposure, duration, and fiber content on UHPC containing fine dune sand rich in silica as aggregate and copper-coated plain steel fibers as reinforcement. The study examined four UHPC mixtures with steel fiber contents of 2%, 4%, 6%, and 8% (by mass). Each mixture was exposed to 572°F (300°C) for different durations: 60, 120, 180, 240, and 300 minutes. The heating rate was 54°F/min (30°C/min), and cylindrical specimens 2.95 in. (75 mm) in diameter, 5.9 in (150 mm) in height were tested under uniaxial compression following ASTM C39.

Explosive spalling occurred in all UHPC mixtures at approximately 662°F (350°C), suggesting that a higher heating rate 54°F/min (30°C/min) better simulates real-world fire conditions. The study further revealed that prolonged exposure increased compressive strength, while modulus of elasticity decreased due to matrix-fiber bond degradation. After 300 minutes of exposure, compressive strength increased in the range of 37% to 41%, while modulus of elasticity decreased in the range 27% to 31% compared to control specimens at room temperature. The modulus of toughness increased in the range of 121% to 149%, but flexural strength decreased in the range of 13% to 27% due to fiber-matrix bond deterioration for varying duration of heat exposure. The study concluded that increasing steel fiber content beyond 6% (2% by volume) provided no additional benefits at elevated temperatures.

Use of Natural Fibers for Thermal Spalling Resistance

Zhang et al. (2020) investigated natural fibers as a sustainable alternative to polypropylene (PP) fibers for improving spalling resistance in UHPC. The study examined jute fiber incorporation at 0.19, 0.31 and 0.62 lb/ft³ (3, 5, and 10 kg/m³) and evaluated compressive strength, hot permeability, and thermal stability. Additionally, four mixtures were prepared with steel fiber contents ranging from 0 to 0.62 lb/ft³ (0 to 10 kg/m³).

Specimens were exposed to 392°F (200°C), 752°F (400°C), 1,112°F (600°C) and 1,472°F (800°C) to assess residual mechanical properties and dimensional stability. Thermal analysis examined dimensional changes in jute fibers and their potential to reduce explosive spalling.

The results showed that compressive strength increased up to 392°F (200°C) but declined beyond 752°F (400°C). Under ambient condition, UHPC with 0.19 lb/ft³ (3 kg/m³) of jute fibers showed no strength change compared to UHPC without jute fibers. However, at a higher fiber dosage of up to 0.62 lb/ft³ (10 kg/m³), compressive strength decreased by up to 13%. At 392°F (200°C), strength increased regardless of fiber presence. Between 392°F (200°C) and 752°F (400°C), changes in strength were minimal. However, at temperatures exceeding 752°F (400°C), strength loss became more pronounced with increasing fiber content, suggesting that higher fiber dosages negatively impact high-temperature performance.

131

7.3.2 Optimization of Mechanical Performance of UHPC

Concrete Strength

The compressive strength of UHPC is influenced by multiple factors, including the water-to-cement (w/cm) ratio, binder composition, aggregate gradation, fiber content, and curing conditions. Several studies have investigated the effects of these parameters to optimize UHPC strength development.

Effect of Water-to-Cement Ratio and Binder Composition

Talebinejad et al. (2004) examined the impact of w/cm ratio, cement content, and silica fume percentage on UHPC compressive strength. A total of 38 mixture proportions were tested, with w/cm ratios ranging from 10% to 20%, cement contents between 81.16 – 131.48 lb/ft³ (1300–2105 kg/m³), and silica fume percentages of 20–35%. The study found that reducing the w/cm ratio from 20% to 11.5% increased compressive strength by approximately 46%.

Later, Park et al. (2004) investigated the role of each UHPC ingredient in strength development, varying water-to-binder (w/b) ratios (0.16–0.24), silica fume content (0–0.35), sand size (below 5 mm), filler powder type and content (0–0.4), and steel fiber content (0.20–0.24). The results indicated that compressive strength increased as the w/b ratio decreased. However, further reducing the w/b ratio to achieve a target strength of 26,107 psi (180 MPa) of UHPC mixtures became challenging, as failures occurred at the interface between the cement paste and fine aggregates rather than within the paste itself. Therefore, a w/b ratio of 0.20 was required to achieve compressive strength of 26,107 psi (180 MPa) or greater. According to results, for a constant silica fume/cement ratio of 0.25, the highest compressive strength of 20,305 MPa (140 MPa) was obtained with a w/b ratio of 0.16. The strength gradually decreases to 15,954 psi (110 MPa) for further increase in w/b ratio to 0.24.

Effect of Cement Type and Air Content

Dils et al. (2013) studied six different Belgian cement types and their effects on workability, rheology, and compressive strength in UHPC mortar. The research also examined the influence of vacuum mixing on microstructure and air content. The findings highlighted that higher entrapped air content reduced workability and rheology, which in turn negatively impacted compressive strength. However, when all mixtures achieved a fresh air content below 0.5%, a significant improvement in compressive strength was observed. Additionally, the study demonstrated that reducing air bubble content not only enhanced mechanical performance but also improved workability and rheology effects of vacuum mixing on microstructure and air content.

Effect of Nanomaterials on Strength Enhancement

A study in 2016, examined the effects of graphite nanoplatelets (GNPs) and carbon nanofibers (CNFs) on UHPC strength and mechanical behavior (Meng & Khayat, 2016). Nanomaterial content ranged from 0% to 0.3% by weight, with compressive strength increasing from 25,382 psi (175 MPa) at 0% nanomaterials to approximately 26,397 psi (182 MPa) at 0.3%. Beyond compressive strength, incorporating nanomaterials significantly enhanced tensile and flexural

properties. Increasing carbon nanofiber (CNF) content from 0% to 0.3% resulted in a 56% increase in tensile strength, a 108% improvement in energy absorption capacity, a 59% rise in flexural strength, and a 276% enhancement in toughness. Similarly, increasing graphene nanoplatelet (GNP) content from 0% to 0.3% led to a 40% increase in tensile strength and a 187% improvement in energy absorption capacity for GNP-C, while GNP-M exhibited a 45% increase in tensile strength and a 153% improvement in energy absorption capacity. At 0.2% GNPs, UHPC mixtures exhibited strain-hardening behavior in both tension and flexure, further enhancing structural resilience. CNFs demonstrated superior tensile strength compared to GNPs, reinforcing their effectiveness in improving UHPC's ductility and crack resistance.

Impact resistance

The impact resistance of UHPC is a critical factor in its performance under dynamic loading conditions, particularly in applications requiring high energy absorption and crack resistance. Researchers have explored various cementitious materials and nanoparticles to enhance fiber-matrix bonding and microstructural density, thereby improving mechanical performance under impact loading.

Wu et al. (2018) investigated the static and dynamic mechanical properties of UHPC incorporating Portland cement, fly ash, slag, silica fume, nano-$CaCO_3$, and nano-SiO_2 (Wu et al., 2018). Dynamic load testing was performed using an Instron CEAST 9340 impact testing machine, applying a maximum load of 4,496 lb (20 kN) from a drop height of 43.3 in (1.1 m), with an impact velocity ranging from 0.00787 to 0.063 in/s (0.2 to 1.6 mm/s). Microstructural analysis using mercury intrusion porosimetry (MIP) revealed that UHPC mixtures incorporating 20% slag and 3.2% nano-$CaCO_3$ exhibited enhanced fiber-matrix bonding and superior flexural performance. The inclusion of supplementary cementitious materials (SCMs) and nanoparticles significantly refined the microstructure, reduced porosity, and improved impact resistance, demonstrating their effectiveness in optimizing UHPC's dynamic performance.

Bond behavior

The bond behavior of reinforcing steel in (UHPC) is critical for ensuring structural integrity and load transfer efficiency. Several studies have investigated the effects of embedment length, bar size, fiber content, and reinforcement orientation on bond strength and development length in UHPC.

Influence of Embedment Length, Concrete Cover, and Bar Type

Graybeal (2014) conducted an extensive study on the bond behavior of reinforcing steel in UHPC girders using direct tension pullout tests through the FHWA. Over 200 tests were performed to analyze the effects of embedment length, concrete cover, bar spacing, bar size, bar type, and concrete strength on bond strength.

The study tested various reinforcing bars (Figure 7.2), including uncoated and epoxy-coated bars of different sizes and grades. According to the results, bond strength increases with an increase in embedment length. The bar stress at bond failure increased from 90 ksi (621 MPa) to 166 ksi

(1,145 MPa) for an increase in embedment length from 3.88 in (98.5 mm). to 6.31 in. (160.2 mm), with a side cover of 2.24 in (56.89 mm).

Design recommendations for embedding deformed reinforcing bars in UHPC were provided to ensure adequate bond strength. The recommended conditions include:

- Bar sizes from No. 4 to No. 8, with either uncoated or epoxy-coated bars
- Minimum embedment length of 8db and minimum side cover of 3db
- Bar clear spacing between 2db and the lap splice length
- UHPC with a minimum compressive strength of 13.5 ksi (93 MPa)
- Lap splice reinforcement requiring a lap splice length of at least 75% of the embedment length
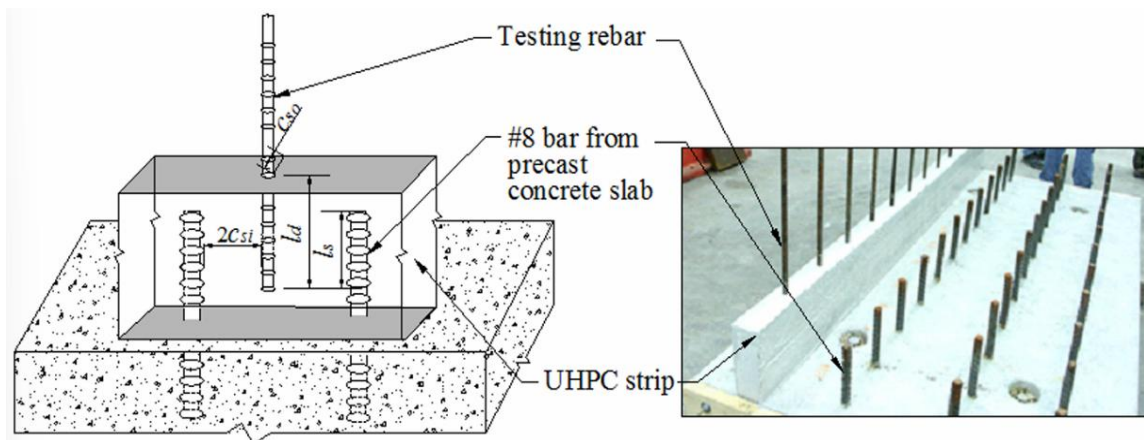
Figure 7.2. Configuration of test specimens

Effect of Fiber Volume and Orientation on Bond Strength

Roy et al. (2017), investigated how fiber volume and orientation affect the pullout behavior of steel reinforcement bars embedded in UHPC. The study tested steel fiber contents ranging from 0% to 3%, with fibers oriented parallel, perpendicular, or randomly distributed relative to the reinforcement bars. All specimens contained #3 and #4 rebars, with concrete cover values of 2.17db and 1.5db, respectively.

The results showed that pullout load increased with fiber volume. The highest pullout resistance was recorded in specimens with perpendicular fiber orientation, while parallel fibers resulted in the lowest pullout capacity. Specimens with random fiber orientation exhibited intermediate bond performance. Additionally, higher fiber content enhanced resistance to pullout forces and allowed for greater deformation before failure, suggesting improved energy absorption and crack resistance in UHPC reinforced with well-distributed fibers.

Development Length and Bond Strength in Non-Proprietary UHPC

Montana State University, in collaboration with the Montana Department of Transportation, developed a non-proprietary UHPC and conducted tests to evaluate rebar bond strength and development length (Berry & Scherr Kirsten Matteson, 2021). The study focused on reinforcing

steel embedded in UHPC curbs, cast on top of conventional concrete slabs, and subjected to direct tension pullout tests. A total of 56 pullout tests were performed, with 40 specimens systematically varying bar size, embedment depth, clear spacing, and clear cover to isolate the effects of these parameters. The remaining 16 specimens were designed to meet the FHWA-recommended minimum embedment depth for UHPC. The embedment length was 8 inches, and testing was conducted until yielding but before rupture to ensure safety. The study examined No. 4, 5, 6, and 7 reinforcing bars, all of which were Grade 60 conventional reinforcement. Notably, none of the specimens failed due to bond failure, confirming UHPC's exceptional bond strength and its ability to fully develop reinforcing bars within relatively short embedment lengths.

Summary of Bond Behavior in UHPC

- Longer embedment lengths, increased side cover, and optimized bar spacing enhance bond strength in UHPC
- UHPC exhibits superior bond performance compared to conventional high-strength concrete, even at shorter development lengths
- Recommended embedment conditions for UHPC include bar sizes No. 4 to No. 8, minimum embedment of 8db, and a minimum side cover of 3db
- Pullout resistance increases with fiber volume, with perpendicular fibers yielding the highest bond strength
- Non-proprietary UHPC demonstrated sufficient bond strength to prevent bond failure, reinforcing its effectiveness in infrastructure applications

Durability

The durability of UHPC is a critical factor in its long-term performance, particularly in aggressive environments where resistance to carbonation, chloride ingress, chemical attack, alkali-silica reaction (ASR), and freeze-thaw cycles are essential. Several studies have evaluated the resistance of UHPC to deterioration mechanisms, comparing it to conventional and high-performance concrete.

Pierard et al. (2013), conducted an extensive durability assessment on various types of UHPC, testing resistance to carbonation, chloride diffusion, chemical attack, ASR, and freeze-thaw cycling, both with and without de-icing salts. The study included lab-produced and precast UHPC, evaluating three different mixture compositions with cement contents ranging from 31.22 to 51.84 lb/ft³ (500 to 830 kg/m³) and silica fume between 6.24 lb/ft³ (100 kg/m³) and 10.35 lb/ft³ (166 kg/m³).

The carbonation test, conducted over one year in a 1% CO_2 atmosphere, showed that UHPC exhibited a carbonation depth of only 0.06 to 0.0787 in (1.5 to 2 mm), significantly lower than conventional concrete. Compared to required cover depths for 100-year carbonation resistance, UHPC required less than 0.196 in (5 mm), while ordinary concrete required 2.56 in (65 mm) and high-performance concrete (HPC) needed 0.98 in (25 mm). The chloride diffusion test demonstrated exceptionally low chloride penetration, reaching only 0.0787 to 0.118 in (2 to 3 mm) after 90 days of accelerated exposure, confirming UHPC's high resistance to chloride ingress.

In freeze-thaw testing, UHPC showed minimal mass loss after 112 cycles, even in the presence of sodium chloride (NaCl) solution, highlighting its resilience in de-icing conditions. The ASR test indicated no expansion or deterioration, even when the total alkali content exceeded 0.25 lb/ft³ (4 kg/m³), ensuring UHPC's stability against ASR-induced cracking. Sulfate resistance tests revealed no expansion or deterioration even after 500 days in sodium sulfate solution, confirming UHPC's robustness in sulfate-rich environments. However, the sulfuric acid attack test indicated relatively low resistance, with 0.031 in (0.8 mm) expansion and 0.051 in (1.3 mm) material loss after 12 weeks, whereas ordinary concrete containing blast furnace slag cement exhibited only 0.0039 in (0.1 mm) expansion and no material loss under similar conditions.

Alkaysi et al. (2016) further examined the influence of silica powder and cement type on UHPC durability, evaluating resistance to freeze-thaw cycles, chloride ingress, and air void distribution. The study tested three cement types, including portland Type I, portland Type V, and a 50:50 blend of portland Type I with ground granulated blast furnace slag (GGBFS). Each cement type was tested with three different cement-to-silica powder ratios of 1:0.25, 1:0.15, and 1:0 to assess the effect of silica powder content.

Results confirmed that all UHPC mixtures exhibited exceptional freeze-thaw resistance, with mass loss well below acceptable limits after more than 60 cycles. Although variations in silica powder and cement type slightly influenced freeze-thaw resistance, the overall mass loss remained minimal. The study found no direct correlation between air content (ranging from 3.0% to 7.5%) and freeze-thaw resistance, indicating that UHPC durability is more dependent on low water uptake rather than air voids. Furthermore, all UHPC mixtures demonstrated excellent chloride penetration resistance, with the portland Type I/GGBFS cement blend exhibiting the lowest permeability. Notably, the silica powder content did not significantly impact ion permeability or overall durability, suggesting that it could be removed or reduced to lower material costs without compromising performance.

These studies confirm that UHPC exhibits superior durability compared to conventional concrete, with outstanding resistance to carbonation, chloride ingress, freeze-thaw cycles, ASR, and sulfate attack. However, its resistance to sulfuric acid remains a limitation, requiring potential modifications to improve acid resistance in highly aggressive environments.

7.3.3 Environmental Impact

The environmental impact of Ultra-High Performance Fiber-Reinforced Concrete (UHPFRC) has been a key concern due to its high cement content and associated carbon emissions. Efforts have been made to mitigate these impacts by incorporating alternative materials such as ground granulated blast furnace slag (GGBS), silica fume (SF), recycled glass cullet (RGC), natural sand, and limestone powder.

In 2008, UHPFRC was successfully applied in dam repairs, bridge deck overlays, coupling beams in high-rise buildings, and other structural applications (S. L. Yang et al., 2009). Despite its advantages, the high cost of production is limited to wider adoption. Studies explored the partial replacement of cement with GGBS and SF, which helped reduce both environmental and economic

impacts without significantly affecting mechanical performance. Researchers also investigated replacing the commonly used silica sand with locally sourced natural sand and recycled glass cullet (RGC). The results showed that natural sand produced similar strength and ductility as silica sand, while RGC resulted in approximately 15% lower performance (i.e. flexural strength, compressive strength, fracture energy) compared to silica sand.

A more recent study explored methods to reduce the environmental footprint of UHPC by incorporating high-volume limestone powder (P. P. Li, Brouwers, et al., 2020). Five different UHPC mixtures were tested, with limestone powder replacing 0% to 80% of the binder volume. The optimal mixture contained 50% limestone powder, which reduced embedded CO_2 emissions by 47% (474 kg/m³) and lowered production costs by 0.722 €/ft³ (25.5 €/m³), while still achieving a 28-day compressive strength of 22,190 psi (153 MPa) with a cement content of only 34.96 lb/ft³ (560 kg/m³).

7.3.4 Economic Considerations/Aspects

The cost of UHPC remains a major barrier to widespread implementation, primarily due to its high binder and fiber content. Several studies have aimed to develop cost-effective UHPC mixtures by optimizing material composition while maintaining adequate performance.

A study in 2008 explored the economic impact of UHPC by incorporating GGBS and SF as partial cement replacements (S. L. Yang et al., 2009). In this study, cement was replaced with 35% GGBS and 10% SF by weight, while steel fibers were included at 2% by volume. To further reduce costs, researchers evaluated the use of local natural sand and RGC as alternatives to silica sand. Natural sand provided similar mechanical properties and ductility, whereas RGC led to a 15% reduction in strength performance in comparison to silica sand.

Alkaysi et al. (2016) conducted a study to balance cost and performance in UHPC, testing various combinations of silica fume, silica powder, and different types of cement. The study evaluated three types of cement (white cement Type I, portland cement Type V, and a blend of portland Type I with GGBS), along with steel fibers at 0.5%, 1.0%, and 1.5%. The cost of each mixture was measured as a cost index relative to a baseline mixture published in 2011. Results showed that mixtures containing white cement had the highest costs, while using portland Type I cement reduced costs. For every 1% increase in steel fiber content, cost index increases by 1. The most cost-effective mixture, GG-25-00, contained portland Type I cement blended with GGBS, 25% silica fume, 0% silica powder and 1.0% to 1.5% steel fibers, achieving the lowest cost index of 0.52. Although this mixture did not have the highest mechanical performance, it was considered sufficient for reducing cracking and structural durability at a lower cost. The study ultimately excluded silica powder due to its high cost and limited performance benefits.

7.4 Applications of UHPC

7.4.1 Bridges

UHPC has significantly advanced bridge construction, offering higher strength, durability, and reduced maintenance requirements. Its applications range from pedestrian and highway bridges to

rehabilitation and accelerated bridge construction (ABC) methods, enabling faster, more cost-effective, and longer-lasting infrastructure solutions.

Early Applications of UHPC in Bridges

The world's first major structure built with Reactive Powder Concrete (RPC) was the Sherbrooke pedestrian and bike bridge in Quebec (Figures 7.3 & 7.4), Canada, completed in July 1997 (Blais et al., 1999). The 197-foot span bridge was constructed using precast, prestressed RPC, consisting of six prefabricated, match-cast segments. The top and bottom chord members incorporated RPC with a compressive strength of 29,000 psi (200 MPa), while the diagonal web members, confined in stainless steel tubes, achieved 50,000 psi (345 MPa) in compression. The project aimed to demonstrate the lightweight, durable, and aesthetic potential of RPC, serving as a real-world research model. Due to its high strength, the bridge used significantly less concrete, reducing weight and allowing for rapid on-site assembly within four days. The structure was also instrumented with sensors to monitor long-term performance.
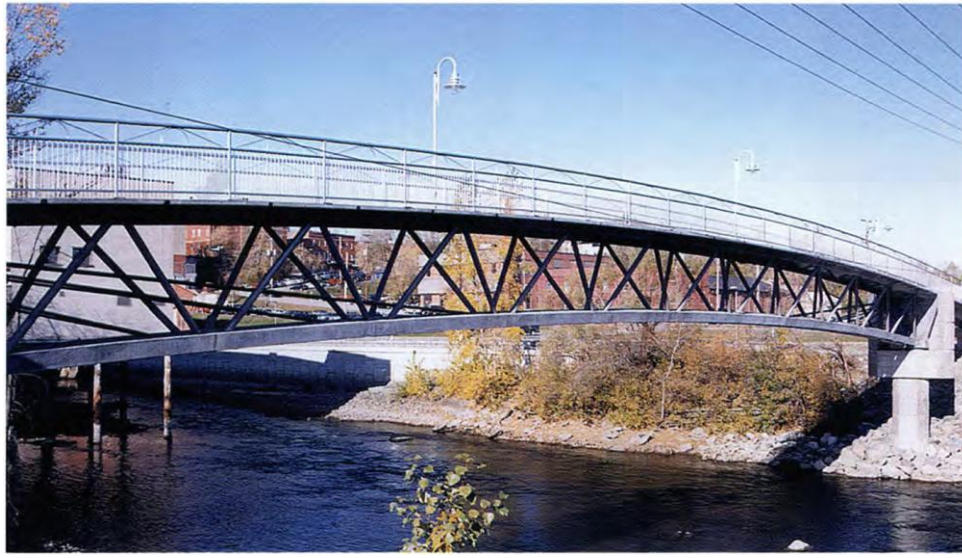

Figure 7.3. The Sherbrooke Footbridge in Sherbrooke, Quebec, spans across the Magog River

Figure 7.4. View of completed bridge

By 2001, UHPC was first used in road bridge construction with two overpasses on the Bourg-lès-Valence bypass in France (Ziad Hajar, 2004). These two-span structures incorporated 39.37 ft (12 m) wide decks made from π-shaped precast UHPC beams, significantly reducing the self-weight of the bridge. The beams, produced with self-compacting UHPC containing 3% steel fibers, achieved a compressive strength of 24,656 psi (170 MPa) and tensile strength of 1,160 psi (8 MPa). The deck thickness was reduced to 9.84 in (0.25 m), compared to 29.52 in (0.75 m) in conventional prestressed slab bridges, making it three times lighter. Extensive pre-construction testing verified the material performance and prestress distribution, while efficient prefabrication allowed for rapid installation using truck-mounted cranes. This project successfully showcased UHPC's structural efficiency, durability, and accelerated construction benefits.

UHPC in Bridge Rehabilitation and Seismic Retrofitting

The Mission Bridge rehabilitation project in Canada (Figure 7.5), completed in 2014, utilized UHPC for seismic strengthening and durability enhancement. The bridge, originally built in 1973, spans 3,691 ft (1,125 m) and consists of post-tensioned concrete, steel I-girders, and steel box beams (Kennedy & Habel, 2015). A seismic assessment in the early 2000s identified significant vulnerabilities, particularly in the S4 pier, which was predicted to experience 15.74 in (400 mm) of lateral spreading during an earthquake. To address this, an 8.85 in (225 mm) thick UHPFRC column jacket was applied, reinforcing pier ductility and spalling resistance. Field-cured UHPC reached an average 28-day compressive strength of 21,465 psi (148 MPa), providing an efficient and unobtrusive retrofit compared to traditional methods.

Figure 7.5. Casting of UHPC Jacquet of Pier S4

UHPC in Accelerated Bridge Construction (ABC)

Aaleti et al. (2010) investigated the use of UHPC waffle deck systems for accelerated bridge construction (ABC), particularly in the Wapello Bridge in Iowa. The goal was to determine whether UHPC waffle deck panels (Figure 7.6) could provide a durable, efficient, and rapid construction method, reducing maintenance needs and life-cycle costs. Two full-depth precast UHPC waffle deck panels (8 ft × 9 ft 9 in × 8 in) were tested under service, fatigue, and ultimate load conditions.

The study evaluated different connection systems, including shear pocket connections, longitudinal panel-to-girder connections, and panel-to-panel connections. The shear pocket connection used embedded shear hooks within UHPC-filled pockets, while the longitudinal connection employed dowel bars to create a positive moment connection. Fatigue testing demonstrated no damage under service loads, and deck displacements remained well below AASHTO limits. The findings confirmed that UHPC waffle decks offer superior durability, stiffness, and accelerated construction potential, making them an ideal solution for prefabricated bridge decks.
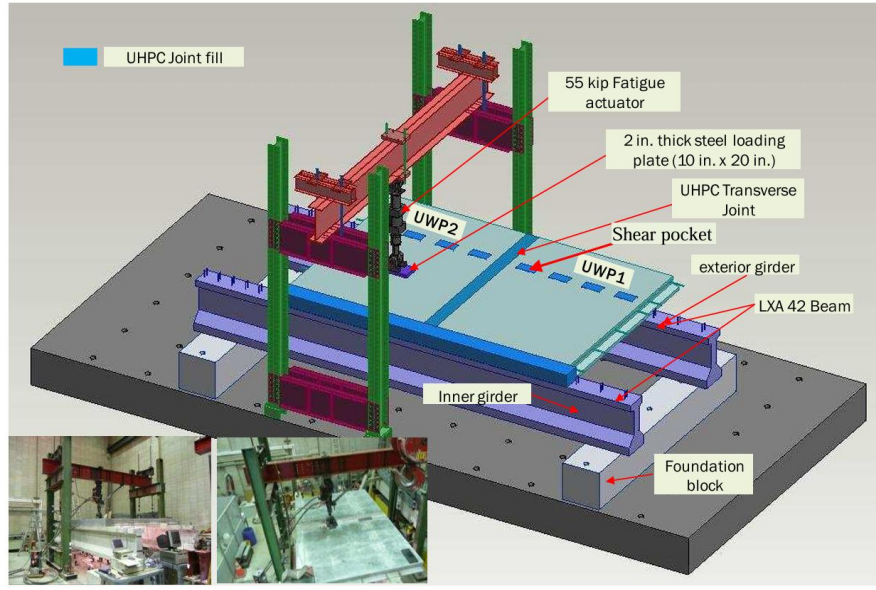
Figure 7.6. Schematic of the setup used for testing of the UHPC Waffle deck panel system

Optimization of UHPC in Bridge Design

Almansour et al. (2010) conducted a comparative study to evaluate the efficiency of UHPC in girder bridge design, focusing on reducing girder size, minimizing material use, and enhancing structural performance. The study considered two- and three-lane simply supported bridges and compared UHPC girders with HPC girders. The results demonstrated that using UHPC could reduce concrete volume by up to 49% for CPCI 1200 girders and 65% for CPCI 900 girders. The required prestressing steel area for UHPC-CPCI 900 girders was only 14% higher than for UHPC-CPCI 1200 girders, while the concrete volume reduction for girders was 33%, making UHPC a more efficient structural material.

7.4.2 Buildings

UHPFRC has been widely utilized in iconic architectural structures, offering exceptional durability, structural efficiency, and aesthetic flexibility. Its application in museums and stadiums showcases its ability to support intricate designs, reduce material usage, and enhance long-term performance.

Fondation Louis Vuitton, Paris

The Fondation Louis Vuitton pour la Création (Figure 7.7), completed in 2014, is a museum characterized by its complex geometric design, a hallmark of the architect's vision (Aubry et al., 2014). The cladding consists of 19,000 unique prefabricated panels cast in white Ductal® UHPFRC, each individually molded and installed with butt joints. The 492.1 ft (150 m) long, 164 ft (50 m) wide, and 147.6 ft (45 m) high structure is enveloped by twelve large glass sails, creating a visually striking effect.

The panel design balanced architectural intent, fabrication limits, economic considerations, weight constraints, and structural resistance. To enhance strength without increasing thickness, a stainless-

141

steel reinforcement system was bonded to the back of each UHPFRC panel using a shear-resistant epoxy adhesive. This composite section allowed the UHPFRC to absorb compressive forces while the stainless-steel strip provided tensile reinforcement, improving structural efficiency. Stainless steel was preferred over carbon fiber due to its superior compatibility with structural demands and installation requirements.

Figure 7.7. UHPFRC cladding, the "Iceberg" at Fondation Louis Vuitton pour la Création, Paris, France (designed by Gehry Partners)

Qatar National Museum, Doha

The Qatar National Museum (Figure 7.8), completed in 2019, utilized UHPFRC cladding to achieve a smooth, uniform, and curved exterior surface while maintaining a massive, mineral-like appearance (Menétrey, 2019). The cladding system consisted of ribbed decks supported by a primary steel structure, an insulation and waterproofing membrane, a secondary steel structure, and UHPFRC cladding panels.

By using UHPFRC, the panel thickness was reduced to 40 mm, significantly lowering material usage and weight while still meeting high durability requirements. Expansion joints were incorporated every four meters to accommodate extreme temperature variations. Covering an area of 29.65 acres (120,000 m²), the UHPFRC solution provided a structurally efficient and aesthetically seamless façade, demonstrating its ability to perform under extreme environmental conditions while reducing material consumption.

Figure 7.8. Qatar National Museum (nmoq.org.qa)

Museum of European and Mediterranean Civilizations, Marseille

The Museum of European and Mediterranean Civilizations (MuCEM) (Figure 7.9), completed in 2013, was the first building in the world to extensively incorporate UHPFRC in both structural and aesthetic elements (Mazzacane et al., 2013). The material was used for tree-like façade columns, bridge decks, brackets, roof lattices, and footbridges.

The museum features two pedestrian footbridges: the Saint Laurent Church (ESL) footbridge, spanning 226.37 ft (69 m), and the Fort Saint-Jean (FSJ) footbridge, with spans of 55.83, 251 and 60.36 ft (17.02, 76.52, and 18.40 m). Lattice structures, both horizontal and vertical, were integrated into the design, and UHPFRC brackets were employed to support the footbridges, replacing traditional steel elements due to UHPFRC's higher fire resistance and structural efficiency.

The primary challenge was in the connection zones, where stress concentrations were highest. These zones were cast in situ, making them less resistant than prefabricated elements. However, the innovative use of UHPFRC ensured structural integrity and enhanced longevity, demonstrating its effectiveness in modern architectural applications.

Figure 7.9. MuCEM / Museum of Civilizations of Europe and the Mediterranean © Roland Halbe (https://arquitecturaviva.com/works/mucem-museum-of-civilizations-of-europe-and-the-mediterranean#lg=1&slide=0)

Stade Jean Bouin, Paris

The Stade Jean Bouin, renovated and reopened in 2013, features 5.19 acres (21,000 m²) of undulating UHPFRC latticework, used for both the façade and the roof (Mazzacane et al., 2013). The double-curved geometry of the roof ensures waterproofing and structural efficiency, while the stadium's seating capacity was increased from 5,000 to 20,000 spectators.

To achieve a lighter appearance, titanium dioxide was added to the UHPFRC mixture. The panel-to-panel connections (Figure 7.10) utilized an innovative male-female system with a 0.98 in (25 mm) spacing, functioning as a gutter to ensure compliance with French building codes. Despite its complex geometry, the facade was designed using a modular approach, employing lightweight, isostatic triangular panels with a limited number of angles to simplify erection and reduce construction time.

Figure 7.10. Pattern and connections and view from the roof

The 1.37 in (35 mm) panel thickness was optimized for both cost-efficiency and structural feasibility, and the integration of glass inserts within the panels demonstrated UHPFRC's ability to meet design and performance requirements for transparency, weight reduction, and structural resilience.

Olympic Museum, Lausanne

The Olympic Museum in Lausanne (Figure 7.11), Switzerland, underwent an extension and modernization, incorporating a new UHPFRC roof to accommodate increasing visitor numbers and contemporary museum standards (Muttoni et al., 2013). Various material alternatives were considered for the roof, including timber, aluminum, and hybrid combinations, but each presented durability, thermal, or cost limitations.

Timber was ruled out due to its poor long-term durability in exterior applications, even with chemical treatments. Aluminum required thermal joints and was considered less energy-efficient, while a hybrid timber-aluminum solution was deemed too costly and lacking sufficient implementation experience. Ultimately, UHPFRC was selected for its superior durability, structural efficiency, and ability to meet the museum's aesthetic and functional requirements.

Figure 7.11. Views of the roof of Olympic Museum, Lausanne

7.4.3 Other Structures

UHPC has been increasingly explored for specialized infrastructure, including nuclear power plants, tunnel systems, and wind turbine towers, due to its exceptional mechanical properties, durability, and resistance to environmental and mechanical stresses. Besides, it is also gaining traction in deep foundations, bridge structures, protective infrastructure, and specialized applications such as radiation shielding and functionally graded composite beams. Its exceptional strength, durability, and versatility allow for significant advancements in structural design, reducing material usage while enhancing performance.

UHPC in Wind Turbine Towers

A new wind turbine tower concept utilizing precast UHPC was developed in 2013 to enable the construction of taller towers while addressing transportation and assembly challenges associated with traditional steel towers (Sritharan & Schmitz, 2013). Steel tower sections, particularly at the base, often require multiple pieces for transport and on-site assembly, complicating logistics. The

precast UHPC design offers a more efficient solution, facilitating easier transportation and faster on-site construction while maintaining high structural performance.

Three precast UHPC tower designs were developed, each with a hub height of 328 ft (100 m), for potential field implementation. The structural system incorporates UHPC, high-strength concrete (HSC), and high-strength prestressing strands, optimizing both cost-efficiency and structural integrity. The tower features six exterior UHPC columns connected by bracing elements, forming a composite system that enhances stability without requiring rigid foundation connections. Concrete panels can be added between the columns to further reinforce the structure and enclose the interior.

Two assembly methods (Figure 7.12) were proposed for constructing the UHPC towers. The first method involves preassembling sections of the tower at ground level, stacking them in place, and post-tensioning the strands to secure the structure. The second method follows a layer-by-layer construction approach, installing the columns first, followed by the panels, and post-tensioning the tendons at each level before proceeding to the next stage. Both methods offer efficiency and precision, reducing on-site labor requirements and construction time.

A structural load test (HCUP-BC test) was conducted, with the tower subjected to a maximum load of 150 kips (670 kN). At the operational load of 100 kips (445 kN), the UHPC columns remained uncracked, and the connections exhibited no inelastic behavior, demonstrating high load-bearing capacity and structural resilience. Only minor microcracking was observed around the embedded connection plates in the panels, confirming the durability and reliability of the design.

The use of precast UHPC with post-tensioning enhances both economic feasibility and structural efficiency. Compared to traditional steel towers, this design reduces transportation constraints, as large steel sections are difficult to maneuver. Additionally, the increased tower height allows turbines to harness stronger winds at higher elevations, maximizing energy production efficiency. This innovative UHPC tower system offers a viable and scalable alternative to conventional steel wind turbine towers, supporting the expansion of renewable energy infrastructure.
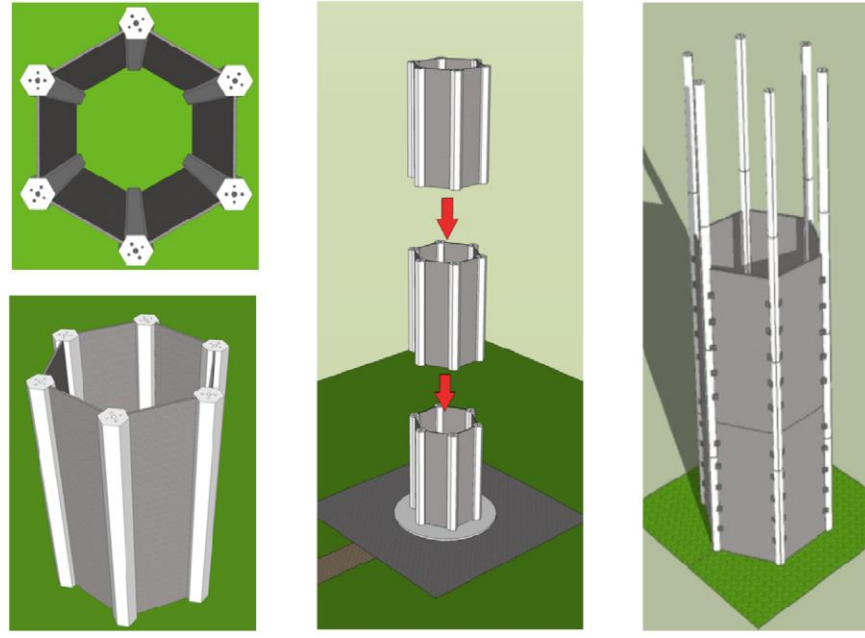
Figure 7.12. a) Tower cross section; b) Assembly method 1; c) Assembly method

UHPC in Deep Foundations

In 2008, the Iowa Highway Research Board and Iowa DOT conducted studies on UHPC piles to assess their drivability, strength, and economic viability (T. Vande Voort et al., 2008). A 10×10 in. tapered H-shaped prestressed UHPC pile was designed, incorporating low-relaxation prestressing strands. The UHPC pile had a cross-sectional area of 56.8 in² (366.45 cm²), significantly larger than the 16.8 in² (108.38 cm²) of an equivalent steel pile yet maintained a similar unit weight of 61.1 lb/ft (902.56 N/m). The moment of inertia for UHPC was 795 in⁴ (32,876 cm⁴), almost three times that of the steel pile 294 in⁴ (12,141.8 cm⁴), highlighting its superior stiffness and structural efficiency.

A drivability analysis using GRLWEAP software confirmed that UHPC piles could withstand driving stress without exceeding allowable limits, demonstrating their potential as a durable and cost-effective alternative to steel piles. Laboratory and field tests validated the moment-curvature response, and PDA measurements confirmed that UHPC piles could be driven without cushions in certain conditions. Additionally, UHPC piles showed no cracking or damage after driving, performing comparably to steel piles. Their axial load capacity was 86% greater than steel piles, suggesting that fewer piles could be required for bridge foundations, potentially reducing overall project costs.

UHPC in Long-Span Bridge Girders

Zhang et al. (2013) investigated UHPC pi-girders optimized for longer spans. Using finite element analysis (FEA), the study refined key girder parameters, including deck thickness, girder height, and prestressing strand count, to maximize UHPC's mechanical efficiency. The optimized girder sections, with depths of 47 inches or less, successfully supported spans of up to 135 feet (41.1 m) while meeting AASHTO LRFD Strength I load criteria.

147

A three-girder bridge model confirmed compliance with AASHTO deflection limits, while deck thickness analysis determined that a 4-inch (101.6 mm) deck was ideal for accommodating construction tolerances. Additionally, an optimal 15-foot (4.57 m) diaphragm spacing was identified to enhance transverse bending resistance. The findings provided a design framework for UHPC pi-girders, enabling span customization by adjusting prestressing strand quantities.

UHPC Bridge Deck Overlays

Khayat and Valipour (2018) explored the use of UHPC for bonded bridge deck overlays, focusing on cost-effectiveness and shrinkage mitigation. The researchers optimized UHPC mixtures by incorporating GGBS, LWS, and expansive cement (EXC) to reduce autogenous and drying shrinkage. Shrinkage decreased from 530 to 35 $\mu\varepsilon$ when 60% LWS was added, while a combination of 5–10% EXC and 60% LWS minimized shrinkage further.

UHPC overlays were applied of 0.98, 1.49 and 1.96 in (25, 38, and 50 mm) thicknesses, and temperature, humidity, and cracking behavior were monitored. Results showed no delamination or cracking after 200 days, confirming long-term durability. A life cycle cost analysis (LCCA) indicated that UHPC overlays provide superior flexural strength, faster construction, and reduced maintenance, making them a cost-effective alternative to latex-modified concrete (LMC) in large-scale applications.

A related study by Haber et al. (2018) evaluated UHPC overlay bond behavior using hydrodemolition and scarification surface treatments. Direct tension pull-off tests showed that hydrodemolition-treated surfaces achieved a peak bond strength of 3.42 MPa, whereas scarified surfaces only reached 113.12 psi (0.78 MPa). Field testing of the first UHPC bridge deck overlay in the U.S. demonstrated that well-consolidated UHPC achieved strong bonding with existing concrete, even when interface voids remained below 10%.

Functionally Graded UHPC Beams

Li et al. (2010) developed functionally graded UHPC beams (FGCB) by integrating UHPC, Two-Stage Concrete (TSC), and Slurry-Infiltrated Fibrous Concrete (SIFCON). The FGCB consisted of a SIFCON bottom layer and a TSC top layer, designed to enhance flexural strength and impact resistance.

Using three types of steel fibers 0.511 in (13 mm) straight, 1.18 in (30 mm) hooked, and 2.36 in (60 mm) 5D fibers, the researchers tested the flexural strength of concrete. Results show that the flexural strength of FGCB increased from 1,305 psi (9 MPa) to 2,088.5 psi (14.4 MPa) for 1% fiber content. The strength reaches a value of 6,309 psi (43.5 MPa) for 3% medium fiber inclusion. The impact resistance is predicted to vary linearly based on the flexural properties. These demonstrate the superior durability of functionally graded UHPC beams compared to traditional UHPC and SIFCON beams. The findings support FGCB as a high-performance alternative for impact-resistant structures.

UHPC for Nuclear Radiation Shielding

Khan et al. (2020) explored heavyweight UHPC (HWUHPC) for nuclear radiation shielding by partially replacing sand with hematite powder, a high-density material. Six HWUHPC mixtures were tested, with hematite powder content ranging from 0 to 57.57 lb/ft³ (0 to 922.48 kg/m³) and a water-to-binder ratio between 0.14 and 0.17. The dry density ranged from 162.33 to 181 lb/ft³ (2600 to 2900 kg/m³), meeting heavyweight concrete classification.

Gamma-ray shielding tests showed that higher hematite content reduced radiation penetration, with a required thickness of 8.18 in (208 mm) for 99% attenuation, compared to 9.72 in (247 mm) for UHPC without hematite. When compared to conventional heavyweight concrete (HWCC), HWUHPC required up to 30% less thickness for equivalent radiation shielding, confirming its superiority for nuclear applications.

7.4.4 Intelligent Design and Manufacturing of UHPC

Gosselin et al. (2016) developed a processing route for a 3D printing process for a large-scale complex geometry without the need for temporary support, achieving a new levels of design complexity. The system used a 6-axis industrial robot with HAL Robotics software, allowing a non-horizontal and non-straight slicing, unlike conventional 3-axis systems that lack precision when printing non-vertical elements.

The 3D printing process consists of two key steps. First, a finely graded mortar premixture is prepared with rheological properties optimized for pumping, characterized by a fine particle-size distribution, low critical shear stress, and slow hardening quality. To prevent premature setting due to its thixotropic nature, the premixture is continuously mixed in a shearing mixer. It is then conveyed via a peristaltic pump to a mixing screw within the printhead, where additives are introduced to accelerate the setting and enhance mechanical properties immediately after extrusion.

The premixture composition includes original portland cement CEM I 52.5N (30−40% w), crystalline silica (40−50% w), silica fume (10% w) and limestone filler (10% w). When mixed with a minimal amount of water (water-to-cement and sand mass ratio, w/(c+s) =0.1), the material forms an ultra-high performance self-placing mortar paste. A polymer-based gripping resin is added to improve the bounding between printed layers, while an accelerating and thresholding agent ensures the desired rheology, and a setting time required for 3D printing applications.

In this study, structural elements like a multifunctional wall element (Figure 7.13) and an acoustic damping wall (Figure 7.14) element were 3D printed. The multifunctional wall element serves as formwork that can be filled with either ultra-high performance fiber-reinforced concrete for structural support or an insulating material like foam for thermal efficiency. Additionally, some sections are intentionally left hollow to accommodate pipes or electrical wiring. The acoustic damping wall is designed as a modular element that provides both structural integrity and enhanced soundproofing performance. The varying hole geometries influence acoustic wave attenuation, optimizing the material's soundproofing properties based on cell structure and composition.
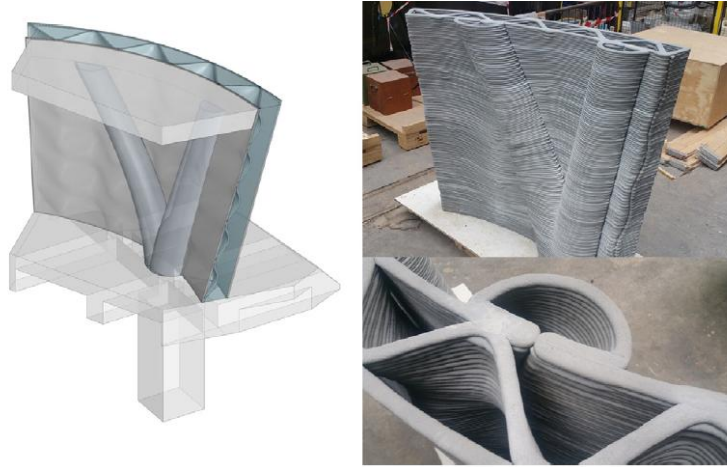
Figure 7.13. CAD model for the multifunctional wall and the 3DP-UHPC multifunctional wall

Figure 7.14. 3DP-UHPC acoustic damping wall element

Arunothayan et al. (2020) developed and characterized the properties of 3D-printable UHPFRC evaluating both fresh and hardened properties for UHPC with and without 2% steel fibers. The results were compared to conventionally mold-cast UHPFRC to assess performance differences.

A custom-built small-scale 3D printer was used to simulate the extrusion-based 3D concrete printing (3DCP) process. The printer was equipped with a piston-type extruder and a 45-degree inclined rectangular nozzle. Immediately after printing, the specimens were sealed for 24 hours to minimize evaporative water loss and prevent premature drying.

Flow tests were conducted in accordance with ASTM C1437 to assess workability. A qualitative evaluation of extrudability was performed using a piston-type extruder, where the acceptance criterion required the successful extrusion of five consecutive layers without blockage, tearing, segregation, or bleeding. The buildability was similarly assessed by printing seven layers of the UHPFRC matrix and composite to ensure structural stability.

For inter-layer bond strength, at least six 1.96 in × 0.98 in × 0.98 in (50 mm × 25 mm × 25 mm) specimens (Figure 7.15) were sawn from the printed layers. Two T-shaped metallic brackets were attached to the top and bottom of each specimen using epoxy adhesive to enable uniaxial pull-out testing without shear support.
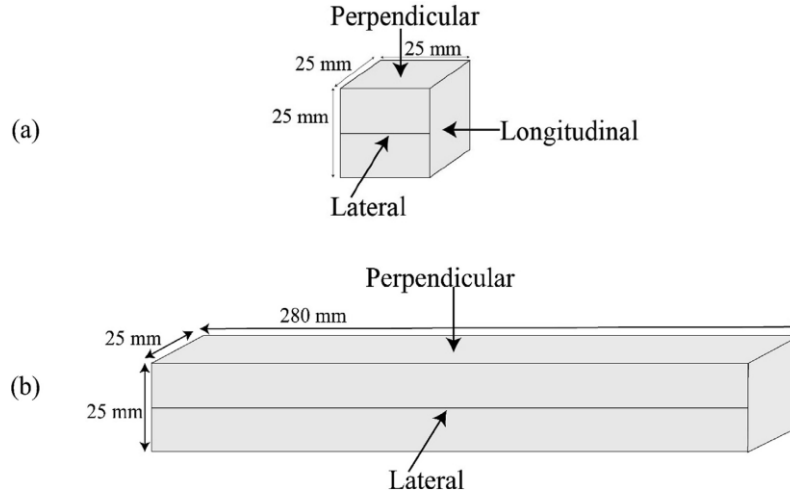
Figure 7.15. Loading directions of printed specimens; a) compression test; b) flexural test

Results indicate that the compressive strength (Figure 7.16) of mold-cast specimens was higher than that of 3D-printed specimens, regardless of the loading direction. However, in printed specimens, compressive strength was direction-dependent (Figure 15), with the highest values observed in the longitudinal direction. The MOR (Figure 16) of printed UHPFRC was slightly higher in the perpendicular direction than in the lateral direction. Additionally, printed specimens exhibited significantly higher MOR values compared to mold-cast specimens, demonstrating the effectiveness of layer-by-layer printing in enhancing flexural properties.
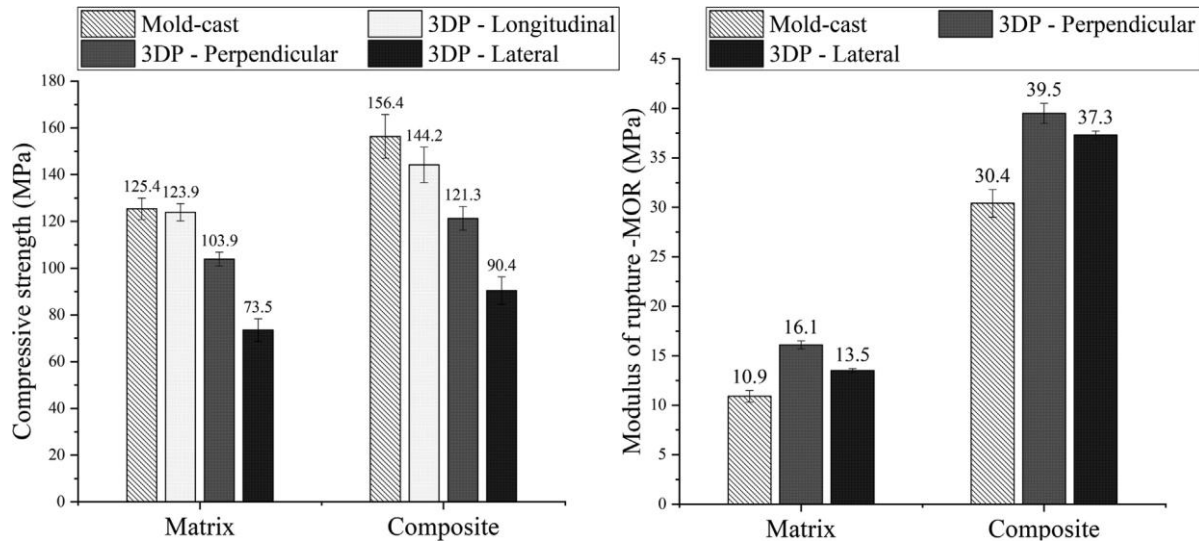
Figure 7.16. MOR of the UHPC matrix and composite

The UHPFRC composite exhibited stronger inter-layer bonding than the matrix alone, indicating that the inclusion of steel fibers improved inter-layer bond strength despite the predominantly parallel fiber orientation within the printed layers. These findings indicate the suitability of 3DCP-UHPFRC for structural applications, with enhanced mechanical properties and buildability.

Arunothayan et al. (2021) explored the effects of fiber orientation in 3D-printed UHPC. The study aimed to quantitatively assess the distribution of steel fibers and evaluate the impact of extrusion nozzle size, Cartesian print speed, and fiber volume fraction on fiber orientation. The subsequent influence of fiber orientation on the mechanical properties of 3D-printed specimens was also examined, with results compared to those of conventionally mold-cast specimens (Figure 7.17).

To analyze these effects, variations in fiber volume, nozzle diameter, and Cartesian printing speed were implemented. The fiber volume ranged from 0 to 2%, the nozzle diameter varied from 0.39 to 1.57 in (10 to 40 mm), and the printing speed was adjusted between 0.78 and 1.96 in/s (20 and 50 mm/s). Following the printing process, all printed slabs were covered with plastic sheets for 48 hours at room temperature 73.4 ± 5.4°F (23 ± 3°C) to control moisture loss. Mold-cast specimens were demolded after 24 hours and kept at room temperature for an additional 24 hours.
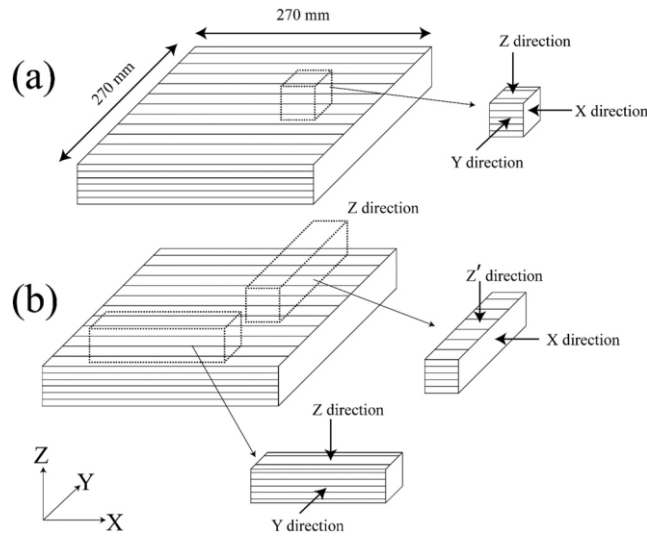
Figure 7.17. Schematic illustration of printed slabs and loading direction of specimens under; a) compression; b) flexure

After a seven-day curing period, 1.96 in (50 mm) cubes were sawn from the printed slabs for compressive strength testing, while 0.96 in × 0.96 in × 7.87 in (50 mm × 50 mm × 200 mm) prisms were prepared for flexural strength testing. Compression tests were conducted in three loading directions, whereas flexural tests were performed in four directions to assess the anisotropic behavior of the printed UHPFRC.

The inclusion of steel fibers increased compressive strength (Figure 7.18) in both mold-cast and 3D-printed specimens, regardless of the loading direction. However, in printed specimens, compressive strength was direction-dependent, regardless of the steel fiber content.

152
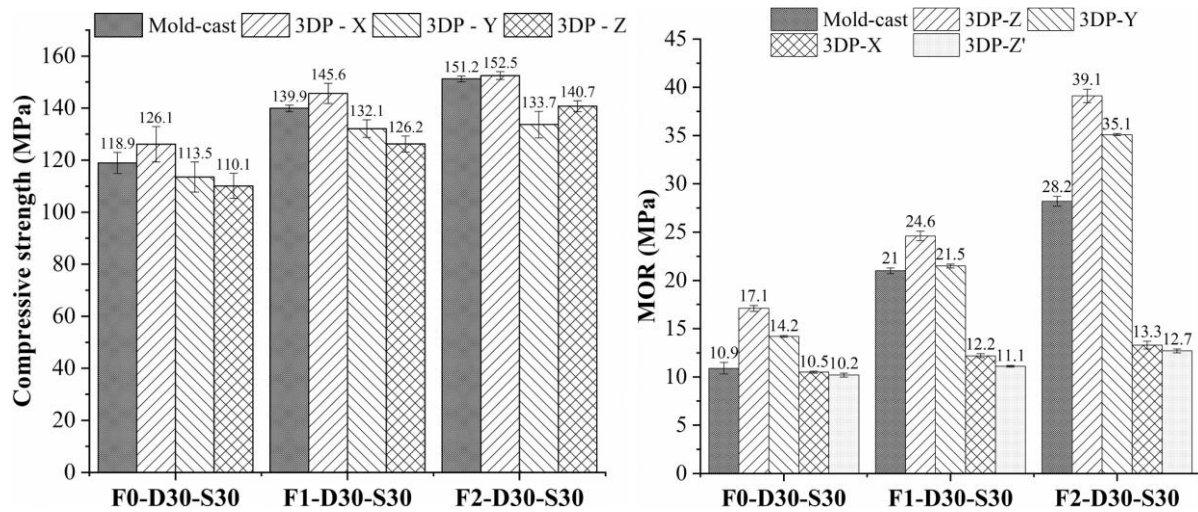
Figure 7.18. Compressive strength and MOR of mold cast and 3DP-UHPC

Similar anisotropic behavior was observed in the modulus of rupture (MOR) results. Specimens loaded in the Z and Y directions exhibited higher MOR values compared to those loaded in the X and Z′ directions (Figure 7.17). This indicates that fiber alignment along the span direction played a significant role in bridging flexural cracks and resisting crack propagation, thereby enhancing flexural performance in specific loading orientations.

The MOR of specimens printed in the X direction (3DP-Z and 3DP-Y) increased as nozzle diameter increased, indicating that fiber orientation is influenced by nozzle size. Specifically, an increase of up to 27% in MOR values was observed in UHPFRC specimens having 1% fiber content with a 10mm diameter nozzle compared to UHPFRC specimens having 1% fiber content with a 40 mm diameter nozzle. However, MOR values remained similar for specimens printed with 1.18 in and 1.57 in (30 mm and 40 mm) nozzles, suggesting the presence of an upper limit in the nozzle diameter-to-fiber length ratio, beyond which fiber orientation becomes independent of nozzle size.

Print speed had negligible influence on MOR values, supporting the hypothesis that fiber orientation remains unaffected by print speed. Additionally, deflection-hardening failure behavior was observed in specimens printed in the X direction (3DP-Z and 3DP-Y) at 1% and 2% steel fiber content, further reinforcing the role of fiber orientation in improving mechanical performance.

Bai et al. (2021) explored the limitations of reinforcement in 3D-printed concrete (3DP-C) and proposed a dual-printing method to enhance mechanical performance. This approach enables the simultaneous deposition of UHPC and conventional 3DP-C, where UHPC acts as an integral reinforcement component within the printed structure. To ensure precise coordination between the two materials, a specialized dual-material extrusion system (Figure 7.19) was developed.
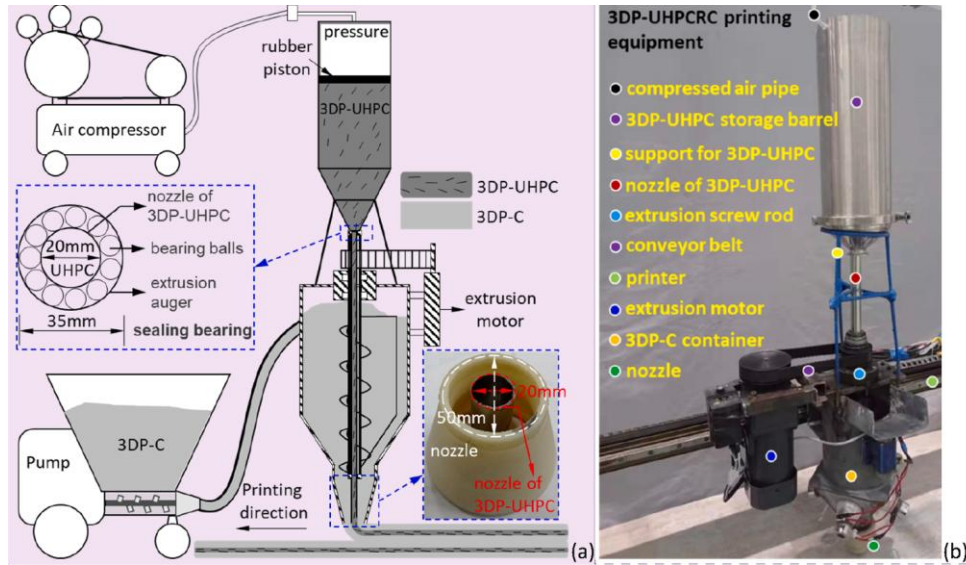
Figure 7.19. Extrusion system for dual 3DCP; a) schematic; b) set-up

The dual-printing process (Figure 7.19) allows UHPC and ordinary 3DP-C to be extruded concurrently, ensuring that 3DP-UHPC encapsulates 3DP-C in a continuous, integrated manner. This method improves the structural integrity of the printed composite. Three identical prismatic specimens of 3DP-UHPCRC (3D-printed ultra-high performance reinforced concrete) were fabricated and subjected to the same curing conditions as standard 3DP-UHPC specimens before undergoing four-point bending tests.

Experimental results indicate that the average flexural strength of conventional 3DP-C specimens was 623.6 psi (4.3 MPa), whereas 3DP-UHPCRC specimens achieved a flexural strength of 1,624 psi (11.2 MPa), representing an improvement of 160.5%. These findings demonstrate that UHPC reinforcement in 3D-printed concrete significantly enhances flexural performance, offering a reinforcement effect similar to that of steel bars in conventional concrete structures.

Prem et al. (2024) investigated damage evolution and crack formation in 3DP-UHPC prisms using Acoustic Emission (AE) testing. The study examined 3DP-UHPC prisms with and without coarse aggregates, tested under lateral (Y-direction) and perpendicular (Z-direction) loading relative to the printing direction. To enhance structural performance, micro steel fibers with a 2% volume fraction were incorporated into the 3D-printed specimens.

Two mixture variations were evaluated: 3D-UHPC-F, containing fine aggregate <0.078 in (<2 mm), and 3D-UHPC-CA, which included coarse aggregate 0.196 – 0.236 in (5–6 mm). The specimens were subjected to displacement-controlled testing at a loading rate of 0.00787 in/min (0.2 mm/min), with testing continued until softening behavior was evident. Prisms were tested in both Z-direction (orthogonal to the printing direction) and Y-direction (parallel to the printing layers) to assess anisotropic mechanical behavior.

An 8-channel PCI-Express Bus AE system was employed for data acquisition, utilizing six R6I-AST sensors with a peak sensitivity of 117 dB, an operating frequency range of 40–100 kHz, and

a resonant frequency of 55 kHz. Silicone grease was applied as a coupling agent to ensure optimal sensor placement and signal transmission.

Using AE source localization techniques, the study aimed to identify the locations of AE events (Figure 7.20) and specimen failures, providing insights into anisotropic damage mechanisms in 3DP-UHPC.
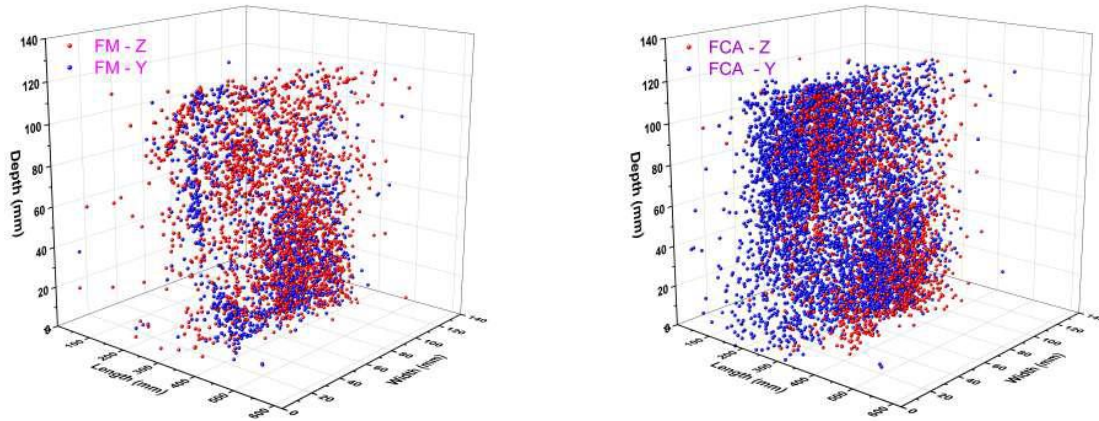
Figure 7.20. Maps of acoustic emission events for UHPC-F and UHPC-CA

Cracks in concrete were classified as shear or tensile by clustering data from RA value and Average Frequency (AF) plots (Figure 7.20). The RA value, defined as the ratio of rise time to amplitude, represents the time required for the AE signal to increase from a threshold level to its peak, while amplitude indicates the maximum signal intensity.

The results revealed distinct trends in crack propagation behavior based on the loading direction. In UHPC-F printed beams, the RA values were higher in the Z direction compared to the Y direction, while AF values in tensile cracks showed an inverse trend, with lower values in the Z direction. Similar trends were observed in shear cracks.

For UHPC-CA printed beams, the opposite trend was found for tensile cracks, where RA values and AF values were higher in the Y direction than in the Z direction. In shear cracks, however, the RA values remained higher in the Y direction, reinforcing the influence of fiber distribution and aggregate size on crack formation.

These findings highlight the anisotropic failure mechanisms in 3D-printed UHPC, demonstrating how aggregate composition and fiber orientation influence crack propagation in different loading directions.

7.4.5 Current Challenges and Future work

Current Challenges

UHPC faces several challenges related to cost, material requirements, sustainability, production efficiency, and large-scale implementation. One of the primary obstacles is the high cost of raw materials, particularly steel fibers, cement, silica fume, and superplasticizers, which significantly

impact its economic feasibility. Additionally, UHPC requires specialized curing conditions, such as heat or steam curing, to achieve its characteristic high strength and durability, further increasing production complexity and costs.

Another major concern is sustainability, as UHPC contains a high cement content, contributing to increased carbon emissions. The availability of SCMs is also becoming a concern, given the decline in coal-fired power plants, which has resulted in shortages of traditional SCMs such as fly ash, slag, metakaolin, and silica fume. Ensuring a sustainable and cost-effective supply chain for UHPC ingredients is crucial for its broader adoption.

From an implementation perspective, the limited industry experience with precast and cast-in-place UHPC applications poses a significant challenge for large-scale construction. Additionally, compliance with federal Buy America provisions necessitates further research into the use of domestically produced steel fibers or alternative non-steel fibers that can maintain UHPC's mechanical properties. Addressing this regulatory requirement is essential for expanding UHPC's use in federally funded infrastructure projects.

Structural and seismic applications of UHPC remain another area requiring further exploration. Large-scale experimental studies are needed to evaluate the structural and seismic behavior of grouted duct connections in non-proprietary UHPC mixes. Furthermore, current UHPC production processes are time-consuming, with mixing times exceeding 20 minutes, which can introduce delays and logistical challenges in field construction. Optimizing mixing efficiency and placement techniques is necessary to improve construction workflows and scalability.

Future Work

To facilitate the broader adoption of UHPC, comprehensive cost-benefit analyses are needed to demonstrate its economic advantages in bridge construction and other infrastructure projects. Large-scale demonstration projects will be critical for showcasing UHPC's performance, durability, and long-term cost savings, ultimately fostering confidence among stakeholders.

The sustainability of UHPC materials is another key research priority. Given the declining availability of traditional SCMs, further investigations are required to identify and evaluate alternative SCMs that can enhance UHPC performance while reducing environmental impact. Developing eco-friendly mixture designs with optimized binder compositions can help improve UHPC's sustainability profile.

There is also a strong need for standardized design and construction guidelines tailored to UHPC applications. A comprehensive design and construction document aligned with AASHTO LRFD Bridge Design Specifications and AASHTO LRFD Bridge Construction Specifications will provide engineers with clear guidance on structural design, reinforcement detailing, and quality control measures. Additionally, new test procedures must be established for mixture development, quality control, and performance evaluation of fresh and hardened UHPC.

A critical gap in UHPC research involves reinforcement detailing for both non-prestressed reinforcement and prestressing strands. Since UHPC requires high flowability and fiber stability, further studies are necessary to determine the optimal workability characteristics for various

construction applications. Additionally, fiber stability during batching and casting is a crucial factor affecting UHPC's mechanical performance. The development of a standardized test method for fiber dispersion and alignment will help ensure consistency and reliability in large-scale production.

Another important research focus is workability retention. Given that UHPC is highly viscous and tends to lose workability rapidly, studies should explore methods to extend its workability period without compromising strength and durability. This is particularly important for large-scale construction projects, where prolonged placement times may be required.

By addressing these challenges and advancing research in key areas, UHPC can achieve greater affordability, sustainability, and practicality, facilitating its integration into mainstream infrastructure development.

8. SUMMARY

This report presents a comprehensive feasibility analysis of UHPC for use in prestressed concrete bridge applications in New Mexico, based on research conducted between 2009 and 2024. Given the widespread use of prestressed concrete girders in the state, the integration of UHPC offers a promising solution to improve structural strength, durability, and service life.

The study began with an extensive literature review of UHPC's material characteristics and concluded with its application as an overlay material on an existing bridge structure. The research was conducted in five phases, covering both laboratory development and field validation.

A parametric study evaluated the influence of design parameters on flexural and shear performance in multi-span bridge configurations, including case studies from the I-25/Doña Ana Interchange and the Sunland Park River Crossing. An economic analysis was conducted to assess the feasibility of producing locally optimized UHPC mixtures, aiming to reduce cost while maintaining high performance.

Various UHPC mixtures were tested by adjusting parameters such as SCMs (silica fume, fly ash), sand content and gradation, w/cm, steel fiber type and dosage, admixture type, and curing conditions. The optimized mixtures were selected based on workability, compressive strength, and flexural strength, and further evaluated for modulus of elasticity, modulus of rupture, unit weight, durability, shrinkage, and creep.

To validate structural performance, the study included testing on Bridge 5296, a structurally deficient bridge, where longitudinal and transverse flexural tests were performed on girders, along with compressive tests on girder and cube specimens. Additional applications of UHPC in joint connections, shear keys, and composite beams were also evaluated. The bond performance of UHPC as an overlay was assessed through direct tension pullout tests on Bridge 7032 in Socorro, NM.

The report concludes with a practical roadmap for UHPC implementation, outlining lessons learned from global research and local applications. It identifies remaining challenges, such as workability retention, the lack of standardized design guidelines, reinforcement detailing, and sustainability concerns, and provides recommendations to guide future research and support broader adoption of UHPC in New Mexico's transportation infrastructure.

REFERENCES

Aaleti, S. R., Sritharan, S., Bierwagen, D., Wipf, T. J., Engineering, W., & Chair, A. (2011). Experimental Evaluation of Structural Behavior of Precast UHPC Waffle Bridge Deck Panels and Connections. *Proceedings of the 90th annual meeting (pp. 23-27).* Transportation Research Board, Washington, DC.

AASHTO (American Association of State Highway and Transportation Officials). (2017). *AASHTO LRFD bridge design specifications, customary U.S. units, (6th ed.).*

AFGC-SETRA (Association Française de Génie Civil-Service d'Études Techniques des Routes et Autoroutes). (2002). Ultra-High Performance Fibre-Reinforced Concretes - Interim Recommendations. *AFGC Scientific and Technical Documents.*

Ahmad, S., Rasul, M., Adekunle, S. K., Al-Dulaijan, S. U., Maslehuddin, M., & Ali, S. I. (2019). Mechanical properties of steel fiber-reinforced UHPC mixtures exposed to elevated temperature: Effects of exposure duration and fiber content. *Composites Part B: Engineering*, *168*, 291–301. https://doi.org/10.1016/j.compositesb.2018.12.083

Alkaysi, M., & El-Tawil, S. (2016). Effects of variations in the mix constituents of ultra high performance concrete (UHPC) on cost and performance. *Materials and Structures/Materiaux et Constructions*, *49*(10), 4185–4200. https://doi.org/10.1617/s11527-015-0780-6

Alkaysi, M., El-Tawil, S., Liu, Z., & Hansen, W. (2016). Effects of silica powder and cement type on durability of ultra-high performance concrete (UHPC). *Cement and Concrete Composites*, *66*, 47–56. https://doi.org/10.1016/j.cemconcomp.2015.11.005

Almansour, H. (2010). Innovative precast bridge superstructure using ultra high performance concrete girders. https://www.researchgate.net/publication/44091977

Alsalman, A., Dang, C. N., & Micah Hale, W. (2017). Development of ultra-high performance concrete with locally available materials. *Construction and Building Materials*, *133*, 135–145. https://doi.org/10.1016/j.conbuildmat.2016.12.040

Arunothayan, A. R., Nematollahi, B., Ranade, R., Bong, S. H., & Sanjayan, J. (2020). Development of 3D-printable ultra-high performance fiber-reinforced concrete for digital construction. *Construction and Building Materials*, *257*. https://doi.org/10.1016/j.conbuildmat.2020.119546

Arunothayan, A. R., Nematollahi, B., Ranade, R., Bong, S. H., Sanjayan, J. G., & Khayat, K. H. (2021). Fiber orientation effects on ultra-high performance concrete formed by 3D printing. *Cement and Concrete Research*, *143*. https://doi.org/10.1016/j.cemconres.2021.106384

Aubry, S., Bompas, P., Vaudeville, B., Corvez, D., Lagrange, T., Mazzacane, P., Brizou, A., & Sabla, B. (2013). A UHPFRC Cladding Challenge: The Fondation Louis Vuitton Pour La Création "Iceberg." *In 2nd RILEM-fib-AFGC international Symposium on ultra-high performance fibre-reinforced concrete.*

Azmee, N. M., & Shafiq, N. (2018). Ultra-high performance concrete: From fundamental to applications. *Case Studies in Construction Materials*, *9*. https://doi.org/10.1016/j.cscm.2018.e00197

Bache, H. H. (1981). *Densified Cement Ultra Fine Particle Based Materials. Denmark.*

Bagheri, A., Zanganeh, H., Alizadeh, H., Shakerinia, M., & Marian, M. A. S. (2013). Comparing the performance of fine fly ash and silica fume in enhancing the properties of concretes containing fly ash. *Construction and Building Materials*, *47*, 1402–1408. https://doi.org/10.1016/j.conbuildmat.2013.06.037

Bai, G., Wang, L., Wang, F., & Ma, G. (2021). In-process reinforcing method: dual 3D printing procedure for ultra-high performance concrete reinforced cementitious composites. *Materials Letters*, *304*. https://doi.org/10.1016/j.matlet.2021.130594

Berry, M., & Scherr Kirsten Matteson, R. (2021). Feasibility of non-proprietary ultra-high performance concrete (UHPC) for use in highway bridges in Montana: phase II field application (No. FHWA/MT-21-002/9578-606). *Montana Department of Transportation Research Programs.*

Blais, P. Y., and Couture, M., Operations Manager, P. E., Bolduc, B., & Beauce, Ste.-M. (1999). Precast, Prestressed Pedestrian Bridge World's First Reactive Powder Concrete Structure. *PCI journal*, *44*(5).

Carey, A. S., Howard, I. L., Scott, D. A., Moser, R. D., Shannon, J., & Knizley, A. (2020). Impact of materials, proportioning, and curing on ultra-high-performance concrete properties. *ACI Materials Journal*, *117*(1), 213–222. https://doi.org/10.14359/51719076

Deeb, R., Ghanbari, A., & Karihaloo, B. L. (2012). Development of self-compacting high and ultra high performance concretes with and without steel fibres. *Cement and Concrete Composites*, *34*(2), 185–190. https://doi.org/10.1016/j.cemconcomp.2011.11.001

Dils, J., Boel, V., & De Schutter, G. (2013). Influence of cement type and mixing pressure on air content, rheology and mechanical properties of UHPC. *Construction and Building Materials*, *41*, 455–463. https://doi.org/10.1016/j.conbuildmat.2012.12.050

Ebrahimpour, A., Mashal, M., Casanova, M., Rashique, U., Clauson, C., & Shokrgozar, A. (2018). Effectiveness of High-Early Strength Concrete Class 50AF with Polypropylene Fibers as a Cost-Effective Alternative for Field-Cast Connections of Precast Elements in Accelerated Bridge Construction. *No. FHWA-ID-16-246. Idaho Transportation Department*. https://itd.idaho.gov/alt-programs/?target=research-program

Ferdosian, I., & Camões, A. (2016). Effective low-energy mixing procedure to develop high-fluidity cementitious pastes. *Materia*, *21*(1), 11–17. https://doi.org/10.1590/S1517-707620160001.0002

Gesoglu, M., Güneyisi, E., Muhyaddin, G. F., & Asaad, D. S. (2016). Strain hardening ultra-high performance fiber reinforced cementitious composites: Effect of fiber type and concentration.

Composites Part B: Engineering, *103*, 74–83. https://doi.org/10.1016/j.compositesb.2016.08.004

Gosselin, C., Duballet, R., Roux, P., Gaudillière, N., Dirrenberger, J., & Morel, P. (2016). Large-scale 3D printing of ultra-high performance concrete - a new processing route for architects and builders. *Materials and Design*, *100*, 102–109. https://doi.org/10.1016/j.matdes.2016.03.097

Graybeal, B. A. (2006). Material Property Characterization of Ultra-High Performance Concrete (No. FHWA-HRT-06-103). *United States. Federal Highway Administration. Office of Infrastructure Research and Development*.

Haber, Z. B., Munoz, J. F., De la Varga, I., & Graybeal, B. A. (2018). Bond characterization of UHPC overlays for concrete bridge decks: Laboratory and field testing. *Construction and Building Materials*, *190*, 1056–1068. https://doi.org/10.1016/j.conbuildmat.2018.09.167

Huang, H., & Ye, G. (2017). Examining the "time-zero" of autogenous shrinkage in high/ultra-high performance cement pastes. *Cement and Concrete Research*, *97*, 107–114. https://doi.org/10.1016/j.cemconres.2017.03.010

Iman Talebinejad, S. A. (2004). Optimizing Mixture Proportions of Normal Weight Reactive Powder Concrete with Strengths of 200-350 MPa. *In Proceedings of the International Symposium on UHPC, Kassel, Germany,* pp. 133-141. 2004.

Ji, T., Chen, B., Zhuang, Y., Li, F., Huang, Z., & Liang, Y. (2011). Effects of sand particle size and gradation on strength of reactive powder concrete. *Advanced Materials Research*, *261–263*, 208–211. https://doi.org/10.4028/www.scientific.net/AMR.261-263.208

Kennedy, D., & Habel, K. (2015). Ultra High-Performance Concrete Column Jacket Retrofit for the Mission Bridge. In *Proceedings of the 11th Canadian Conference on Earthquake Engineering, Victoria, BC, Canada*, pp. 21-24. 2015.

Khan, M. U., Ahmad, S., Naqvi, A. A., & Al-Gahtani, H. J. (2020). Shielding performance of heavy-weight ultra-high-performance concrete against nuclear radiation. *Progress in Nuclear Energy*, *130*. https://doi.org/10.1016/j.pnucene.2020.103550

Khayat, K. H., & Eng, P. (2018). Final Report Prepared for Missouri Department of Transportation Design and Performance of Cost-Effective Ultra High Performance Concrete for Bridge Deck Overlays. No. cmr 18-006. Missouri. *Dept. of Transportation. Construction and Materials Division.* https://orcid.org/0000-0002-0739-0211

Lankard, D. R. (1984). Slurry Infiltrated Fiber Ccncrete (Sifcon): Properties and Applications. *MRS Online Proceedings Library*, *42*(1), pp.277-286.

Li, P. P., Brouwers, H. J. H., Chen, W., & Yu, Q. (2020). Optimization and characterization of high-volume limestone powder in sustainable ultra-high performance concrete. *Construction and Building Materials*, *242*. https://doi.org/10.1016/j.conbuildmat.2020.118112

Li, P. P., Sluijsmans, M. J. C., Brouwers, H. J. H., & Yu, Q. L. (2020). Functionally graded ultra-high performance cementitious composite with enhanced impact properties. *Composites Part B: Engineering*, *183*. https://doi.org/10.1016/j.compositesb.2019.107680

Li, P. P., Yu, Q. L., & Brouwers, H. J. H. (2018). Effect of coarse basalt aggregates on the properties of Ultra-high Performance Concrete (UHPC). *Construction and Building Materials*, *170*, 649–659. https://doi.org/10.1016/j.conbuildmat.2018.03.109

Li, S., Cheng, S., Mo, L., & Deng, M. (2020). Effects of steel slag powder and expansive agent on the properties of ultra-high performance concrete (UHPC): Based on a case study. *Materials*, *13*(3). https://doi.org/10.3390/ma13030683

Liang, X., Wu, C., Su, Y., Chen, Z., & Li, Z. (2018). Development of ultra-high performance concrete with high fire resistance. *Construction and Building Materials*, *179*, 400–412. https://doi.org/10.1016/j.conbuildmat.2018.05.241

Liu, J., Han, F., Cui, G., Zhang, Q., Lv, J., Zhang, L., & Yang, Z. (2016). Combined effect of coarse aggregate and fiber on tensile behavior of ultra-high performance concrete. *Construction and Building Materials*, *121*, 310–318. https://doi.org/10.1016/j.conbuildmat.2016.05.039

Ma, J., & Orgass, M. (2004). Comparative Investigations on Ultra-High Performance Concrete with and without Coarse Aggregates. In *International symposium on ultra high performance concrete, Kassel, Germany*, pp. 205-212. 2004. https://www.researchgate.net/publication/238104255

Mazzacane, P., Ricciotti, R., Lamoureux, G., & Corvez, D. (2013). Roofing of the stade Jean Bouin in UHPFRC. In *Proceedings of international Symposium on ultra-high performance fibre-reinforced concrete*. Vol. 10, p. 9781118557839.

Menétrey, P. (2013). UHPFRC Cladding for The Qatar National Museum. In *Proceedings of the International Symposium on Ultra-High Performance Fiber-Reinforced Concrete, Marseille, France*, pp. 1-3. 2013.

Meng, W., & Khayat, K. (2017). Effects of saturated lightweight sand content on key characteristics of ultra-high-performance concrete. *Cement and Concrete Research*, *101*, 46–54. https://doi.org/10.1016/j.cemconres.2017.08.018

Meng, W., & Khayat, K. H. (2016). Mechanical properties of ultra-high-performance concrete enhanced with graphite nanoplatelets and carbon nanofibers. *Composites Part B: Engineering*, *107*, 113–122. https://doi.org/10.1016/j.compositesb.2016.09.069

Muttoni, A., Brauen, U., Jaquier, J.-L., & Moullet, D. (2013). A New Roof for The Olympic Museum At Lausanne, Switzerland. In *Proceedings of International Symposium on Ultra-High Performance Fiber-Reinforced Concrete*, pp. 69-76.

Park Jung Jun, K. S. (2004). Influence of the Ingredients on the Compressive Strength of UHPC as a Fundamental Study to Optimize the Mixing Proportion. In *Proceedings of the second*

international symposium on ultra high performance concrete, pp. 105-112. Kassel University Press GmbH, Kassel, Germany, 2008.

Piérard, J., Dooms, B., & Cauberg, N. (2013). Durability Evaluation of Different Types of UHPC. In *Proceedings of the RILEM-fib-AFGC International Symposium on Ultra-High Performance Fiber-Reinforced Concrete*, pp. 275-284.

Prem, P. R., Ingle, V., Kumar, V., & Darssni, R. (2024, January 7). Acoustic Emission Characterization Of 3d -Printed Ultra-High Performance Concrete Beams Under Bending. *11th International Conference on Fracture Mechanics of Concrete and Concrete Structures*. https://doi.org/10.21012/fc11.092372

Pyo, S., Kim, H. K., & Lee, B. Y. (2017). Effects of coarser fine aggregate on tensile properties of ultra high performance concrete. *Cement and Concrete Composites*, *84*, 28–35. https://doi.org/10.1016/j.cemconcomp.2017.08.014

Richard, P., & Cheyrezy, M. (1995). 0008-8846(95)00144-l COMPOSITION OF REACTIVE POWDER CONCREXES. In *Cement and Concrete Research* (Vol. 25, Issue 7).

Roy, M., Hollmann, C., & Wille, K. (2017). Influence of volume fraction and orientation of fibers on the pullout behavior of reinforcement bar embedded in ultra high performance concrete. *Construction and Building Materials*, *146*, 582–593. https://doi.org/10.1016/j.conbuildmat.2017.04.081

Soliman, A. M., & Nehdi, M. L. (2014). Effects of shrinkage reducing admixture and wollastonite microfiber on early-age behavior of ultra-high performance concrete. *Cement and Concrete Composites*, *46*, 81–89. https://doi.org/10.1016/j.cemconcomp.2013.11.008

Sritharan, S., & Schmitz, G. M. (2013). Design Of Tall Wind Turbine Towers Utilizing UHPC. In *2nd International Symposium on Ultra-High Performance Fibre-Reinforced Concrete (UHPFRC). Marseille, France*, pp. 433-442.

Stéphanie Staquet, B. E. (2004). Early-age autogenous shrinkage of UHPC incorporating very fine fly ash or metakaolin in replacement of silica fume. *In International Symposium on UHPC,* pp. 587–599.

Teng, L., Zhu, J., Khayat, K. H., & Liu, J. (2020). Effect of welan gum and nanoclay on thixotropy of UHPC. *Cement and Concrete Research*, *138*. https://doi.org/10.1016/j.cemconres.2020.106238

Vande Voort, T. L., Suleiman, M. T., & Sritharan, S. (2008). Design and Performance Verifi cation of Ultra-High Performance Concrete Piles for Deep Foundations. *No. IHRB Project TR-558.*

Wang, X., Yu, R., Song, Q., Shui, Z., Liu, Z., Wu, S., & Hou, D. (2019). Optimized design of ultra-high performance concrete (UHPC) with a high wet packing density. *Cement and Concrete Research*, *126*. https://doi.org/10.1016/j.cemconres.2019.105921

Weldon, B. D., Jáuregui, D. V, Newtson, C. M., Taylor, C. W., Montoya, K. F., & Allena, S. (2009). Feasibility Analysis of Ultra High Performance Concrete for Prestressed Concrete Bridge Applications. No. NM09MSC-01. *New Mexico. Dept. of Transportation. Research Bureau.*

Wille, K., & Naaman, A. (2011). Ultra-High Performance Concrete with Compressive Strength Exceeding 150 MPa (22 ksi): A Simpler Way. In *ACI Materials Journal* (Vol. 108, Issue 1).

Wu, Z., Shi, C., He, W., & Wu, L. (2016). Effects of steel fiber content and shape on mechanical properties of ultra-high performance concrete. *Construction and Building Materials*, *103*, 8–14. https://doi.org/10.1016/j.conbuildmat.2015.11.028

Wu, Z., Shi, C., Khayat, K. H., & Xie, L. (2018). Effect of SCM and nano-particles on static and dynamic mechanical properties of UHPC. *Construction and Building Materials*, *182*, 118–125. https://doi.org/10.1016/j.conbuildmat.2018.06.126

Xercavins, P., Demarthe, D., & Shushkewich, K. (2008). Eugene Freyssinet-The Invention of Prestressed Concrete and Precast Segmental Construction. *Paper on the Association Eugène Freyssinet website.*

Yuan, J., & Graybeal, B. A. (2014). Bond Behavior of Reinforcing Steel in Ultra-High Performance Concrete (No. FHWA-HRT-14-090). *United States. Federal Highway Administration. Office of Infrastructure Research and Development.*

Yang, R., Yu, R., Shui, Z., Gao, X., Xiao, X., Fan, D., Chen, Z., Cai, J., Li, X., & He, Y. (2020). Feasibility analysis of treating recycled rock dust as an environmentally friendly alternative material in Ultra-High Performance Concrete (UHPC). *Journal of Cleaner Production*, *258*. https://doi.org/10.1016/j.jclepro.2020.120673

Yang, S. L., Millard, S. G., Soutsos, M. N., Barnett, S. J., & Le, T. T. (2009). Influence of aggregate and curing regime on the mechanical properties of ultra-high performance fibre reinforced concrete (UHPFRC). *Construction and Building Materials*, *23*(6), 2291–2298. https://doi.org/10.1016/j.conbuildmat.2008.11.012

Yoo, D. Y., Kim, J. J., & Chun, B. (2019). Dynamic pullout behavior of half-hooked and twisted steel fibers in ultra-high-performance concrete containing expansive agents. *Composites Part B: Engineering*, *167*, 517–532. https://doi.org/10.1016/j.compositesb.2019.03.022

Zhang, D., Tan, K. H., Dasari, A., & Weng, Y. (2020). Effect of natural fibers on thermal spalling resistance of ultra-high performance concrete. *Cement and Concrete Composites*, *109*. p.103512. https://doi.org/10.1016/j.cemconcomp.2020.103512

Zhang, G., Graybeal, B., & Chen, L. (2013). Development of a Family of Ultra-High Performance Concrete Pi-Girders. No. FHWA-HRT-14-027. *United States. Department of Transportation. Federal Highway Administration. Office of Infrastructure Research and Development.*

Zhang, Y., Zhu, Y., Qu, S., Kumar, A., & Shao, X. (2020). Improvement of flexural and tensile strength of layered-casting UHPC with aligned steel fibers. *Construction and Building Materials*, *251*. https://doi.org/10.1016/j.conbuildmat.2020.118893

Zhao, S., Fan, J., & Sun, W. (2014). Utilization of iron ore tailings as fine aggregate in ultra-high performance concrete. *Construction and Building Materials*, *50*, 540–548. https://doi.org/10.1016/j.conbuildmat.2013.10.019

Zhu, L., Wang, J. J., Li, X., Zhao, G. Y., & Huo, X. J. (2020). Experimental and numerical study on creep and shrinkage effects of ultra high-performance concrete beam. *Composites Part B: Engineering*, *184*. https://doi.org/10.1016/j.compositesb.2019.107713

Ziad Hajar, D. L. (2004). *Design and Construction of the world first Ultra-High Performance Concrete road bridges*. 39–48.

APPENDIX A

After analyzing the effects of various curing regimens and mixture proportions, including w/cm ratios, steel fiber content, fly ash supplementation, fine aggregate content, and aggregate top size, findings from previous UHPC studies identified a few mixtures as the most cost-effective options. Additionally, the mixture proportions used for applications in Chapter 6 of this document are listed.

Mixture proportions (UHPC Phase II): Type I/II portland cement, w/cm of 0.14, 50% replacement of silica fume by Class F fly ash, No. 4 aggregate as the maximum aggregate size, and 1.5% steel fibers by volume.

Table A-1. Recommended mixture proportions (UHPC Phase II, Table 16.1)

Constituents	Unit	Amount/yd^3 (Amount/m^3)
Cement	lb (kg)	1263.9 (749.8)
Silica fume	lb (kg)	158 (93.7)
Fly ash	lb (kg)	158 (93.7)
Sand	lb (kg)	1900 (1127)
Steel fibers	lb (kg)	200 (118.7)
HRWRA	gal (L)	8.6 (42.5)
Water	lb (kg)	221.2 (131.2)

Mixture proportions for prestressed concrete members (UHPC Phase III, used in the field for girders of Bridge 9706) are shown in Table A-2.

Table A-2. Recommended mixture proportions (UHPC Phase III, Table 518-C-2.1:1)

Material	Weight (lbs./CY)	Source
Cement	1267	Tijeras Type I/II
Fly Ash	119	SRMG Four Corners Class F
Silica Fume	198	BASF
Fine Aggregate (SSD)	1900	Placitas Pit Manufactured Washed Concrete Sand
Water	222	Public Water Supply
High Range Water Reducer	72 (8.6 gal.)	BASF Glenium 3030
Steel Fiber	200	Nycon-SF Type I Steel Fibers

Table A-2: Cementitious Materials

Tijeras Type I/II Cement shall comply with the physical and chemical requirements of ASTM C150 Type I/II.

SRMG Four Corners Class F Fly ash and BASF silica fume shall comply with the physical and chemical requirements of ASTM C618 and ASTM C1240 respectively.

The mill certifications representing the shipments for this mixture shall report physical and chemical properties of the cementitious materials for the lots delivered to the batching facility.

Table A-2: Fine Aggregate

Placitas Pit manufactured fine aggregate shall comply with the deleterious materials limits, quality requirements, and gradation requirements for Fine Aggregate of Section

509: Portland Cement Concrete Mixture Designs.

Note: the top aggregate size being considered is #4.

Table A-2: Water

The source of water shall be considered as potable.

Table A-2: High Range Water Reducer

BASF Glenium 3030 High range water reducing admixture shall comply with ASTM C494 requirements.

Table A-2: Steel Fiber

Steel fibers used for UHPC shall be Nycon-SF Type I Steel Fibers.

Mixture proportions used in the laboratory for strength gain tests under thermal and ambient curing regimens were representative of the trail production batches, each with a volume of 1.25 ft^3.

Table A-3. Mixture proportions used in UHPC Phase IV on batches of 1.25 ft^3 (Phase IV, Table 4.13)

Material	Quantity	
Sand	85.0 lb	(38.5 kg)
Type I/II Portland Cement	60.6 lb	(27.5 kg)
Silica Fume	9.47 lb	(4.30 kg)
Class F Fly Ash	5.68 lb	(2.58 kg)
Water (w/cm = 0.140)	10.6 lb	(4.81 kg)
High-Range Water-reducing Admixture	50.7 fl oz	(1499 mL)
High Strength Steel Fibers (volumetric content of 1.50%)	9.19 lb	(4.17 kg)

NOTE: Values based on aggregates at oven-dry conditions and must be adjusted for moisture content and absorption.

Mixture proportions used in the laboratory tests for investigating the tensile behavior of locally produced UHPC are presented in Table A-4.

Table A-4. Mixture proportions for direct tension tests (UHPC Phase IV, Table 4.97).

Constituent	Quantity
Cement	50.9 lb
Silica Fume	6.4 lb
Fly Ash	6.4 lb
Sand	62.3 lb
Steel Fibers	7.4 lb
HRWRA	1/3 gal
Water	10.2 lb

The following mixture proportions (Tables A-5 and A-6) are used in laboratory tests when investigating the possibility of additional applications of UHPC for joint application and UHPC shear keys.

Table A-5. Joint application mixture proportions (UHPC Phase IV, Table 5.2)

Cement, lb/yd^3 [kg/m3]	Silica Fume, lb/yd^3 [kg/m^3]	Fly Ash, lb/yd^3 [kg/m^3]	Fine Sand, lb/yd^3 [kg/m^3]	Steel Fibers, lb/yd^3 [kg/m^3]	Water, lb/yd^3 [kg/m^3]	HRWRA, gal/yd^3 [L/m^3]
1374 [815]	172 [102]	172 [102]	1700 [1010]	200 [119]	258 [153]	9.31 [46.1]

Table A-6. UHPC shear keys mixture proportions (UHPC Phase IV, Table 5.9)

Material	Cement	Silica Fume	Class F Fly Ash	Sand	HRWRA gal/yd^3 (L/m^3)	Water	Steel Fibers
lb/yd^3 (kg/m^3)	1377 (817)	172 (102)	172 (102)	1700 (1009)	9.0 (45)	258 (153)	200 (119)

Cement, Class F Fly ash and sand were obtained from local sources when testing shear keys (Table 13). Silica fume, HRWRA and steel fibers were sourced from regional suppliers. HRWRA is Master Glenium 3030 and a water to cement ratio is 0.15. The steel fibers used for this test were Dramix® OL 13/0.2, produced by Bakaert, and had a length of 0.51 in. and tensile strength of 399 ksi.

Table A-7. UHPC composite beams mixture proportions (UHPC Phase IV, Table 5.19)

Constituent	Quantity, /1 yd^3	Quantity, /1 m^3
Cement	1374 lb	815 kg
Silica Fume	173 lb	103 kg
Fly Ash	173 lb	103 kg
Sand	1682 lb	998 kg
Steel Fibers	200 lb	119 kg
HRWRA	9 gal	44.6 l
Water	276 lb	164 kg

The following mixture proportions were used on UHPC Phase V for overlay mock-up placements.

Table A-8. UHPC overlay mock-up mixture proportions (UHPC Phase V, Table 4.1)

Constituents	Unit	[kg/m³]
Cement	lb. [kg]	1248 [740.5]
Silica Fume	lb. [kg]	195 [116]
Fly Ash	lb. [kg]	117 [69.4]
Sand	lb. [kg]	1602 [950.5]
Fibers [1]	lb. [kg]	230 [137]
HRWRA	gal. [L]	8.50 [42.1]
Water	lb. [kg]	244 [145]

[1] - Mixture contains 1.75% by volume of steel fibers.

Table A-9. Baseline mixture proportions for the optimization from chapter 3 (UHPC Phase II, Table 12.3)

Category	Mixture	Cement, lb/yd³ (kg/m³)	Silica fume, lb/yd³ (kg/m³)	Fine sand, lb/yd³ (kg/m³)	Steel fibers, lb/yd³ (kg/m³)	Water, lb/yd³ (kg/m³)	HRWRA, gal/yd³ (l/m³)	w/c	w/ (c+sf)[1]
D	DL00	1500 (890)	375 (222)	1411 (837)	-	375 (222)	6.00 (29.64)	0.25	0.20
E	EL00	1500 (890)	375 (222)	1347 (799)	200 (119)	375 (222)	6.00 (29.64)	0.25	0.20

[1]water-to-cement plus silica fume